

**The Effect of Cage Positioning on Lumbosacral Vertebral
Endplate Failure in Compression**

Robert David Labrom

**MB, BS, University of Queensland, 1992
FRACS (Orth)**

**A thesis submitted in partial fulfillment of the requirements of
for the degree of**

Master of Science

**In
The Faculty of Graduate Studies
(Department of Surgery)**

**We accept this thesis as conforming
to the required standard**

THE UNIVERSITY OF BRITISH COLUMBIA

October 2002

© Robert Labrom, 2002.

In presenting this thesis in partial fulfilment of the requirements for an advanced degree at the University of British Columbia, I agree that the Library shall make it freely available for reference and study. I further agree that permission for extensive copying of this thesis for scholarly purposes may be granted by the head of my department or by his or her representatives. It is understood that copying or publication of this thesis for financial gain shall not be allowed without my written permission.

Department of Surgery

The University of British Columbia
Vancouver, Canada

Date OCTOBER 1ST, 2002.

Abstract

Anterior column cage or graft subsidence remains a biomechanically and clinically serious problem that affects the performance and patient outcome of any spinal arthrodesis surgery. To assess the best position to place an interbody fusion cage, a posterior interbody fusion construct was simulated.

Specifically, the hypothesis to be tested was *that two smaller, posterolaterally positioned interbody cages would provide superior construct stiffness and strength in compression.*

Nine human cadaver spine specimens from L3-S1 were dissected and continuously posteriorly instrumented with pedicle screws and rods. This continuously instrumented construct was then potted in dental cement and plaster of Paris in such a way as to enable sequential individual axial compression testing of each functional spinal unit (FSU) from L3/4 to L5/S1.

All specimens were x-rayed, and scanned with DEXA for bone mineral density pre-testing. Stiffness properties of the FSU's with intact disc and without disc were tested. Three patterns of titanium mesh cages were then used to test stiffness and gross failure under compression: one large central, two small central, or two small posterolaterally positioned cages.

After digitizing points on the cage and vertebral bodies pre-test, an optoelectronic camera system was used to track motion of the cage and vertebrae.

The compressive stiffness of the construct at all spinal levels was significantly higher with the intact disc compared to without the disc, and with any of the three cage patterns, and these differences were significant. Mean failure loads for the three cage positions ranged between 2000 N and 2500 N and were not significantly different, though tended to be higher for the 2 posterolateral cage position.

Mean bone mineral density values for both superior and inferior vertebrae of the FSU tested, were significantly correlated with failure load values, yet did not appear predictive of cage subsidence direction.

Motion analysis of the cage- either single or double combinations, revealed no trend for either superior or inferior subsidence into the endplates. Mode of endplate failure appears to involve a mass shear displacement of the underlying trabecular bone, with condensation of the trabecular architecture in the immediate sub-endplate region.

Results of this study have supported the biomechanical validity of PLIF and TLIF type surgeries, with the preferred placement of two smaller posterolaterally positioned mesh cages (Harms et al, 1997).

Table of Contents

Abstract.....	ii
Table of Contents	iii
List of Tables	vi
List of Figures.....	vii
Acknowledgements.....	xiii
1.0 Introduction.....	1
1.1 Clinical Problem.....	1
1.2 Background Literature	5
1.2.1 Anatomy of Vertebral Bone.....	5
1.2.2 Anatomy and Development of Vertebral Endplates.....	11
1.2.3 Mapping the Structural Properties of the Lumbosacral Vertebral Endplates	13
1.2.4 Biomechanical Analyses of Interbody Fusion Constructs	15
1.3 Hypothesis and Questions Asked in this Study.....	32
1.4 Clinical Applications and Long-Term Goals	34
1.5 Scope of Study	35
2.0 Materials and Methods	36
2.1 Experimental Overview- Model Selection and Justification, Protocol	36
2.2 Human Cadaver Spine Specimen Selection	45
2.3 Dual Energy X-Ray Absorptiometry Scan (DEXA) Pre-testing	46
2.4 Dissection of Specimen	47
2.5 Instrumentation of Spinal Columns	47
2.6 Potting of Specimens.....	50
2.6.1 Lower Column Potting	50
2.6.2 Upper Vertebra Potting	54

2.7	Cage Size and Position Pattern Selection Criteria.....	56
2.8	Validation for Packing Bone Graft into Titanium Mesh Cages	60
2.9	Human Bone Graft Preparation and Insertion into Titanium Mesh Cages	63
2.10	Measurement of Cage- Bone and Bone- Bone Motion and Pre-test Validation of Digitization Method	66
2.11	Compressive Stiffness Testing- FSU's with Intact Disc and with Disc Removed... 73	
2.12	Compressive Failure Testing- FSU's with One of Three Cage Patterns Positioned	79
2.13	Post Compression Testing Vertebral Endplate Analysis	85
2.14	Mode of Endplate Failure Analysis- Macro and Microscopic Qualitative Examination	85
2.15	Data Analysis	86
2.16	Statistical Analysis	87
3.0	Results	89
3.1	Construct Stiffness Characteristics.....	89
3.2	Construct Failure Characteristics	95
3.3	Motion Analysis of Cage Subsidence	98
3.4	Mode of Endplate Failure-Macro and Microscopic Qualitative Examination	103
3.5	FSU Intervertebral Disc Degenerative Grading Values	108
4.0	Discussion	110
4.1	Effect of Cage Position Between Lumbosacral Endplate on Construct Stiffness and Failure in Compression.....	110
4.2	Effect of Bone Mineral Density	115
4.3	Direction of InterbodyCage Subsidence in the Lumbosacral Spine	117
4.4	Theoretical Mode of Endplate Failure with Bone Graft Packed Titanium Mesh Cages.....	119
4.5	Support of the Proposed Lumbosacral Endplate Strength Map	120
4.6	Strengths and Weaknesses of the Experimental Model.....	122
4.7	Clinical Correlations to Posterior Lumbar Interbody Fusion (PLIF) and Transforaminal Lumbar Interbody Fusion (TLIF).....	125
4.8	Future Directions and Further Study.....	126

5.0 Conclusions	127
6.0 References	129
7.0 Appendices	137
Appendix A - Load-Displacement Graphs for all FSU's Tested.....	138
Appendix B - Translation and Rotation Graphs for Single Cages, and Qualitative Description of Motion for Single Cage Position Tests.....	152

List of Tables

Table 2.1 Physiological profile of cadaver spine columns included in study	46
Table 2.2 Random cage position allocation for specimens and FSU levels.....	60
Table 2.3 Width (mm) x Length (mm) of endplates and surface area (mm ²) (assuming ovoid shape) and percentage of cage(s) used covering the mean of the two available endplate surface areas of the FSU tested	62
Table 3.1 Load-displacement values data spread sheet for spinal level.....	91
Table 3.2 Load-displacement values data spread sheet for cage position	92
Table 3.3 Motion analysis summary for single and double cage compression tests at failure.....	101
Table 3.4 Effect of bone mineral density on cage subsidence. Lowest bone mineral density of each FSU tested with single cage versus direction of cage subsidence	102
Table 3.5 Intervertebral disc degenerative grades from 1-4 for each level tested for all specimens	109

List of Figures

Figure 1.1	Lateral view- typical appearance and basic anatomy of a human lumbar vertebra.....	6
Figure 2.1	Experimental protocol for study	43
Figure 2.2	Schematic diagram of lateral view of the test spinal column (L3-S1) with details of general method for experiment	44
Figure 2.3	Typical appearance of instrumented, continuous spinal column from L3-Sacrum	49
Figure 2.4	Anterior (left) and lateral view of instrumented, and potted spinal column, to level of middle of S1, with L5/S1 disc space horizontal to floor.....	51
Figure 2.5	Plaster of Paris layer to mid-level of L5, leaving L4/5 disc exposed for testing as a separate FSU, and covering L5/S1 disc (last tested FSU)	52
Figure 2.6	Second Plaster of Paris layer potted (left) to mid-level of L4 body, and third layer of Plaster of Paris potted (right) to mid-level of L5 body.....	53
Figure 2.7	Typical example of superior vertebra of the FSU level being tested, with shallow dental cement and aluminum mounting cap for compression testing.....	55
Figure 2.8	Typical titanium mesh cage used- close up of 22x28mm cage...	57
Figure 2.9	Pairs of cages used in experiment (left) with 2x14 mm diameter cages and 17x22 mm (equivalent surface areas) on top, with 2x16 mm diameter cages and 22x28 mm (equivalent surface areas) on bottom. Lateral view of 9mm high 14 mm diameter cage and 9 mm high 17x 22 mm cage (right)	58
Figure 2.10	Pneumatic bone mill (left) and bone graft made from human sacrum for experiment (right).....	64
Figure 2.11	Divided portions of graft for each one of nine specimens tested.	64

Figure 2.12	Customized metal tip plunger to pack graft within each size cage (left) and standardized force (variable weights for cages) with gravity only (right)	65
Figure 2.13	Lateral and axial view of 14 mm diameter cage packed with graft	66
Figure 2.14	Cages with braided wire attaching 4 LED 's for assessment of cage motion	67
Figure 2.15	Close-up of braided wires coupled to vertebrae and cages	68
Figure 2.16	Optotrak camera system and global cartesian coordinate system based upon the center camera	69
Figure 2.17	Clear plate with 3 LED markers to establish a local coordinate system with cartesian coordinate system as marked	70
Figure 2.18	Example of points digitized on each cage for calculation of center point of cage	71
Figure 2.19	FSU with all markers attached mounted in 3 plane leveling vice ready for compression testing in Instron machine	73
Figure 2.20	Close-up of cross-wire assessment to accurately mark the center of the superior vertebral body for direct axial compression	75
Figure 2.21	Specimen 1082-L4/5, intact disc before 2 mm non-destructive compression for stiffness assessment	78
Figure 2.22	Close up of cleared disc space and endplates before 2 mm non-destructive compression test for stiffness assessment	79
Figure 2.23	Close up view of typical position of 2 central cages (post-test) ...	80
Figure 2.24	Close up view of typical position of 2 central cage position with cages removed (post-test)	81
Figure 2.25	Close up view of typical appearance of a titanium mesh cage that has been filled with graft, and preferentially compressed on the endplate side that the cage mostly subsided	82
Figure 3.0	Typical appearance of a load-displacement curve for a FSU with intact disc, no disc, and any of the three cage positions	89

Figure 3.1	Mean stiffness (N/mm) and SD's for all FSU's tested with either Disc Intact (1), No Disc (2), or Cage(s) (3).....	93
Figure 3.2	Stiffness properties of FSU's with intact disc, without disc, and with cage(s) positioned, with respect to spinal level	93
Figure 3.3	Stiffness properties of FSU's with intact disc, without disc, and with cage(s) positioned, with respect to cage position.....	94
Figure 3.4	Failure load (N) for each FSU with a cage position tested (note- key for subgroups), versus average bone mineral density for that FSU.....	96
Figure 3.5	Mean peak failure loads (N) and standard error of the mean versus cage position.....	96
Figure 3.6	Mean peak failure loads (N) and ranges versus spinal levels	97
Figure 3.7	Specimen 1061 L4/5 - Load-displacement curves for disc intact, without disc, and 1 central cage.....	97
Figure 3.8	Cartesian coordinate system used in describing motion of cage and vertebrae for translation and rotation	99
Figure 3.9	Translation (T) and Rotation (R) in both axial- up or down (y plane) and sagittal- forward flexion (x plane) of the single cage in specimen 1061, L4/5, versus time	100
Figure 3.10	Macroscopic cross-section in coronal plane of Specimen 1067 - L4 Failed superior endplate post-test, single cage.....	103
Figure 3.11	2 mm wafer of vertebral body of Specimen 1036- Inferior endplate of L3 highlighted (2 central cages tested)	105
Figure 3.12	2 mm wafer of vertebral body in coronal plane of Specimen 1036- L5 inferior endplate highlighted (1 central cage)	106
Figure 3.13	2mm wafer of vertebral body cut in coronal plane of Specimen 1067- L5 superior endplate highlighted (2 central cages)	107
Figure A.1	Specimen 1061 L3/4- Load-displacement curves for disc intact, without disc, and 2 posterolateral cages	138
Figure A.2	Specimen 1061 L4/5 - Load-displacement curves for disc intact, without disc, and 1 central cage.....	138

Figure A.3	Specimen 1061 L5/S1- Load-displacement curves for disc intact, without disc, and 2 central cages	139
Figure A.4	Specimen 1067 L3/4- Load-displacement curves for disc intact, without disc, and 1 central cage	139
Figure A.5	Specimen 1067 L4/5- Load-displacement curves for disc intact, without disc, and 2 central cages	140
Figure A.6	Specimen 1067 L5/S1- Load-displacement curves for disc intact, without disc, and 2 posterolateral cages	140
Figure A.7	Specimen 1009 L3/4- Load-displacement curves for disc intact, without disc, and 2 central cages	141
Figure A.8	Specimen 1009 L4/5- Load-displacement curves for disc intact, without disc, and 1 central cage	141
Figure A.9	Specimen 1009 L5/S1- Load-displacement curves for disc intact, without disc, and 2 posterolateral cages	142
Figure A.10	Specimen 1027 L3/4- Load-displacement curves for disc intact, without disc, and 2 posterolateral cages	142
Figure A.11	Specimen 1027 L4/5 Load-displacement curves for disc intact, without disc, and 1 central cage	143
Figure A.12	Specimen 1027 L5/S1 Load-displacement curves for disc intact, without disc, and 2 central cages	143
Figure A.13	Specimen 1082 L3/4- Load-displacement curves for disc intact, without disc, and 1 central cage	144
Figure A.14	Specimen 1082 L4/5- Load-displacement curves for disc intact, without disc, and 2 posterolateral cages	144
Figure A.15	Specimen 1082 L5/S1- Load-displacement curves for disc intact, without disc, and 2 central cages	145
Figure A.16	Specimen 1031 L3/4- Load-displacement curves for disc intact, without disc, and 2 posterolateral cages	145
Figure A.17	Specimen 1031 L4/5- Load-displacement curves for disc intact, without disc, and 2 central cages	146

Figure A.18	Specimen 1031 L5/S1- Load-displacement curves for disc intact, without disc, and 1 central cage.....	146
Figure A.19	Specimen 1090 L3/4- Load-displacement curves for disc intact, without disc, and 1 central cage.....	147
Figure A.20	Specimen 1090 L4/5 Load-displacement curves for disc intact, without disc, and 2 central cages	147
Figure A.21	Specimen 1090 L5/S1- Load-displacement curves for disc intact, without disc, and 2 posterolateral cages	148
Figure A.22	Specimen 1030 L3/4- Load-displacement curves for disc intact, without disc, and 2 central cages	148
Figure A.23	Specimen 1030 L4/5 Load-displacement curves for disc intact, without disc, and 2 posterolateral cages	149
Figure A.24	Specimen 1030 L5/S1- Load-displacement curves for disc intact, without disc, and 1 central cage.....	149
Figure A.25	Specimen 1036 L3/4- Load-displacement curves for disc intact, without disc, and 2 central cages	150
Figure A.26	Specimen 1036 L4/5- Load-displacement curves for disc intact, without disc, and 2 posterolateral cages	150
Figure A.27	Specimen 1036 L5/S1- Load-displacement curves for disc intact, without disc, and 1 central cage.....	151
Figure B.1	Translation (T) and Rotation (R) in both axial- up or down (y plane) and sagittal- forward flexion (x plane) of the single cage in specimen 1061, L4/5, versus time	152
Figure B.2	Translation (T) and Rotation (R) in both axial- up or down (y plane) and sagittal- forward flexion (x plane) of the single cage in specimen 1067, L3/4, versus time	153
Figure B.3	Translation (T) and Rotation (R) in both axial- up or down (y plane) and sagittal- forward flexion (x plane) of the single cage in specimen 1009, L4/5, versus time	154
Figure B.4	Translation (T) and Rotation (R) in both axial- up or down (y plane) and sagittal- forward flexion (x plane) of the single cage in specimen 1027, L4/5, versus time	155

Figure B.5	Translation (T) and Rotation (R) in both axial- up or down (y plane) and sagittal- forward flexion (x plane) of the single cage in specimen 1082, L3/4, versus time	156
Figure B.6	Translation (T) and Rotation (R) in both axial- up or down (y plane) and sagittal- forward flexion (x plane) of the single cage in specimen 1031, L5/S1, versus time	157
Figure B.7	Translation (T) and Rotation (R) in both axial- up or down (y plane) and sagittal- forward flexion (x plane) of the single cage in specimen 1090, L3/4, versus time	158
Figure B.8	Translation (T) and Rotation (R) in both axial- up or down (y plane) and sagittal- forward flexion (x plane) of the single cage in specimen 1030, L5/1, versus time	159
Figure B.9	Translation (T) and Rotation (R) in both axial- up or down (y plane) and sagittal- forward flexion (x plane) of the single cage in specimen 1036, L5/1, versus time	160

Acknowledgements

I would like to thank my thesis committee for all of their support and valuable input over the time it has taken to design and complete this study.

Special thanks to my co-supervisors, Drs Oxland and Reilly, for their always excellent advice and teaching.

Sincere thanks to my friend and engineering mentor, Juay Seng Tan, whose help and patience has been greatly appreciated.

I would also like to thank all others who have contributed from both biomechanical and clinical perspectives, including Dr Heather McKay and Leslie Bryant MacLean for their contribution to the DEXA scanning part of this study.

Thank you to Dr Stephen Tredwell who has taught me many good things, including how to "be academic".

Thank you to my wife and family for travelling so far and for making anything possible.

Implants supplied by DePuy, Canada, are gratefully acknowledged.

Thank you to the George W. Bagby Research Fund for generous financial support.

1.0 Introduction

1.1 Clinical Problem

The role for anterior reconstruction and fusion of intervertebral levels in the spinal column has been expanded with the advent of better understanding of anterior spinal column biomechanics (White and Panjabi, 1990; Panjabi et al, 1989; Panjabi et al, 1994), laproscopic and mini-approach surgery, improved segmental anterior and posterior instrumentation systems, and the more recent introduction of various intervertebral cage type implants. Historically, surgery for spinal deformity secondary to tuberculosis infection of the anterior spinal column has been a prelude to more contemporary technical procedures via an anterior approach that address degenerative conditions of the lumbosacral spine (Cloward, 1953). Interbody fusion can be achieved successfully with tricortical iliac crest graft, ring allograft, or an implantable cage that is either of a screw-in type, cylindrical or cube/trapezoidal shape. A significant clinical and biomechanical problem for interbody fusion is that of cage or graft subsidence into the endplates of the adjacent vertebral bodies (Wetzel and LaRocca, 1990). This compromises the biomechanical performance of an anterior column reconstruction, and may result in significant clinical problems for the patient. Improved knowledge of vertebral endplate biomechanical properties (Grant et al, 2001) supports the concept that there may be a most ideal position on the vertebral endplates to position a cage or a pair of cages to avoid excessive subsidence secondary to endplate failure.

Despite debate over the role for spinal arthrodesis for degenerative spinal conditions, without deformity, the role of selective spinal arthrodesis for painful isthmic dysplastic spondylolisthesis in the young population has been well established. Similarly, the role of segmental spinal arthrodesis for degenerative instability and spondylolisthesis has been well established. Several studies have supported the effectiveness of posterior only *in situ* fusion of Meyerding Grades 1 and 2 (Meyerding, 1932) in children that have failed non-operative measures (Butterman, et al, 1998; Lenke, et al, 1992).

Molinari et al, 2002, have presented a study that compared the long-term clinical outcome of two groups of paediatric patients with high-grade spondylolisthesis with different surgical procedures for each group. The authors acknowledged that there remains considerable controversy regarding the treatment of higher grades (Meyerding Grades 3, 4, and 5) of isthmic spondylolisthesis (Edwards and Bradford, 1994). There exist several good long-term results of posterior *in situ* fusion for high grades of isthmic spondylolisthesis (Dick and Schnebel, 1988; Freebody et al, 1971; Freeman and Donati, 1989; Frennered et al, 1991; Harris and Weinstein, 1987; Johnson and Kirwin, 1983; Poussa et al, 1993). However, problems with increased slip progression and pseudarthrosis have also been reported in children with only posterior *in situ* fusion for high grades of spondylolisthesis (Edwards and Bradford, 1994; Seitsalo et al, 1990).

Importantly, neurological complications have also been reported for *in situ* fusion of high grade isthmic spondylolisthesis (Maurice and Morley, 1989; Schoenecker et al, 1990). Reduction of high grades of isthmic spondylolisthesis has been reported to have a high rate of complication (Boos et al, 1993; Boxall et al, 1981; Gaines and Nichols, 1985; Poussa et al, 1993; Tiusanen et al, 1996).

Molinari et al, 2002, aimed to evaluate the clinical and radiographic outcomes between patients treated for high-grade spondylolisthesis with posterior only procedures and posterior procedures combined with anterior column support. With 31 patients, with an average age of 13.5 years (9-20years) and 37 surgical procedures, they performed the study by dividing the patients, all with Meyerding Grade 3 or 4 isthmic spondylolisthesis, into two surgical arms. Group 1 (18 patients) were divided into Group 1A- (11 patients) posterior *in situ* fusion L4-sacrum fusion without decompression or instrumentation; Group 1B- (7 patients) posterior decompression with posterior instrumentation and posterior fusion (6 of the seven also had reduction). Group 2 (19 patients) were those who had posterior decompression and reduction with posterior instrumentation and circumferential fusion including anterior structural grafting (16 of 19 patients had anterior structural grafting through a separate anterior approach and 3 had posterior lumbar interbody fusions in place of the separate anterior approach. The patients were not randomized in the study and the tendency was for the patients with the highest degree of slippage to be treated with reduction and internal stabilization.

Results of the Molinari et al, (2002) study, based on an average radiographic follow-up of 3.1 years (2-10 years 1 month), include the incidence of pseudarthrosis as 39% (7 of 18) in Group 1, and 0% (0 of 19) in Group 2. All seven patients who had pseudarthroses achieved solid fusion with a second procedure involving circumferential fusion with anterior column structural grafting. Other quality of life outcomes such as pain, function, and satisfaction were best in those patients who achieved solid fusion regardless of surgical procedure.

Favourable clinical results such as that mentioned above with the successful reconstruction and arthrodesis of the anterior spinal column for deformity, such as spondylolisthesis, encourage the need to continue refinement of surgical techniques to achieve optimal clinical outcomes. Biomechanical studies aim to refine the techniques available, including the positioning of cages, to achieve successful and safe anterior column reconstruction and arthrodesis.

The *purpose* of this biomechanical study therefore was to address the question of where is the best position to place an interbody fusion cage or graft for greatest anterior column structural support in the lumbosacral spine, and to minimize cage subsidence into the endplates. The well-described surgical techniques of transforaminal and posterior lumbar interbody fusion (TLIF/PLIF) require the reconstruction and solid arthrodesis of the anterior spinal column,

using a posterior surgical approach. Despite the well-reported use of the techniques for deformity and degenerative conditions, and the multitude of available cage designs and shapes, little has been reported on what is the best position, with respect to the vertebral endplates, to place an interbody fusion cage to minimize cage subsidence. In this human cadaver experiment, careful attention was made to simulate a posterior interbody fusion construct, with pedicle screw instrumentation, followed by placing titanium mesh cages in one of three positions between the vertebral endplates. Failure loads in compression, endplate strength, and direction of cage subsidence were assessed in the experiment, with attention paid to the relationship of vertebral bone mineral density.

1.2 Background Literature

1.2.1 Anatomy of Vertebral Bone

1. Lumbar Vertebrae

The lumbar vertebrae have an excellent design for bearing load through their anterior and posterior portions. The anterior vertebral body has a drum shaped, light weight, blood filled, therefore dynamic, load bearing shape. The vertebral body has a shell of cortical bone and an inner cancellous bone portion. The complex vertical and horizontal trabeculae of this cancellous bone allows transfer of loads in many directions. The in-vivo state of blood filled trabecular bone allows better dynamic force distribution by the means of a hydraulic state.

Vertebral bodies also contain bone marrow cells for maintenance of the haematopoietic system.

The trabeculae found in the cancellous bone of the vertebral body can be seen to sweep into the pedicles that lie posteriorly, permitting a solid connection between the anterior and posterior spinal columns. It appears that this area of confluence between the vertebral body and the pedicle has an underlying trabecular architecture that forms a strong area of the vertebral endplate in the posterolateral corners of the vertebral endplates (Amstutz and Sissons, 1969).

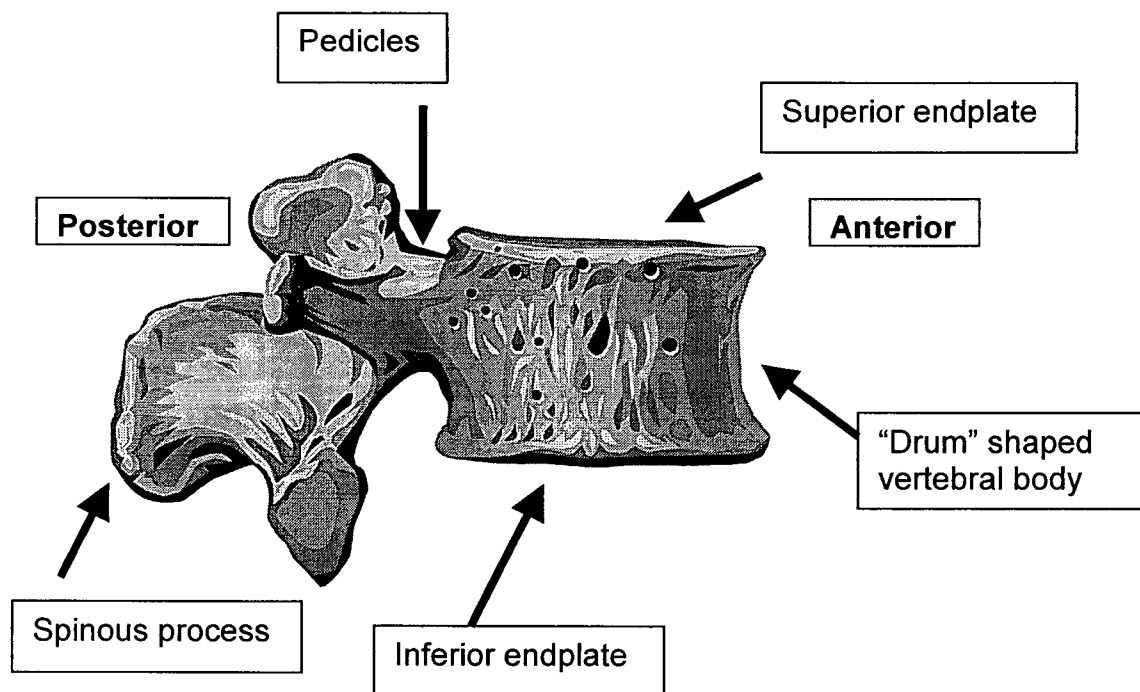


Figure 1.1 Lateral view- typical appearance and basic anatomy of a human lumbar vertebra.

Because vertebral cancellous bone is filled with blood and marrow products, it is sometimes referred to as *vertebral spongiosa*. Schmorl and Junghanns (1959) described the vertebral spongiosa as “consisting of thin bone plates intersecting each other and perforated by numerous openings varying roughly circular to quadrangular in shape”. The same authors also described a variation in the direction of the plates in different parts of the spine that may be attributed to variations in differences in functional stresses.

Amstutz and Sisson (1969) outlined a study that highlighted these functional differences in trabecular bone architecture and bony condensations. In their study, they took the third lumbar vertebra autopsy specimen of a twenty-year-old woman, and decalcified the vertebra and then sectioned it into thin slices on a band saw. Multiple outline drawings and models of the trabeculae allowed them to conclude that the bone near the superior and inferior surfaces of the vertebral body are denser than the intervening central region. They also note the condensations of the trabecular bone nearer the endplates and near the pedicle-vertebral body junction.

It is well reported, and clinically understood, that trabecular bone density can vary greatly between individuals and even between spinal levels in the same individual. Factors such as disease states, trauma, and environmental factors can alter vertebral bone architecture and bone density. Flynn and Cody (1993) report a study on the assessment of vertebral bone macroarchitecture with fine

detail three-dimensional computerized tomography (CT) scanning. Requiring larger doses of radiation than conventional QCT (quantitative computerized tomography), the technique described by Flynn and Cody (1993) revealed vertebral bone properties that highlight the higher density of cancellous bone in the inferior, posterior, and lateral regions of a vertebral body. The authors also concluded that regions with a higher density at the age of 40 have a larger decline with age. They also conclude that the vertebral body cortex thickness declines with age at a slower rate than observed for cancellous bone; however, the decline with age of cortical bone appears to vary substantially amongst subjects.

Other regional variation studies of the trabecular bone of lumbar vertebra include that of Keller et al (1989). The study assessed the compressive mechanical properties of human lumbar vertebral trabeculae on the basis of anatomic origin, bone density, and intervertebral disc degenerative states. The study concluded that the trabecular bone compressive strength and stiffness increased with increasing bone density, as assessed by dual-photon absorptiometry (DPA). After cubing 12 lumbar vertebrae and compressing these sections, regional variations within each segment were found, the most prevalent differences occurring in regions of bone overlying the disc nucleus in comparison with the bone overlying the disc anulus. Using a degenerative disc grading system by Nachemson (1960), they concluded that as disc degeneration became more severe, the difference in bony compressive strength, in the regions beneath the

disc, became less. Normally, they suggested that a region of vertebral bone overlying disc nucleus had a higher compressive strength. They also concluded that there was no recordable difference in compressive properties between superior and inferior ends of the vertebra of the same specimen. This study appears to not be in keeping with the findings of Roberts et al (1997), who demonstrated a difference in the measured thickness of the vertebral subchondral endplate bone. Using a grading system for degenerative disc assessment (Roberts et al, 1989), they noticed a radiologically measured regional variation in thickness of the subchondral bone, being greater adjacent to the annulus than the nucleus, and the endplates cranial to the disc were thicker than those caudal. This reported anatomical finding correlates well with the biomechanical findings by Grant et al, (2001), that the inferior lumbar endplates are stronger than the superior endplates, and have a similar strength to the sacral endplate of L5-S1 articulation.

These findings are consistent with work from Keller et al, (1992), who assessed an autopsy specimen L1 and L2 vertebrae of a 60 year woman with CT scanning through 4 mm sections. Findings included that the superior and inferior sections of the vertebral body were made up of an open-celled network of trabeculae, while the translational and middle sections consisted primarily of plate-like trabeculae forming a closed-cell structure. The most dense and most oriented bone was found in the superior and inferior sections of the posterolateral body,

whereas least dense and least oriented bone was found in the ventral third of the anterior body.

The importance of these background studies was recognized in the hypothesis generation of this study. Regional variations in structure and strength of vertebral bodies, based upon regional anatomical variations, may be a significant factor in the choice of where to position a cage or graft on vertebral endplates in the lumbosacral spine.

2. Sacrum

Internal bony architecture of the sacrum has been less described than that of the lumbar spine. The sacrum has a large vertebral body at the S1 level that has an equivalent surface area of endplate as the overlying inferior endplate of L5. An obvious feature of the sacrum is the large lateral masses that make up the alar of the sacrum and allow a large surface area of attachment to the more lateral pelvis, via the sacroiliac joints. The trabecular pattern of the cancellous bone of the sacrum is similar to that of the lumbar spine, in that it follows lines of tensile and compressive forces that permit a structure that can withstand forces of the full body weight or more. This complex trabecular bone pattern is also seen at the lateral attachment of the sacrum to the pelvis, and is reflective of the complex force directions that must be directed through this articulation.

1.2.2 Anatomy and Development of Vertebral Endplates

Endplates of the human vertebrae are best seen as being composed of both a cartilaginous component that is intimately related to the intervertebral disc, and an osseous component that is a condensation of the subchondral bone that overlies the cancellous bone of the vertebral body. The osseous component is approximately 0.25 mm thick (Tencer et al, 1995), and is a thin layer of bone that resembles a cortical bone layer, but is better understood as a condensation of the underlying trabecular bone. The cartilaginous component of the endplate is between 0.6-1.0 mm thick (Eyring, 1969; Roberts, 1989; Saunders, 1940) and in the vertebral body of a child, appears to have a distinct cleavage plane between it and the osseous component of the endplate. In adulthood, this cleavage plane becomes less defined and the cartilaginous layer appears more adherent to the osseous endplate.

Developmentally, the lumbar vertebrae are not completely ossified at birth, and the vertebral body continues to ossify and grows longitudinally at an equal rate at the upper and lower growth plates (Gooding and Neuhauser, 1965).

Longitudinal growth of the vertebral bodies continues throughout adolescence and slows after age 18, and usually is completed by the age of 25 (Taylor, 1975). The growth plates become thinner as longitudinal growth ends, and the vertebral surface is sealed off from the vertebral body by both a calcified layer of cartilage

and the development of the subchondral bone plate at the end of the vertebral body. The hyaline and fibrocartilage remaining on the surfaces of the body then become the vertebral cartilaginous endplate of the intervertebral disc complex.

Around the edges of the cartilaginous growth plates, a ring of calcification appears and is seen at the ages of 6-8 years in girls, and 7-9 years in boys (Schmorl and Junghanns, 1971). This area of development, called the ring apophysis, does not contribute to growth of the vertebra, but its fusion to the rest of the vertebral body does signal the end of longitudinal growth between the ages of 16- 21years (Calvo, 1957; Walmsley, 1953). The ring is better developed anteriorly and laterally, and as it develops, and ossifies the margins of the cartilaginous growth plate, it incorporates those fibers of the annulus fibrosus that are inserted into the perimeter of the plate. This also explains the "heaped-up" edge that surrounds the peripheral margin of the bony endplate of vertebra in adults.

An understanding of the developmental changes that occur with the growing vertebral body helps in understanding the anatomy that is found in the adult vertebral endplate. Anatomical features, macroscopically and microscopically, are best understood when considering the biomechanical properties of the vertebral endplates, as applied to the seating and positioning of any spinal interbody implant or graft that may be used to support and arthrodese the anterior spinal column.

1.2.3 Mapping the Structural Properties of the Lumbosacral Endplates

Grant et al, (2001) presented a study that addresses the variation in the strength that occurs across the surface of a lumbosacral endplate. This study stands as unique in the way that it specifically aimed to determine whether there are regional differences in endplate strength, and whether any differences identified are affected by spinal level (lumbar versus sacrum) or endplate (superior versus inferior). Keller et al, (1989) assessed the regional variations in compressive properties of the vertebral body trabecular bone in sections that did not allow for the possibility of the subchondral bone condensation of the endplate having a significant contribution to compressive strength, or a variation across levels, or between superior versus inferior endplates.

After performing indentation tests on 27 standardized test sites in 62 bony endplates of intact human vertebrae (L3-S1) using a 3 mm diameter, hemispherical indenter, the failure load and stiffness at each test site was determined using load-displacement curves. Similar regional strength variation studies on subchondral bone have included such bones as the tibia (Behrens et al, 1974), the patella (Weaver et al, 1966), the femur (Nakabayashi et al, 1994), and the glenoid (Anglin et al, 1999). In a well-reported paper, Perey, 1957, studied the endplate strength by using a 1cm² flat indenter. Strength of the

subchondral bone decreased with age, with no difference in the strength between the central, lateral, and anterior regions of the endplate, were some of his conclusions.

After performing the indentation tests, Grant et al (2001), concluded that both the failure load and stiffness varied significantly across the endplate surfaces ($p < 0.0001$), with the posterolateral corners of the endplate being stronger and stiffer than the central regions. The sacral and inferior lumbar endplates were both found to be stronger than the superior lumbar endplates (sacrum $p = 0.054$); (inferior $p = 0.008$) but themselves were not significantly different. The authors also concluded that the center of the bone, where implants are often placed, is the weakest part of the lumbar endplates and is not the strongest region of the sacral endplate.

The study presented by Grant et al, (2001), remains unique in its focus on presenting a regional strength map of the lumbosacral endplates. The size of the 3 mm diameter indenter used, does certainly present as a surface area of contact that is much less than the usual graft/cage implant that may rest upon the endplate. However, the results undoubtedly draw attention to the measured difference that does exist in the biomechanical compressive strength of the lumbosacral endplates, and does serve as a significant basis to the formulation of the methods in the experiment that will be presented in this thesis publication.

1.2.4 Biomechanical Analysis of Interbody Fusion Constructs

Oxland and Lund, (2000), have presented a comprehensive *literature review* of biomechanical properties anterior stand alone cages and cages in combination with posterior fixation for the facilitation of lumbosacral spine interbody fusion. Their objective was to review all literature published regarding the biomechanical properties of interbody cages, with specific focus on their three-dimensional stabilization patterns, and the compressive strength of the bone-implant construct. They also describe the effectiveness of supplementary posterior pedicle screw instrumentation for both stabilization and strength of the interbody fusion constructs.

The study by Oxland and Lund, (2000), logically divides their literature review of basic mechanics of interbody fusion cage fixation in the lumbar spine based on two important aspects of cage performance:

1. Three-dimensional stabilization;
2. Compressive strength of the cage vertebra interface.

The following literature review will use the same two part division as described by Oxland and Lund (2000) and will contain many of the essential references that are cited in their review, as well as similar category subheadings under the

1. Three-dimensional stabilization; and 2. Compressive strength of the cage vertebra interface divisions.

1. Three-dimensional stabilization

Different cage designs

There exists now an array of interbody cages available for the use of anterior spinal column support from either a posterior or anterior direction of insertion. Well-described studies are found from design pioneers of such as Bagby, (1988), Brantigan et al, (1991), Ray, (1993), Kuslich et al, (1993), and Brantigan, (1993).

Comparative studies on cage design have shown no significant differences in either anteriorly or posteriorly inserted cages. Lund et al, (1998), describes a study in which 18 FSU's (9 L2/3, 9 L4/5) were DEXA scanned for BMD values, then tested for flexibility in the intact state, and then with one of three cage – either a porous coated titanium cage designed to fit the endplate contours (Stratec; STRATEC Medical AG, Oberdorf, Switzerland); a rectangular carbon-fibre cage (Brantigan; Acromed Corporation, Cleveland, Ohio); or a cylindrical threaded titanium cage (Ray TFC; Surgical Dynamics Inc., Concord, California). All cages were filled with graft and inserted from a posterior direction. Four test conditions - the intact disc, one of the three cages without instrumentation, one of

the three cages with posterior instrumentation, and then finally with the addition of a cross link to the posterior instrumentation, were described. The authors found no significant difference in the stabilizing potential of the three cage designs. The cages used alone significantly decreased the intervertebral movement in flexion and lateral bending, but no stabilization was achieved in either extension or axial rotation. It was stated that for all types of cage, the greatest stabilization in flexion and extension and lateral bending was achieved by the addition of posterior transpedicular instrumentation. The addition of cross-connectors to the instrumentation had an effect on axial rotation. The bone density of the adjacent vertebral bodies was a significant factor for stabilization in flexion and extension and in lateral bending. The study clearly defines the minimal effect that cage design and shape had on the stabilizing potential of interbody fusion constructs.

Anterior approach

Anterior stand-alone type cage applications have been studied in several human cadaver experiments including studies by Glazer et al, (1997), Nibu et al, Rathonyi et al, (1998). Oxland and Lund (2000) summarized these studies well and conclude that in flexion, the intervertebral motion is always less with the cage, on average being about 60% of the intact motion. In extension, the motion with the cage was approximately the same as the intact motion. In axial rotation, the cages generally stabilized the spine such that the cage motion is about 60%

of the intact motion. In lateral bending, the cages reduced motion to about 50% that of the intact spine.

Posterior approach

As previously described Lund et al, (1998) reported an experiment on human cadaver lumbar spine that uses three different cage types, all inserted from a posterior direction, which examined the effect of posterior pedicle screw fixation on stability of the cage construct. Other studies that look at such effect included that by Hoshijima et al (1997) and Tencer et al, (1995). Oxland and Lund (2000) concluded that in flexion, the intervertebral motion was always less with a cage, on average being about 60% of the intact motion. In extension, the motion with the cage was about the same as the intact motion. This suggested that as with anterior inserted cage constructs, posterior inserted cages did not stabilize the spine well in extension. In axial rotation, the motion of after cage insertion was always more than in the intact spine by around 25%.

Effect of supplementary posterior fixation

It is well accepted that the addition of posterior instrumentation stabilizes an interbody cage construct. Lund et al, (1998) examined the three cage type constructs with and without posterior pedicle screw fixation. Other studies that also examined this effect of posterior instrumentation, whether it be in the form of

pedicle screws, translaminar screw fixation, or transfacet screw fixation, included those of Glazer et al, (1997) and Rathonyi et al,(1998). Brodke et al, (1997) reported the results of an animal study that supports the addition of posterior instrumentation to an interbody construct to increase stability and stiffness. The authors performed an *in vitro* study on eight calf spines and tested a threaded cage, with and without posterior instrumentation, and is one of several animal studies that have been published, that have not always supported the finding of supplemental posterior instrumentation increasing cage construct stability.

Distraction-compression forces adding to intervertebral stabilization

Bagby (1988) described the theory of distraction-compression forces as they apply to intervertebral stabilization. He suggested that intervertebral stabilization is enhanced by distraction of the annulus fibrosis. This idea of distraction of the disc space with interbody cages has been supported by a number of studies including Blecher et al, (1999), Chen et al, (1995), Nibu et al, (1998), Sandhu et al, (1996). It is thought that within the early post-operative period (first 6 weeks) that there is loss of distraction, and this results in decreased stabilization, particularly in flexion-extension and lateral bending (Hoffer et al, 1998).

Bone mineral density

Oxland et al, (1996) demonstrated that for various cage types, increased bone mineral density enhances stabilization in flexion-extension and lateral bending, but not axial rotation.

2. Cage-vertebra interface strength

Effect of bone mineral density

Oxland et al, (1996), outlined a study that specifically looked at the bone mineral density (BMD) of 72 functional spinal units (FSU) using dual energy x-ray absorptiometry (DEXA), and assessed the interrelationship between BMD values and intervertebral disc degeneration, their effect on normal spine motion, and their significance in the biomechanical performance of interbody fixation techniques. Three-dimensional flexibility tests were performed on the 24 FSU's in the intact and posteriorly inserted interbody implant stabilized states. Four different implants were used, and a pre-load of 200N was applied throughout all flexibility testing to simulate *in vivo* compression. Both multidirectional flexibility testing without posterior instrumentation, and axial compression testing with and without posterior instrumentation were performed. The investigators used a macroscopic disc degeneration grading system that was described by Vernon-

Roberts and Pirie (1973), and is similar to a previous grading system as described by Nachemson (1960). The authors concluded that vertebral bone density is a highly important variable in the performance of interbody implants in axial compression and stabilization. It was found that there was a statistically significant non-linear relationship between BMD and disc degeneration. Specifically, the BMD for the moderately degenerated discs, Grade 3, had lower densities than all other grades, including the most severely degenerated discs, Grade 4. It was suggested that the presence of peripheral syndesmophytes around the disc edge, in severely (Grade 4) degenerated discs, could artificially increase the BMD for that vertebral body. The observation of the artificial estimation of BMD by DEXA scanning method, for degenerated discs, has also been reported by Reid et al, (1991). The results of Oxland et al (1996) concluded that the effect of bone density on the implant stabilization most likely resulted from local damage to the vertebral bone in compression adjacent to the implant. It was also suggested that the performance of interbody fixation techniques, whether bone graft or implant, is affected strongly by the density of the host vertebral body. Lower bone densities are correlated strongly to decreased failure loads and less-stable constructs.

Other studies have supported the use of DEXA scanning in the measurement of bone mineral density of vertebral bodies. Keller et al, (1989) defined the use of DEXA in assessing the regional properties in the compressive properties of lumbar vertebral trabeculae, as was discussed in Section 1.3.1. Other work that

has defined the role of DEXA for the assessment of vertebral body bone mineral density includes the work of Rizzoli et al, (1995), where it was proposed that the technique allows an accurate assessment, diagnosis and follow-up of osteoporosis.

Goh et al, (2001) reported a study involving 27 lumbar vertebra from 17 cadavers of Chinese origin. DEXA scanning was performed on the specimens in antero-posterior, lateral, and axial planes. They suggested the potential problem of overestimation of BMD using a lateral DEXA scan of a vertebra with large amounts of syndesmophyte and osteophyte formation secondary to disc degeneration. The extra peripheral bone formations - syndesmophytes and osteophytes, need to be recognized and subtracted in a BMD calculation. A study by Ito et al (1993), using quantitative computerized tomography (QCT) scanning on 203 men found there to be no significant difference in the BMD of trabecular bone in the central region of the vertebral body with large osteophytes and those without. Goh et al, (2001) concluded that it is not necessary to include areas with osteophyte formation in the analysis of DEXA BMD data, when taken from a lateral direction, if the osteophytes are excluded from the region of interest during analysis. They also concluded that axial scanning of the vertebral body provides the best indication of BMD, although this is not possible or practical *in vivo*. Lateral direction DEXA scans were linearly correlated to axial direction DEXA scans in the same study, and the authors concluded that despite axial scan directions being superior for BMD assessment, the lateral direction BMD

scan could be used to accurately determine the condition of bone in the region of interest of the vertebral body.

Tan et al (2000) reports a study that confirms the linear correlation between axial and lateral BMD values of the lumbar spine using DEXA scan ($r=0.87$). The authors detail a study that tested 26 cadaveric lumbar vertebrae, scanned with DEXA, and then used to assess compressive failure loads, stiffness values, and compression failure energy values of the vertebrae after compressing 12mm diameter mesh cages into the endplates, with and without endplate decortication. They concluded that endplate removal did not significantly result in lower failure loads, and they concluded that the strength of a lumbar spine vertebra in supporting loads transmitted through a titanium mesh cage is linearly correlated to the BMD of the vertebra. This unpublished study is in conflict with a recent study by Oxland et al, (2002), that concluded that removal of the lumbar vertebral endplate does significantly reduce the local strength and stiffness magnitudes in the lower lumbar vertebral bodies. More specifically, Oxland et al, (2002) found that removal of the endplate caused greater strength loss posteriorly and laterally on the vertebral surface. The study involved high- speed burr decortication of half of the endplate of the specimens selected, with load-displacement values collected based upon indenting the intact and decorticated endplate surface with a 3 mm diameter indenter to a depth of 3 mm.

Jost et al, (1998), reported a study that compared the compressive strength of three different interbody cages in the lumbar spine using 36 FSU's, and the effect of the cage shapes, effect of posterior instrumentation, and bone density. The bone density, determined by DEXA, was clearly related to compressive strength of the bone-cage interface. Interestingly, the authors DEXA scanned the vertebrae in both posterior-anterior and lateral directions, and statistically analyzed the relationship between failure load and each of the four bone densities for the FSU being tested. The lateral DEXA scan values (upper vertebra $r^2=0.61$; lower vertebra $r^2=0.60$) revealed a higher correlation than the postero-anterior values (upper vertebra $r^2=0.38$; lower vertebra $r^2=0.15$). The authors decided to use the upper lateral DEXA as the covariate in the statistical analysis.

Effect of endplate preparation and graft to endplate surface area ratio

Both the way one should prepare a vertebral endplate- that is, decorticate the osseous endplate surface or not, and the size/surface area of graft/cage required for adequate structural support of the interbody construct, has been considered in the literature for some time. Stauffer and Coventry, (1972), and Gill, (1989), have outlined the importance of both endplate preparation and the size of the graft that should be placed for a successful interbody fusion, though based largely on clinical observation. Cloward, (1953), popularized the surgical technique of lumbar interbody fusion for the treatment of back pain. From his

initial work, which involved anterior approach surgery for such a fusion, he recommended large surface area grafts using struts of tricortical iliac crest. Lin, (1985), and Lee et al, (1995), have been advocates of a Cloward style interbody fusion using large total surface area grafts of packed tricortical iliac crest struts, though performing the fusion through a posterior approach, both with, and without posterior instrumentation.

To answer the question of what is the minimum surface area of graft, albeit bony type structural grafts, or cage type implants, required to be seated upon the endplates for a successful interbody fusion, studies like that of Closkey et al, (1993), have been well received. The study involved the assessment of 35 *thoracic* vertebrae, and had the specimens QCT scanned for bone mineral density, and involved the decortication of part of the thoracic endplate. The amount of decortication was 4.0 cm², which was to match the largest size indenter graft that they tested. The study involved loading the vertebral endplates in compression using one of three sized polymethylmethacrylate blocks- either 4.0cm², 2.4cm², 1.1cm² which was based upon a 55%, 33%, 15% amount of endplate coverage, based upon the calculated average endplate surface area of a T5 vertebral endplate (7.3cm²). They reported that endplate decortication and placement of a graft block between 30% and 40% of total surface area was required to provide adequate graft surface area to carry minimal thoracic physiological loads (400-600N) without trabecular subsidence. They stated that eighty percent of the vertebral bodies with graft area covering

25% of the total area or less failed at loads less than 600N, while 88% of the vertebral bodies with graft covering 30% or more were able to carry a load greater than 600N.

The authors also showed a moderate correlation between BMD and trabecular bone strength ($r^2=0.63$). Importantly, they concluded that their results show that for *thoracic* vertebrae, the *minimum* necessary graft area to prevent subsidence under moderate physiological loads was between 30% and 40%. This is in contrast to literature (Gill et al, 1989) that between 50%-80% of the vertebral body be decorticated and covered by graft.

Steffen et al, (2000), presented the results of a study that assessed the axial compressive strength of an implant with peripheral endplate contact as opposed to full surface contact. The same study assessed whether removal of the central bony endplate affects the axial compressive strength of that implant/bone interface. The authors used 44 vertebrae and four experimental groups, by combining two interbody implants (full-surface versus peripheral surface support) with two endplate preparation techniques (intact bony endplate versus removal of the central bony endplate). They concluded that an implant with only peripheral support resting on the apophyseal ring offers axial mechanical strength similar to that of an implant with full support. They state that neither supplementary struts nor a solid implant face has any additional mechanical advantage, but reduces graft-host contact area. Removal of the bony endplate was recommended by the

authors, because it did not affect the compressive strength of the construct and promoted graft incorporation.

Another, more clinically flavored study, that looked at the effect of endplate preparation for graft was that reported by McAfee et al, (2002). The authors reported a study that prospectively compared the clinical and radiographic outcomes of two groups of patients that underwent lumbar interbody arthrodesis. The first group of 50 patients had a reamed channel discectomy performed through a minilaparotomy (20) or laproscopic anterior approach (30), with the insertion of two interbody cages (BAK, Sulzer-Spine Tech, Minneapolis, MN). The second group of 50 patients underwent a more extensile, wider approach retroperitoneal exposure to the anterior spine, and had what was considered a complete discectomy and removal of the cartilaginous endplate. Similarly, two interbody cages (BAK, Sulzer-Spine Tech, Minneapolis, MN) were inserted. At two years follow-up, all patients in Group 2 who had a complete open operative disc removal achieved solid arthrodesis. There were no revision surgeries. However, in Group 1 there were seven patients who had a pseudarthrosis and an additional patient with early patient with postoperative cage displacement, that which resulted in eight patients in Group 1 requiring revision surgery. A retrospective review of the 100 patients revealed a 14% rate of pseudarthrosis in the group that had the reamed channel discectomies, and not a complete discectomy. The authors suggested that the advantages of complete discectomy are more surface area available for fusion, easier orientation to the midline, less

avascular disc material remaining (theoretically decreasing the infection rate), better reduction of any spondylolisthesis, and easier restoration of the disc space. This clinical study remains an important study because it addresses the features of stand-alone type anterior interbody fusion technique, without anterior or posterior instrumentation.

McAfee et al, (2002) described indications for surgery that appear identical to those described by Kulisch et al, (1998), Ray (1997¹), and Ray (1997²). Six criteria used by Ray (1997¹) are severe, disabling, intractable back pain; no previous interbody fusion at the target level; an absence of degeneration at adjacent neighboring disc spaces; and no greater than a Meyerding Grade 1 spondylolisthesis; the disabling back pain had to be present for more than 1 year, refractory to nonoperative care; and there had to be substantial loss of disc height and mobility. Patients who had a disc space height of greater than 12 mm were excluded.

Hollowell et al, (1996) presented a study of how various interbody grafts and implants would perform under direct axial load on either decorticated or intact endplates. Despite the study's title including "analysis of thoracolumbar interbody constructs", they only examined *thoracic* vertebrae. In total, 63 isolated human thoracic vertebrae were used to test seven different constructs in direct axial load onto prepared endplates using an electrohydraulic testing device. They only tested the *superior* endplates and pre-test DEXA scanned the

vertebrae for BMD values. The seven constructs included 1. Titanium mesh (17mm x 22mm) oval cages on an intact endplate; 2. C Shaped humerus rings on an intact endplate; 3. Tricortical iliac crest on intact endplates; 4. Tricortical iliac crest in a cancellous trough on the endplate; 5. Triple rib struts- with one rib in a cancellous trough and the outer two ribs on the intact endplate; 6. Single rib on intact endplate; 7. Single rib on cancellous bone.

Endplate removal in the Hollowell et al (1996) experiment involved complete removal of the endplate to a depth of 3-4 mm. All grafts were positioned centrally, except the iliac crest grafts which were positioned posterolaterally on the vertebral body. No grafts were positioned posteriorly. With significance, it is noted, from the photograph in their publication, that the titanium mesh cages used in the Hollowell et al, (1996) study were not short type, single level, interbody fusion cages, but rather long vertebral body replacement type cages, which appeared to have a titanium mesh end-cap placed on the end of the long oval cage, with no mention of any bone graft packed inside the cage.

Results of the Hollowell et al, (1996) study, I believe, importantly hang on the acceptance that the deformation occurring at failure represents an interaction between the graft and the vertebral body, and does not always represent only failure of the endplate. This is because no endplate is tested in some of the configurations tested. Considering this aspect, they found that the *titanium mesh cage* had a force to endplate failure that is *greater* than all other constructs tested

in their study ($p=0.028$). The centrally positioned, titanium mesh cage construct tested, with intact endplate, had a mean peak failure load of 1486N with standard error of the mean of 96N, adjusted for BMD. Other mean values for failure included that of the iliac crest on the intact endplate at 1150N (SEM=109), and the single rib on a cancellous endplate at mean peak failure of 236N (SEM=95).

Hollowell et al, (1996) divided the vertebral levels tested into high (T7 or higher), and low (T8 or lower) groups and assessed mean peak failure loads for all constructs and found no significant difference for level ($p=0.17$). BMD, did however, have an effect on mean force to failure ($p<0.001$).

The same study reported a mean percentage of endplate covered by graft/cage in the titanium mesh cage construct as 23.2% (SEM=2.1). This value can be compared to the highest mean percentage of vertebral area covered by graft, in the iliac crest on endplate group, with a value of 47% (SEM=5.1), which highlights the relative success of the titanium mesh cage group, with a 50% less (23.2%) mean surface area covered. The authors concluded, in their *thoracic* only vertebrae study, that the titanium mesh cage construct provided the greatest resistance to subsidence of all constructs tested. They also concluded that the superior thoracic endplate did not show an important contribution in resisting graft subsidence. They stated that certain constructs (e.g., titanium cage, humerus, triple rib) can resist a single uniaxial load in excess of 1000N despite cross-sectional areas of 23-27% of the vertebral body. With respect to the

findings of the possibly small overall contribution of the osseous endplate in the superior endplates of the thoracic spine, one should note morphological data (Hanson et al, 1994), which has found the thoracic endplate to be as thin as 0.12mm. It may be that the overall strength, in compression, of the endplate/subchondral cancellous bone region of the vertebral body, has only a relatively small contribution, to the overall strength, from the osseous portion of the endplate.

Effect of cage design

Both Jost et al, (1998) and Steffen et al, (1998) in their studies concluded, after testing several different cage designs, that there was no significant difference of the cage-vertebra interface strength versus cage design.

Effect of supplementary posterior fixation

Jost et al, (1998) concluded that the effect of supplementary posterior pedicle screw fixation was not to increase the compressive strength of the cage-vertebra interface. In an unpublished study by Wong et al, (2000), there was suggestion that the addition of posterior instrumentation did significantly add to the compressive strength of the cage-vertebra interface. The study aim was to assess the effects of endplate removal and the addition of posterior fixation on the subsidence of titanium mesh cages in the lumbar spine. Using 26 FSU's, the

study involved three- test situations- group 1 (endplate intact, without fixation); group 2 (endplate removed, without fixation); group 3 (endplate removed, with posterior pedicle screw fixation). BMD values were recorded using DEXA pre-test, and the results indicated that removal of the vertebral endplate lead to penetration of the cages into the vertebra, without posterior fixation present. The authors suggested that the penetration was significantly reduced by pedicle screw fixation. Interestingly, they also report that there did not exist a consistent significant relationship between BMD and cage subsidence.

1.3 Hypothesis and Questions Asked in this Study

There is an absence of any clinically flavoured biomechanical study that assesses the best position to place an interbody fusion graft. Therefore, a biomechanical study was planned to address the question of where is the best position to place an interbody fusion cage or graft for greatest anterior column structural support in the lumbosacral spine. Careful attention was made to simulate a posterior interbody fusion construct, with pedicle screw instrumentation, followed by positioning of titanium mesh cages in one of three positions between the vertebral endplates.

Specifically, the hypothesis was that two smaller, posterolaterally positioned interbody cages would provide higher construct stiffness and strength in compression. The basis of this hypothesis was from previous work that demonstrated that the posterolateral corners of the lumbosacral endplates were stronger than the anterior and central regions (Grant et al, 2001). The same work also showed that the sacral and inferior lumbar endplates were both stronger than the superior lumbar endplates, but themselves were not significantly different.

With less emphasis on particular cage design properties, this study specifically addresses the question of best cage position for successful interbody fusion.

The following questions have been asked, and answered in this study-

1. Is there a difference in interbody construct stiffness and peak failure loads in compression, using one larger centrally placed titanium mesh cage, two smaller centrally placed mesh cages, or two smaller posterolaterally positioned cages as detailed in the technique of transforaminal lumbar interbody fusion as described by Blume and Rojas, (1981), and popularized by Harms et al, (1997)?
2. Does the cage(s) subside preferentially into the superior or inferior endplate?
3. Does bone mineral density have an association with load to failure and direction of cage subsidence?

4. Is there a pattern to the anatomical mode of endplate failure for cages/grafts that subside into lumbosacral vertebra?

1.4 Clinical Applications and Long-Term Goals

The biomechanical information presented in this study will add to the existing knowledge of biomechanical information relating to anterior spinal column structural support and reconstruction for the purposes of interbody arthrodesis. The study will particularly address the biomechanical validity of posterior lumbar interbody fusion (PLIF) and transforaminal lumbar interbody fusion (TLIF) surgical techniques, with the often-preferred placement of two smaller posterolaterally-positioned titanium mesh cages.

The study results will also add to the current knowledge of the strength of the lumbosacral endplate complex, and may add to the biomechanical prediction and further testing of other cage designs, and perhaps lend support to the biomechanical basis of the optimal positioning, or seating, of endplate bearing implants, as is found in disc replacement devices.

1.5 Scope of Current Study

The biomechanical study presented in the following publication is an *in vitro* study that utilized human cadaver lumbar and sacral vertebrae. All specimens were harvested and then stored at -20 degrees C, and, although not blood filled as in the dynamic *in vivo* state, were the best representations of actual vertebral biomechanical properties *in vivo*.

Another limitation of the specimens and model, is that no biological healing properties could be assessed, and that the study was only limited to the lumbosacral spine.

The study also only assessed such biomechanical properties over a short period of time, and no allowance for fatigue of instrumentation, or other potential settling possibilities of the cages were allowed for.

2.0 Materials and Methods

2.1 Experimental Overview - Model Selection and Justification and Experimental Protocol

With the relative paucity of clinically applicable biomechanical studies that examine the question of what is the best position to place a cage or graft in the intervertebral space to reconstruct and arthrodesis the anterior spinal column, it was thought that a study, as to be presented, was necessary. With the recently reported regional variation in lumbosacral endplate strength study (Grant et al, 2001), it was proposed that a study to help confirm these results of a stronger osseous endplate in the posterolateral corners of lumbar vertebrae was needed. Published biomechanical validation of the positioning of two smaller posterolaterally positioned cages as used in PLIF and TLIF type surgeries (Harms et al, 1997) also seems absent.

Therefore, what would be an appropriate biomechanical model to assess the effect of cage position, in an interbody fusion construct, on the vertebral endplate strength?

To answer this question, one should consider five factors that are proposed as factors related to success of an interbody fusion cage/graft construct for

reconstruction and arthrodesis of the anterior spinal column. These include cage position, bone mineral density, posterior instrumentation, ratio of graft/cage to endplate surface area, and endplate preparation. These factors have been individually and collectively discussed in the preceding chapter. The options for such an “ideal” interbody fusion cage construct model include, anterior versus posterior cage insertion; with or without posterior instrumentation; variation in cage design; and, endplates either intact or removed.

Cunningham et al, (2002) outlined a biomechanical perspective as to the clinical use of interbody cages. In this study, the authors draw attention to the fact that spinal instrumentation has revolutionized the treatment of spinal deformities, and permits the more successful ability of reconstructing the anterior bony spinal column. The authors also concluded that there exists biomechanical and clinically based support that there should be load sharing between anterior and posterior spinal columns, and that the anterior spinal column remains key to the success of many spinal reconstructions and arthrodesis for deformity caused by various disease states. Comprehensively, Cunningham et al, (2002) outlined the fact that there should be an integration of multiple strategies that can improve both anterior and posterior construct stiffness in the treatment of spinal deformities. The authors suggested that interbody support, including cage insertion, probably is the best method to minimize longitudinal rod (Cunningham et al, 1999; Polly et al, 1998; Polly et al, 2000) and screw-bone interface strain (Spiegel et al, 2000).

These various studies mentioned above are to serve as a reminder of the need to keep biomechanical models as clinically relevant as possible to assist in the formulation of more successful, and clinically achievable surgical techniques.

Considering all that has been reviewed in this section, the answer for the question “what would be an appropriate biomechanical model to assess the effect of cage position, in an interbody fusion construct, on the vertebral endplate strength?” could be justified as follows-

Choice of cage design could be any of the available cages, though favourable results have been reported clinically with the use of the titanium mesh cage (Surgical Titanium Mesh®, DePuy Acromed, Raynham, MA) by several authors for the use in cervical, thoracic, and lumbosacral anterior spinal column reconstruction and fusion for many deformity based conditions (Lenke et al, 2002; Riew et al, 2002; Eck et al, 2002). The titanium mesh cages used in a sheep cervical spine cadaver model had favourable results biomechanically with the highest volume related stiffness in extension, and bending stiffness, with high flexion stiffness compared to all other implants used in the study (Kandziora et al, 2001). Hollowell et al, (1996), in their study that compared several graft/cage constructs under direct axial compression into the superior intact endplates of thoracic vertebrae, found that the titanium mesh cage had a force to endplate failure that is greater than all other constructs tested in their study. The other clinically relevant advantage of the smaller sized round titanium mesh cages is

the fact that they can be inserted posteriorly through monoportal, transforaminal, approaches to achieve anterior interbody fusion (Harms et al, 1997; Lowe and Tahernia, 2002). The advantage of this transforaminal posterior interbody fusion (TLIF) technique is the ability to insert two smaller round cages into the interbody space, through a unilateral posterior bony element exposure. The second cage is rolled “blindly” into the far, unexposed side of the interbody space. Specifically, this requires only one whole, or part of one, facet joint to be excised at the disc space level that is being arthrodesed. Assuming neural foramen decompression is not required on the other non-excised side, the TLIF technique, with the monoportal approach decreases the risk of a neural injury to the unexposed spinal nerve at that level, minimizing what has been reported as a significant clinical operative complication.

Review of the literature has suggested that an anterior approach and cage placement permits better immediate stability to a construct's biomechanical property. The anterior approach requires no facet joint destruction, and being left intact, therefore permits better stabilization in axial rotation and lateral bending (Oxland and Lund, 2000). Facet joints have been clearly demonstrated to play an important role in control of axial rotation (Abumi et al, 1990), and less so in lateral bending. The biomechanical role of facet joints in controlling forward flexion and axial compression has been less well described. One would assume that the facet joints contribute significantly to the load sharing of the posterior spinal column in pure axial compression, and in variable amounts in flexion. A

biomechanical model that retains one or both of the facet joints probably comes closer to simulating what is found *in vivo* in patients who have had a TLIF procedure performed.

Anterior approach technique for a biomechanical model would also allow a better ability to clear the cartilaginous disc and endplate, as well as permit the more accurate positioning and insertion of cages.

Endplate preparation in an “ideal” biomechanical model would be best with intact endplates. Studies reviewed in this thesis have concluded that there is no significant difference in strength of the cage-vertebra interface with either intact or removed endplates (Hollowell et al, 1996). However, the titanium mesh cages studied in the Hollowell et al, (1996) study were upon intact endplates, and more importantly, the study by Grant et al, (2001) assesses the strength of the osseous endplate in intact lumbosacral vertebrae. Therefore, it would be ideal to have the osseous component of vertebral endplates intact, so as to include the contribution that the osseous endplate has to the overall strength and resistance to subsidence of interbody cages in axial compression.

Addition of posterior instrumentation in such an “ideal” interbody cage fusion model to assess the best position to place an interbody cage would seem appropriate. The majority of studies suggest that the addition of posterior instrumentation does not alter compressive strength (Jost et al, 1998) of the

cage-vertebra interface. Assuming this negligible effect of posterior instrumentation, and the well-accepted enhancement of stability that it allows, it would be logical to include it in an axial compression test of an interbody cage construct. The instrumentation would decrease lateral side bending and axial rotation (Jost et al, 1998), and would also better simulate the clinically established surgical constructs found in both posterior interbody fusion (PLIF) constructs, and transforaminal lumbar interbody fusion surgeries *in vivo*.

Finally, an appropriate biomechanical model to assess the effect of cage position, in an interbody fusion construct, on vertebral endplate strength in compression, could therefore be one that contains the following features- a human cadaveric specimen model, with titanium mesh cages (Kandziora et al, 2001; Hollowell et al, 1996; Lenke et al, 2002; Riew et al, 2002; Eck et al, 2002) inserted from an anterior direction, allowing the facet joints to be kept intact for more stability (Oxland and Lund, 2000) and a complete disc clearance, and more accurate cage positioning. Also, with intact osseous endplates (Hollowell et al, 1996) to include the contribution of this structure, and allow further assessment of the osseous endplate based upon known previously studied strength maps (Grant et al, 2001). Also, with posterior pedicular instrumentation to stabilize the construct, without significantly affecting compressive strength of the construct (Jost et al, 1998). The features described above in this idealized model have been employed in the experiment detailed in the body of this thesis. A summary

of the experimental protocol is included as well as a schematic representation of the testing method (Figures 2.1 and 2.1).

Experimental Protocol

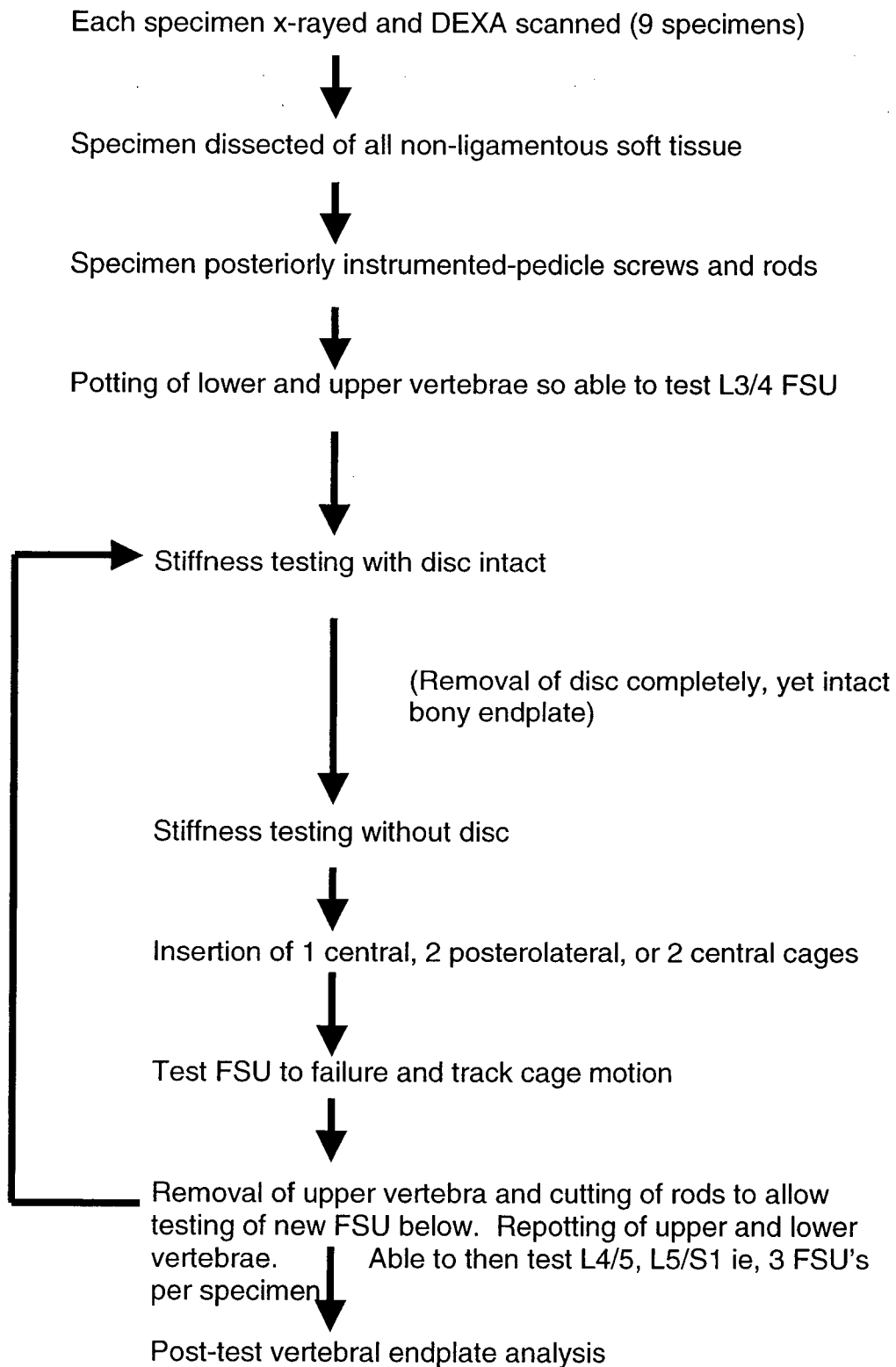


Figure 2.1 Experimental protocol for study

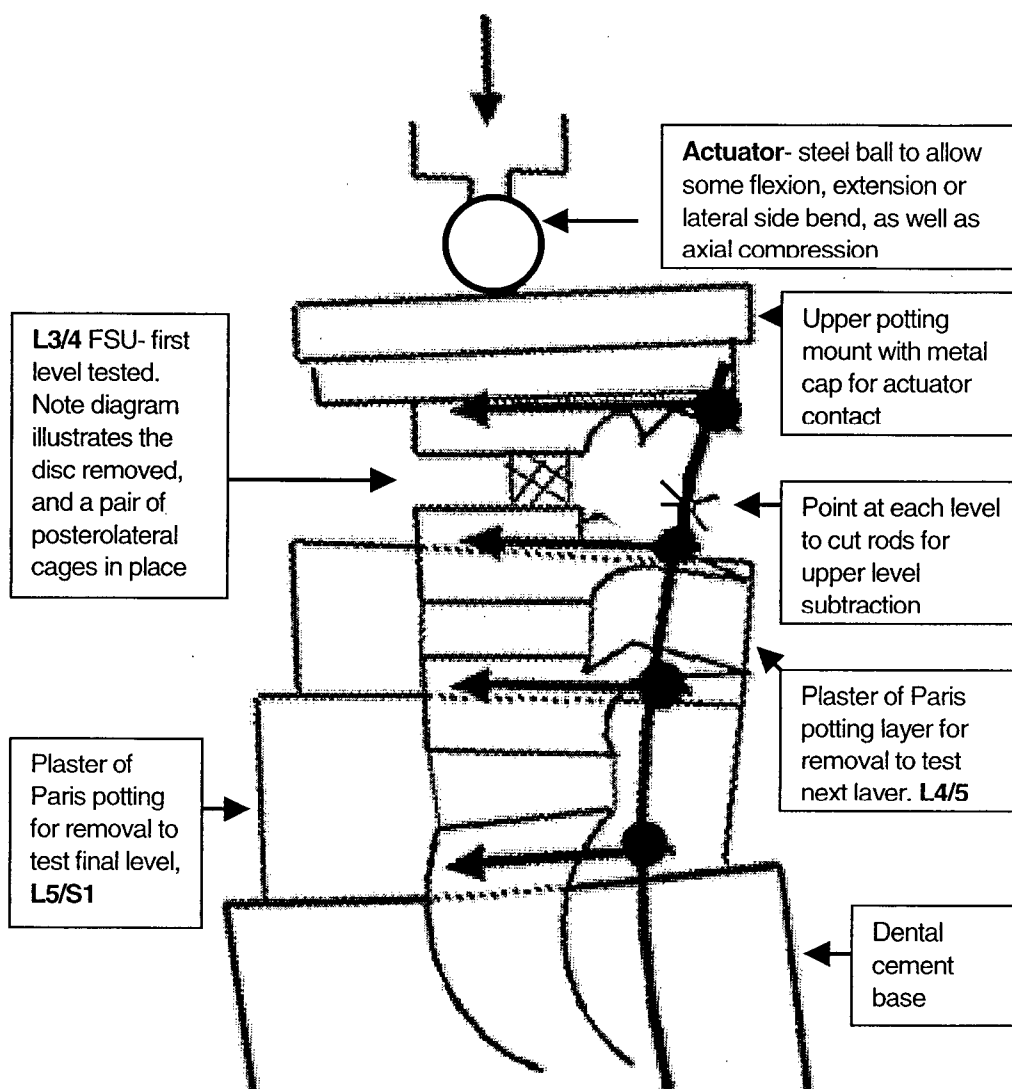


Figure 2.2 Schematic diagram of lateral view of test spinal column from L3-sacrum, with posterior pedicle screws and rods, plus sequentially potted layers for removal. Note the upper vertebra, and instrumentation are cut away after testing that FSU to allow the testing of the next FSU below. Breaking away the Plaster of Paris layer, and re-potting of the new upper vertebra of the next FSU is then required. This sequential subtraction of the upper FSU is repeated until the final FSU, L5/S1, is tested. Light emitting diodes (LED) markers are attached to the cage(s), and vertebra of that FSU tested to assess direction of cage motion using an optoelectronic camera system.

2.2 Human Cadaver Spine Selection

Selection of frozen cadaver spine was made from the frozen musculoskeletal tissue bank at the Division of Orthopaedic Engineering Research, University of British Columbia. A pre-existing database of available spinal columns was utilized, and selection was based upon the required level (L3-sacrum), and after standardized technique antero-posterior and lateral view plain radiographs-assessing for signs of disc degeneration and deformity. Specimens were rejected from the study based upon the presence of excessive (>50% of normal disc height loss at L3/4, 4/5, L5/S1) disc height loss, or deformity (spondylolisthesis or scoliosis). All specimens were visually inspected for excessive osteophyte formation any other signs of damage.

The bone quality (bone mineral density) of the specimen was later confirmed with dual energy x-ray absorptiometry (DEXA) scanning.

Selection of the appropriate specimens was made after the above radiographic screening criteria had been performed, and a total of nine (9) spinal columns from L3-Sacrum were chosen. Table 2.1 summarizes the cadaver spine specimens' physiological history. There included 4 male and 5 female specimens, with an age range from 72 –93 years, with a mean of 77.4 years.

Table 2.1 Physiological profile of cadaver spine columns included in study

Specimen No.	Level	Sex/ Race	Age at death	Smoker
1. 1061	L3-Sacrum	F/Caucas.	73	N
2. 1067	L3-Sacrum	F/Caucas.	88	N
3. 1009	L3-Sacrum	F/Caucas.	70	Y
4. 1027	L3-Sacrum	M/Caucas.	80	N
5. 1082	L3-Sacrum	F/Caucas.	75	Y
6. 1031	L3-Sacrum	M/Caucas.	72	N
7. 1090	L3-Sacrum	F/Caucas.	73	N
8. 1030	L3-Sacrum	M/Caucas.	73	N
9. 1036	L3-Sacrum	M/Caucas.	93	N

2.3 Dual Energy X-ray Absorptiometry (DEXA) Scanning Pre-Test

Lateral and antero-posterior DEXA scans were performed on all vertebrae of all nine (9) spinal column specimens. Vertebra L3, L4, L5 and S1 were scanned on each column, making a total of 36 vertebrae scanned. The scanner, [Hologic QDR4500, Hologic Inc., Bedford, MA] was operated by a single technician and an identical technique was used for all vertebrae. Bags of long-grained white rice with a total vertical height of 4 cm were placed beneath the spine segments to simulate a soft tissue envelope (Keller et al, 1992; Wenger et al, 1999). After

appropriate alignment and calibration, the spinal column from L3- Sacrum was scanned, and post-scanning outlining of the vertebral bodies was performed manually in consultation with the author.

For each vertebra, a record of area of vertebra scanned (cm^2), bone mineral content (BMC-g), bone mineral density (BMD-g/ cm^2), and T score was made.

A cross check comparison was made of the standardized antero-posterior and lateral radiographs taken of the spinal columns for relative indications of excessive radiographic osteopenia.

2.4 Dissection of Specimens

After radiographic and DEXA scanning the specimens, those included were prepared for instrumentation and potting for ultimate testing in the experiment.

The nine (9) spinal columns were cleared of all non-ligamentous soft tissue structures, leaving all posterior capsular and ligamentous structures, using a combination of sharp and blunt dissection in a semi-frozen state.

2.5 Instrumentation of Spinal Columns

After dissection, the spinal columns were instrumented posteriorly with a pair of 6mm poly-axial pedicle screws (Moss® Miami, DePuy Acromed, Raynham, MA) at every L3, L4, L5, S1, and only S2 where anatomy and fixation permitted. A

technique as described by Magerl,(1982) was employed to insert the pedicle screws. An entry point, that is of course variable to the individual anatomy of the specimen, was made in the lumbar spine at a point that has the line across the middle of the transverse processes, and the lateral edge of the zygoapophyseal joint. The sacral pedicle screw entered at a point at the infero-lateral portion of the articular process of S1. All screw tracks were checked for bony canal competence and depth with a pedicle probe and depth gauge. The poly-axial screw of appropriate length was selected and placed to permit motion of the poly axial head. The position of all screws, once placed, were checked with antero-posterior and lateral radiographs. No screw required repositioning or adjustment of more than half a turn of the screw, and all screws were assessed as being solidly fixed in bone.

A pair of 5mm stainless steel rods (Moss® Miami, DePuy Acromed, Raynham, MA) were cut to length and contoured to a normal amount of lumbar lordosis. The rod, on each side, was positioned into the open loading polyaxial screw heads, and after adjustment, secured with first an inner locking nut, and then an outer locking nut (Figure 2.3). After appropriate rod positioning, all inner and outer locking nuts were torque tensioned to a standard value, using a torque wrench.

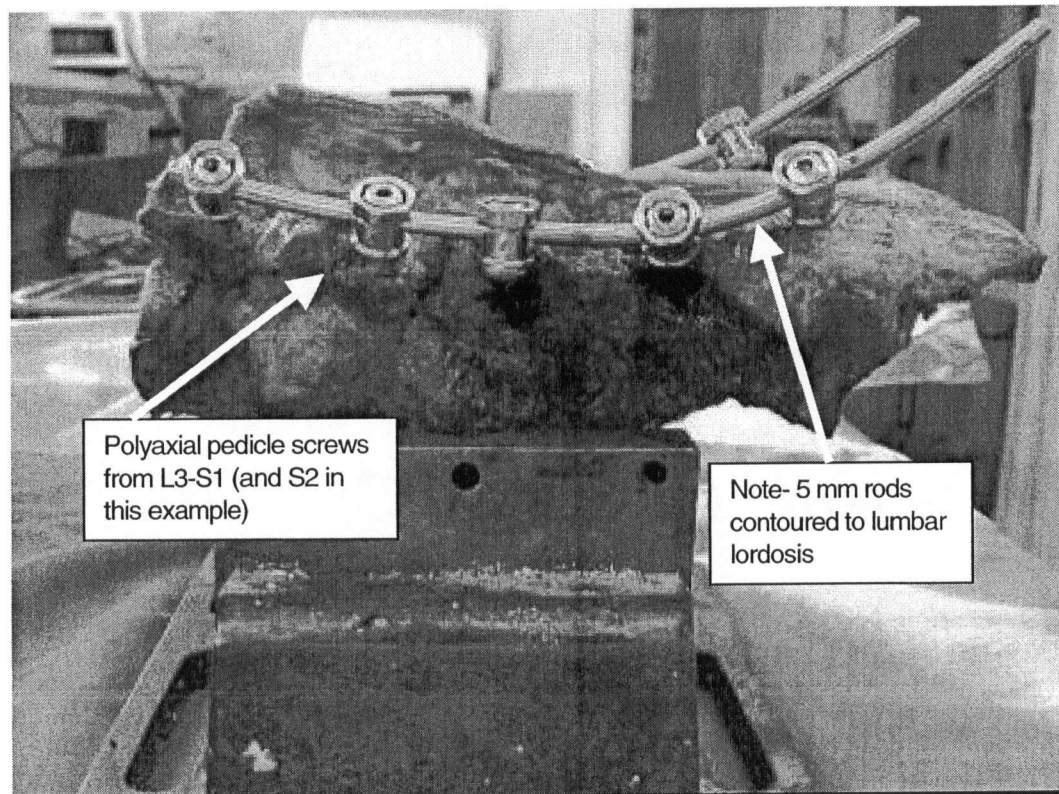


Figure 2.3 Typical appearance of instrumented, continuous spinal column from L3-Sacrum.

The distal (caudad) end of the rod was cut using rod cutters at a mid sacral level, being left longer than the S2 level, to act as an anchor for the embedding in the dental cement. No cross-links were applied to the posterior screw/rod construct, since each functional spinal unit (FSU) was to be tested separately.

The primary investigator, with an identical surgical technique, instrumented all specimens.

2.6 Potting of Specimens

2.6.1 Lower Spinal Column Potting

Each instrumented spinal column was evaluated and had a mid sagittal and mid vertebral body line, from a lateral side view, marked with an ink marker. Reference for this point was largely based upon visualization of the superior endplate of the L3 vertebral body. Accurate mid vertebral positions, based upon this superior most vertebra, permitted extensions of these lines down the spinal column, allowing for the normal lumbar lordosis. A series of 3 mm long sharp metal pins were placed in the vertebral bodies of each level, along these marked mid point lines, to facilitate accurate mid vertebral body positioning, at each FSU test level, of the actuator attached to the servo-hydraulic testing machine used for testing in compression.

The instrumented spinal column had each pedicle screw head covered with a ball of Play-Doh® to avoid cement infiltrating into the screw head complex- making it easier for removal and adjustment of the screws. A pair of aluminum halved box-like retaining molds were machined to enable the pouring of dental cement, and the potting of the sacral portion of each spinal column being tested. After each half of the aluminum mold was taped together, a mix of dental cement and water

was made and poured into the box mold, with necessary metal platform pieces to slightly raise the spinal column specimen, if needed, so that the top of the cement in the mould would become level with the mid portion of S1. The L5/S1 disc space was also made parallel with the top of the cement mould, to allow the metal base to be positioned horizontal for the final L5/S1 level (Figure 2.4).

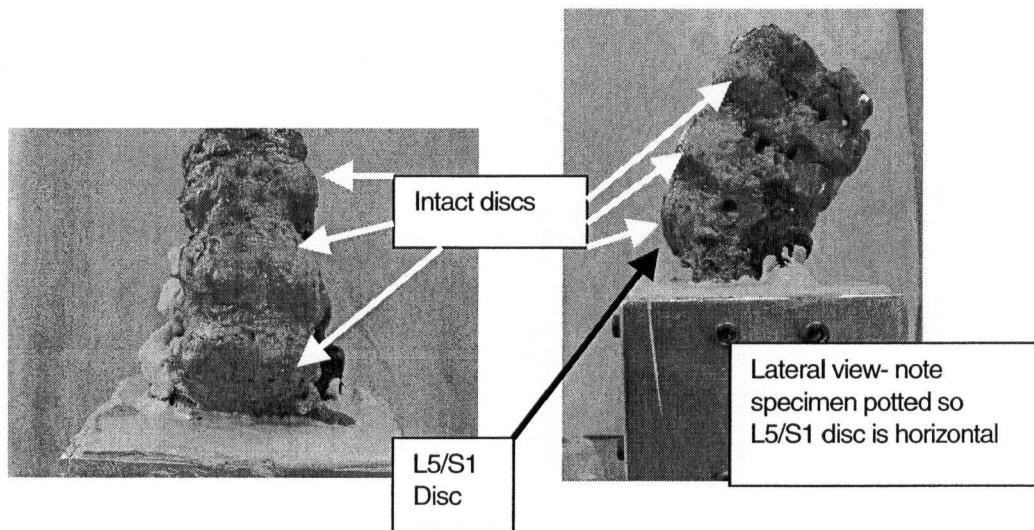


Figure 2.4 Anterior (left) and lateral view of instrumented, and potted spinal column, to level of middle of S1, with L5/S1 disc space horizontal to floor.

Because of the physiological lumbosacral lordosis, the spinal column had to be tilted and held in a special 3-plane vise, during further tests to allow a level disc space for axial compression testing.

The L5/S1 disc space was then surrounded by a plastic molding (plastic container cut into a ring shape) and the Plaster of Paris was poured in a liquid form up the mid-vertebral level of L5. This covered the L5/S1 disc, and made available a new “isolated” instrumented level at L4/5. Play-Doh® was used to

create a layer upon the dental cement, abutting the external peripheral surface of the sacrum, to form a “skirt” like barrier between the dental cement and the overlying poured Plaster of Paris layer. This was to enable easy removal of the solid Plaster of Paris layer (fracturing/cleaving plaster) to reveal a new FSU level for testing.

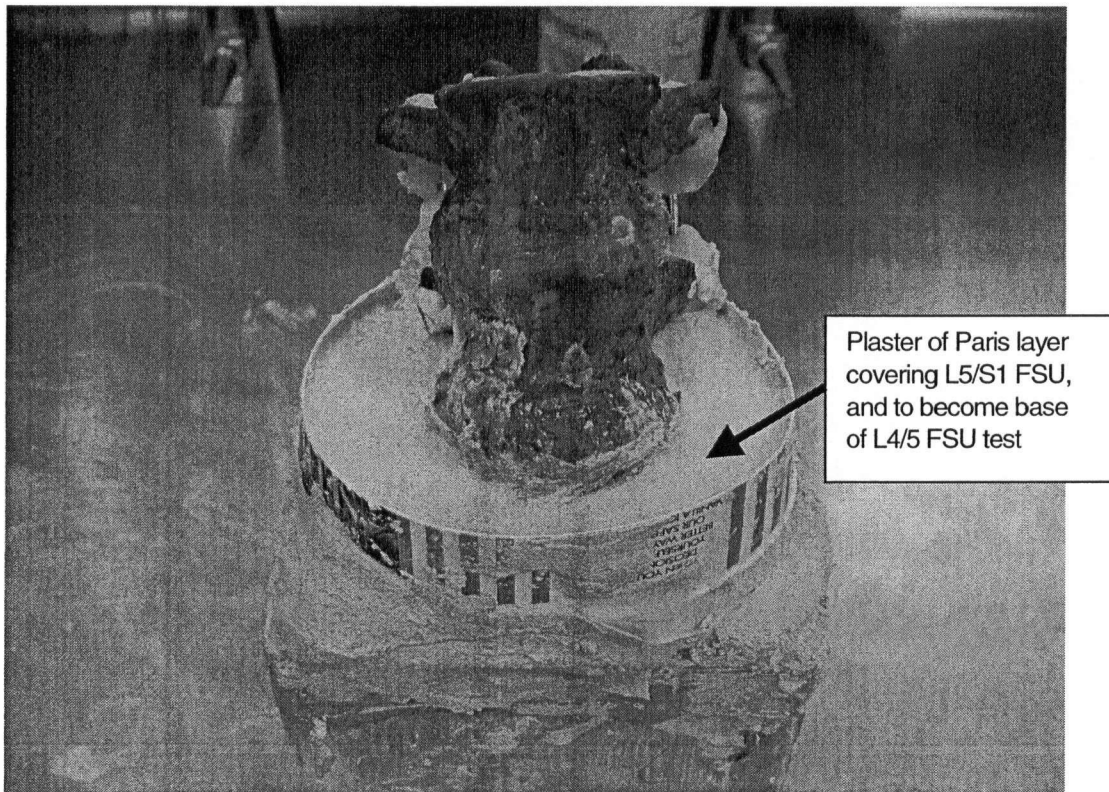


Figure 2.5 Plaster of Paris layer to mid-level of L5, leaving L4/5 disc exposed for testing as a separate FSU, and covering L5/S1 disc (last tested FSU).

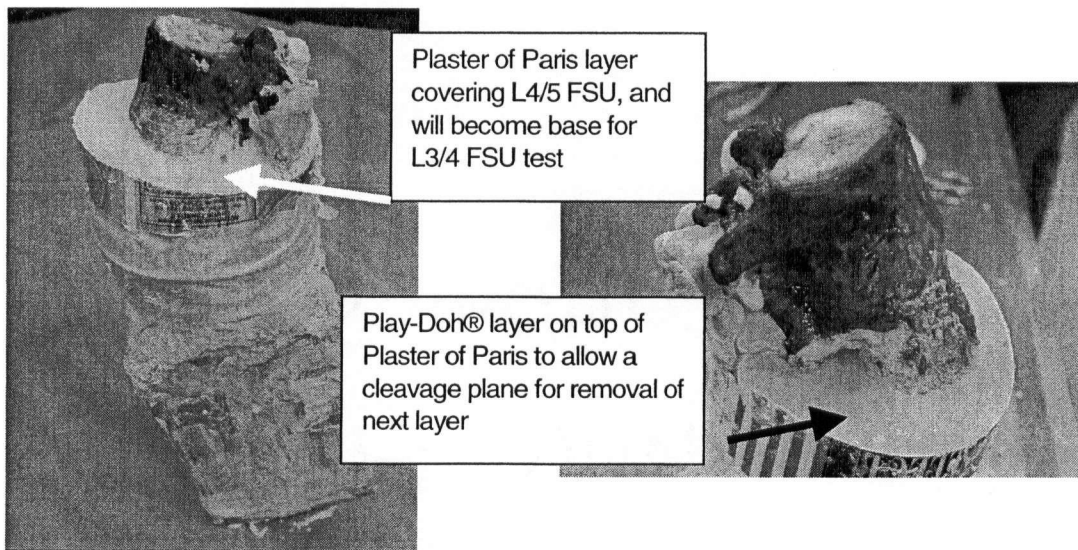


Figure 2.6 Second Plaster of Paris layer potted (left) to mid-level of L4 body, and third layer of Plaster of Paris potted (right) to mid-level of L5 body.

The same technique was performed at the L4/5 disc space level, with the cutting of a plastic ring moulding around the vertebral body of L4, and the same use of Play-Doh® as a “skirt” between the Plaster of Paris layers, and pouring of liquid Plaster of Paris up to the level of mid-vertebral body of L4. This then only left the most superior exposed L3/4 disc FSU to be tested, and the superior endplate, and upper one third of the L3 vertebral body, to be potted in a special aluminum load bearing plate mount, for direct contact with the actuator of the servo-hydraulic compression testing machine. Note that at each FSU level to be tested, the screw head and screw-rod junction were left uncovered by Plaster of

Paris, at the lower vertebral body of the FSU tested, and from dental cement at the upper vertebral body of the FSU being tested.

2.6.2 Upper Vertebra Potting

The superior most vertebra of each test level i.e., L5 of the L5/S1 FSU; L4 of the L4/5 FSU; and L3 of the L3/4 FSU was potted in a way that involved the peripheral and radial placement of 1.5cm long screws into the upper vertebral body, acting as “anchoring pilons” into the cement, and then plunging the spinal column inverted, with the superior test vertebra of that FSU, into wet dental cement that was poured onto a 14x14 cm aluminum plate with a short 1cm plastic PVC molding ring barrier. The specimen would be supported so that the upper endplate of this superior most vertebral body of the FSU being tested would sit flat on the aluminum plate until the dental cement dried solid and fused to the vertebral bodies and anchoring screws. As mentioned, caution was taken to avoid dental cement at this superior vertebral level of the test FSU to become incorporated into the pedicle screw heads. Care was also taken in avoiding Plaster of Paris incorporating into the pedicle screw heads of the lower vertebral body of the FSU being tested. Play-Doh® placed on and around the pedicle screw heads helped avoid this.

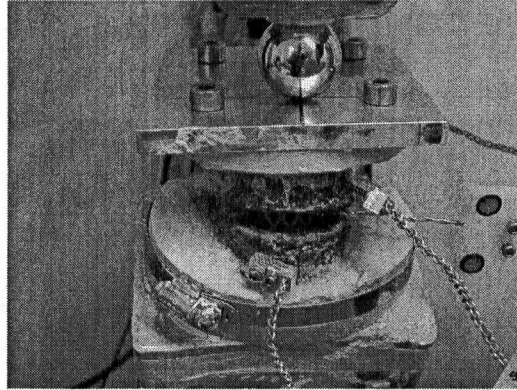


Figure 2.7 Typical example of superior vertebra potting of the FSU, with shallow dental cement and aluminum mounting cap for compression testing.

As will be discussed further, the advantage of this multiple level potting technique of the instrumented spinal column from L3-sacrum, meant that 3 FSU's could be tested on each specimen, instead of having to divide the spinal column through the L4/5 disc, and testing only two 2 FSU's- L3/4 and L5/S1. The spinal column, after various modes of testing- to be discussed, required the cutting of the posterior rods and excision of the facet joint capsules and division of the interspinous ligament, for complete removal of the uppermost vertebral body of that FSU. This exposed that test level disc space and endplates for macroscopic examination. The potting technique as described for the uppermost vertebra of the FSU with the dental cement and aluminum plate, was then performed again permitting a "new" potting isolated and instrumented FSU for testing. The test order therefore, would logically be L3/4 FSU, removal of L3 vertebral body; L4/5 FSU, removal of the L4 vertebral body; and finally L5/S1 level with removal of the L5 vertebral body for inspection of the endplates at that L5/S1 level (Figure 2.2).

This non-destructive plaster removal and repotting technique was repeated for all 9 spinal columns used, and therefore permitted 27 FSU to be tested.

2.7 Cage Size Selections and Randomization of Cage Position Placement

For the 27 cage(s) patterns (Surgical Titanium Mesh®, DePuy Acromed, Raynham, MA) (Figure) inserted in the failure test phase of the experiment (to be outlined), an appropriate and standardized single cage or double cage combination had to be chosen, matched for approximate equivalent surface area of cage available for endplate contact. Once the disc material was removed after the stiffness-testing phase of the experiment (Section 2.11) and the discs were graded (Table 3.6) for degeneration based upon a grading system from 1-4, with 4 being fully dehydrated discs and 1 normal (Vernon-Roberts and Pirie, 1973), calipers were used to measure the maximum antero-posterior and lateral diameter (mm) of the superior and inferior endplates of the FSU being tested, to give two surface area values (mm^2), one for each endplate (Table 3.5). These surface area approximations assumed the endplates to be an elliptical shape (White and Panjabi, 1990).

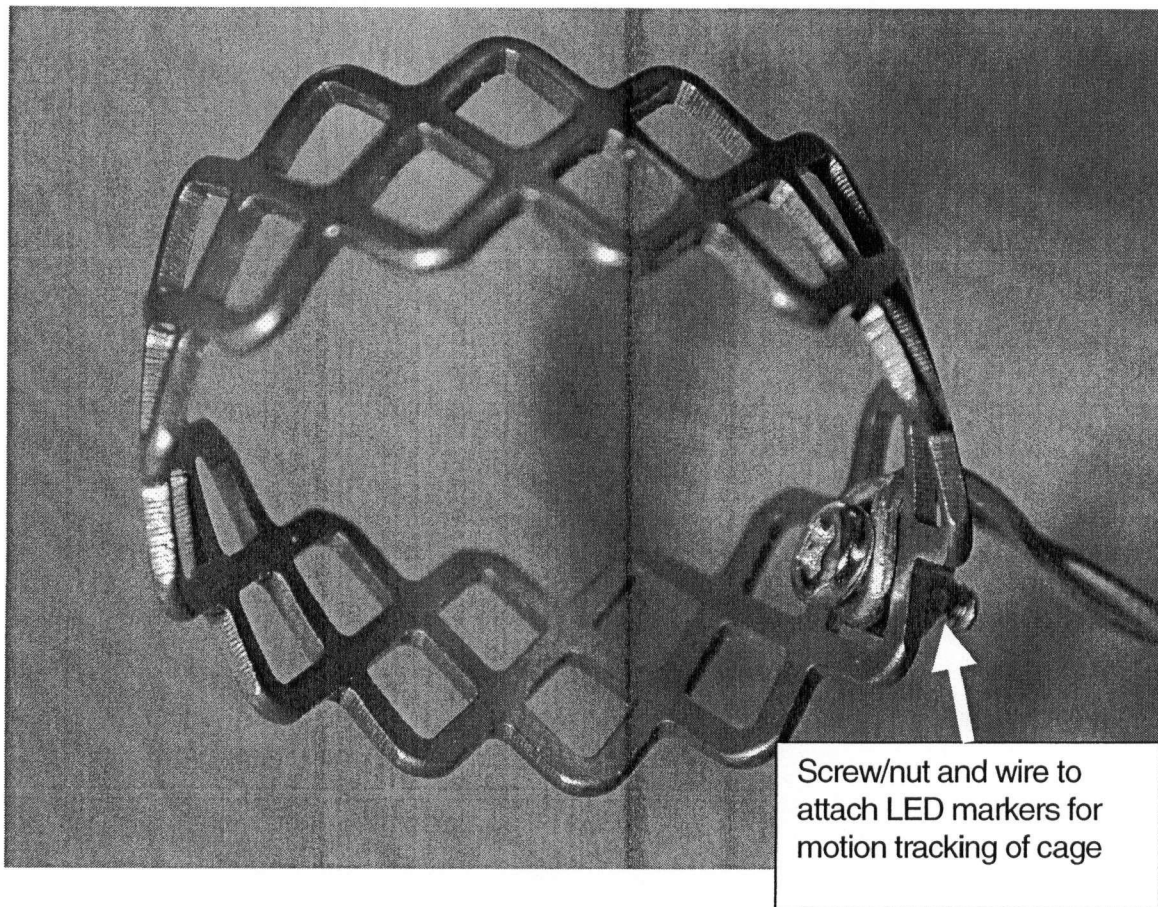


Figure 2.8 Oblique view of typical titanium mesh cage used- close up of 22x28mm cage.

Known cage diameters and surface areas for commonly used cages were used to match a single cage or double cage combination that approximated 20% of the total available mean surface area of the endplates for each FSU. Lowe and Tahernia, (2002) quote a most common cage pair combination, for dual cages in TLIF or PLIF techniques, as being 12-15 mm diameter round cages, with heights from 7-9 mm. Based on this quoted reference and from experience surgically, a pair of round cages with diameters 14mm (surface area potential for graft of 153.9 mm^2 , 307.9 mm^2 for two) and 16mm (surface area potential for graft of 201.1 mm^2 , 402.2 mm^2 for two) were chosen as two common sizes likely to be used in the experiment. Cage height for the 14mm diameter cage was 9 mm , and cage height for the 16mm cage was 10 mm (Figure 2.9).

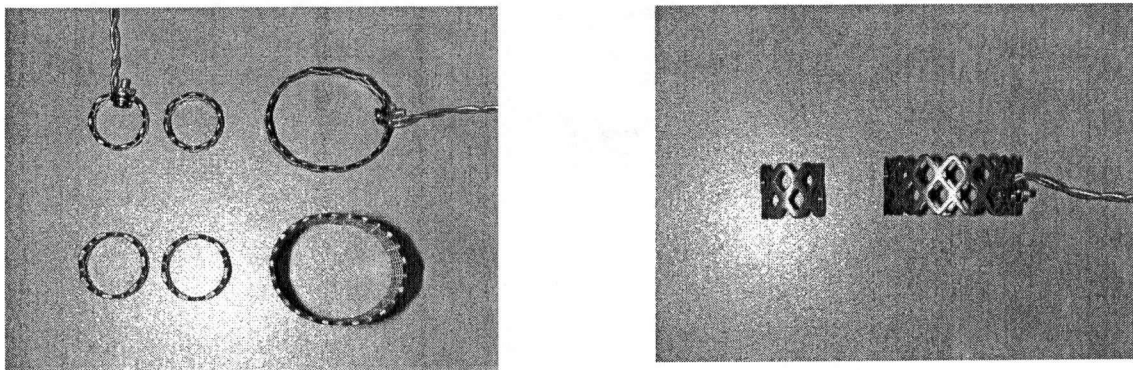


Figure 2.9 Pairs of cages used in experiment (left) with 2x14 mm diameter cages and 17x22 mm (equivalent surface areas) on top, with 2x16 mm diameter cages and 22x28 mm (equivalent surface areas) on bottom. Lateral view of 9mm high 14 mm diameter cage and 9 mm high 17x 22 mm cage (right).

Considering the expected pairs of cages to be used from the above calculation and reference (Lowe and Tahernia et al, 2002), an appropriately sized surface area matched *single* cage had to be selected from the available diameters of cages (Surgical Titanium Mesh®, DePuy Acromed, Raynham, MA) for single level interbody fusion. Two single oval cages were chosen that approximated the combined surface areas of the two paired cage combinations (2x14mm cages= 307.9 mm²; 2x16mm cages= 402.2 mm²) – 1. 17x22 mm (oval) Surface area= 293.7 mm² which approximated closely the 2x14 mm cages; 2. 22x28 mm (oval) Surface area= 483.8 mm², which was approximately 17% greater than the 2x16 mm cage's combined surface area. This 22x28 mm single cage was ultimately only used at *one* FSU tested.

Randomization of the three cage patterns- 2 posterolateral, 2 central, and 1 central, across the 27 FSU's (9 spinal columns) and 3 spinal levels- L3/4, L4/5, L5/S1, was based upon a simple computer generated randomization allocation, to permit a randomized distribution of the three cage patterns.

Table 2.2 Random cage position allocation for specimens and FSU levels

Specimen No.	L3/4 FSU	L4/5 FSU	L5/S1 FSU
1061	2 Posterolateral	1 Central	2 Central
1067	1 Central	2 Central	2 Posterolateral
1009	2 Central	1 Central	2 Posterolateral
1027	2 Posterolateral	1 Central	2 Central
1082	1 Central	2 Posterolateral	2 Central
1031	2 Posterolateral	2 Central	2 Central
1090	1 Central	2 Central	2 Posterolateral
1030	2 Central	2 Posterolateral	1 Central
1036	2 Central	2 Posterolateral	1 Central

2.8 Validation of Placing Bone Graft in Cages

A simple biomechanical study prior to the study was performed to assess the effect of placing mulched human sacrum bone graft into the titanium mesh cages with respect to subsidence in axial compression.

Into both synthetic saw-bone sheets (Last-a Foam FR6712, General Plastics Mfg. Co., Tacoma, WA) of artificial trabecular bone, and into a single human

lumbar vertebra (superior and inferior endplates), cages with and without packed bone graft were compressed. A level metallic surface and a constant velocity, axial compression was provided by a servo-hydraulic testing machine (Instron 8874, Instron Corporation, Canton, MA) was used to push the titanium mesh cages into either the artificial bone or endplate. Load-displacement values were recorded and observation of the effect of the endplate/artificial bone failure was noted. Results from this small experiment, importantly, were applied to the decision to use bone graft in the larger study.

The mean cage(s) and bone graft surface area to vertebral endplate area ratio was 18.9%, with a standard deviation of 2.1%. This intentionally, closely standardized value is summarized in Table 2.3, and is based upon pre-calculated known areas of the cage(s) used, and the exact measurement of the endplates after separation of the FSU post-test.

For both foam block (artificial bone substitute) and human vertebral endplates, the loads for an equivalent displacement (compression the cage \pm graft into the surface) were around three times higher for the titanium mesh cages with graft packed inside. Unlike the empty titanium mesh cages, the graft filled cages left a significant indentation and collapse of the foam block surface. A similar, yet greater, effect was seen on the surfaces of the lumbar vertebral endplate

Table 2.3 Width (mm) x Length (mm) of endplates and surface area (mm²) (assuming ovoid shape), and percentage of cage(s) used covering the mean of the two available endplate surface areas of the FSU tested.

Specimen	L3 Inferior	L4 Superior	L4 Inferior	L5 Superior	L5 Inferior	S1 Superior	Cage L3/4 (%)	Cage L4/5 (%)	Cage L5/S1 (%)
1-1061	28x50 (1400)	28x51 (1428)	30x48 (1440)	30x52 (1560)	32x52 (1664)	32x52 (1664)	2x14mm (21.8)	17x22mm (19.6)	2x14mm (18.5)
2-1067	29x40 (1160)	30x41 (1230)	29x45 (1305)	30x46 (1380)	29x48 (1394)	30x48 (1380)	17x22mm (24.6)	2x14mm (23)	2x14mm (22.7)
3-1009	32x43 (1376)	33x44 (1452)	33x46 (1518)	35x46 (1610)	36x48 (1728)	34x48 (1632)	2x14mm (21.8)	17x22mm (18.9)	2x14mm (18.4)
4-1027	42x58 (2436)	41x56 (2296)	41x58 (2378)	43x58 (2494)	41x53 (2173)	39x59 (2301)	2x16mm (17)	2x16mm (19.9)	22x28mm (18)
5-1082	31x42 (1302)	32x42 (1344)	33x46 (1518)	33x48 (1584)	34x48 (1632)	33x48 (1584)	17x22mm (22.3)	2x14mm (19.9)	2x14mm (19.2)
6-1031	40x56 (2240)	40x55 (2200)	42x58 (2436)	43x60 (2580)	43x60 (2580)	42x60 (2520)	2x16mm (18.1)	2x16mm (16.1)	17x22mm (13.5)
7-1090	33x50 (1650)	33x50 (1650)	36x54 (1944)	39x53 (2067)	36x53 (1908)	36x53 (1908)	17x22mm (17.8)	2x14mm (15.4)	2x14mm (16.1)
8-1030	35x53 (1855)	36x55 (1980)	37x55 (2035)	33x55 (1815)	36x48 (1656)	35x48 (1610)	2x14mm (16.1)	17x22mm (16)	2x14mm (18.1)
9-1036	33x46 (1518)	33x48 (1584)	32x48 (1536)	32x46 (1472)	32x44 (1408)	32x44 (1408)	2x14mm (19.9)	2x14mm (20.5)	17x22mm (20.9)

2.9 Human Bone Graft Preparation and Insertion into Titanium Mesh Cages

Two human frozen sacrum from the musculoskeletal tissue bank at the Division of Orthopaedic Engineering Research, University of British Columbia, were used to mill a standardized grade and quality of bone graft to be packed into the cylindrical titanium mesh cages. After manually dissecting the external surfaces of the sacrum clean of any soft tissue, the sacrum of unknown bone mineral density, were cut into small pieces and passed through a pneumatic bone mill (DePuy, Warsaw, IN) and morsellized using a medium sized blade. The same morsellized bone was passed through for a second time to create a more uniform bone mulch. The total graft specimen was divided into nine equal portions and stored in a freezer at -20°C until required for each FSU tested.

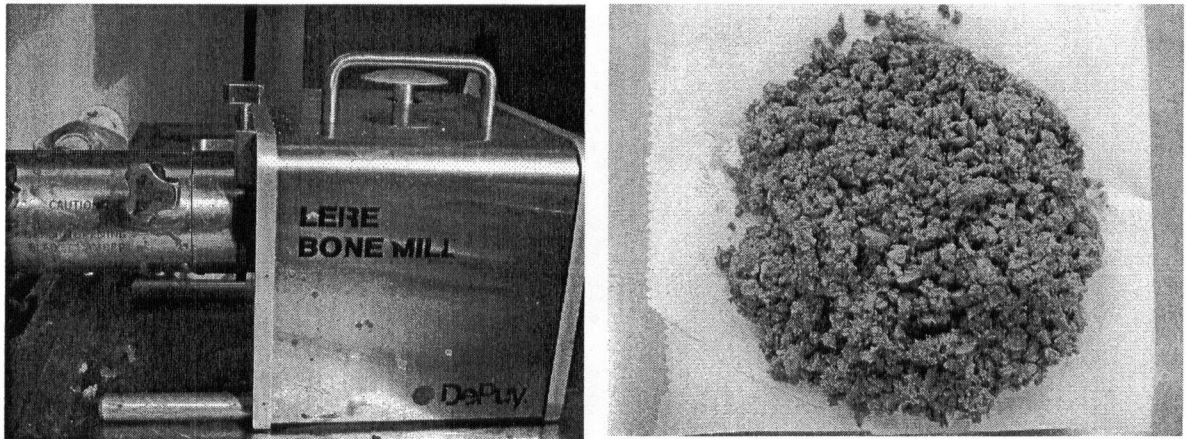


Figure 2.10 Pneumatic bone mill (left) and bone graft made from human sacrum for experiment (right).

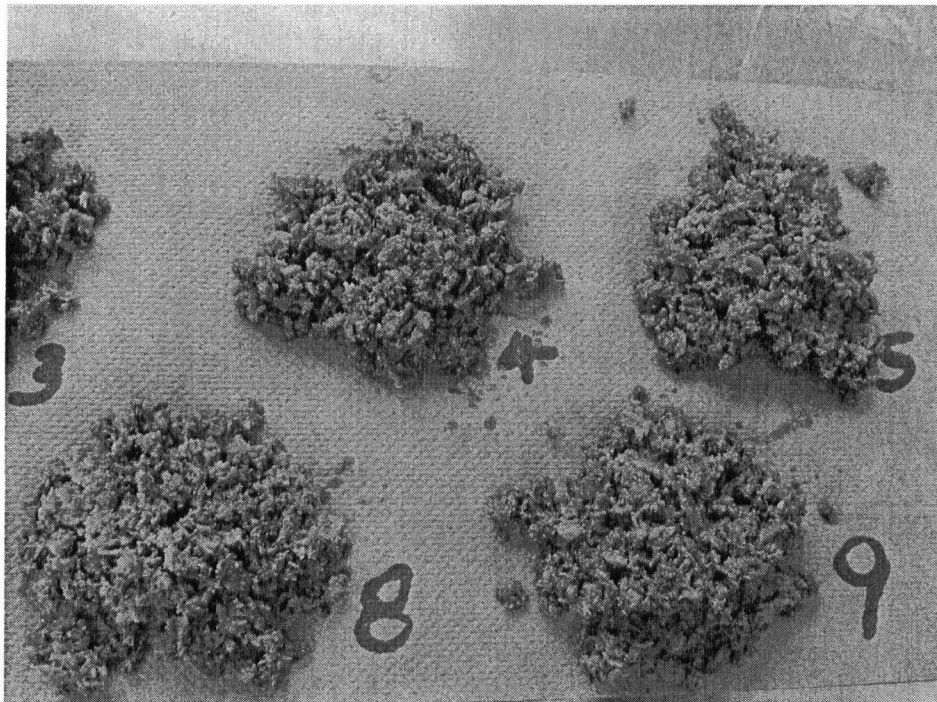


Figure 2.11 Divided portions of graft for each one of nine specimens tested.

The individual titanium mesh cages for each test level, when required, were packed with a macroscopically equivalent quantity of morsellized bone that had been prepared and thawed to room temperature, but frozen at -20°C for storage. Utilizing blocks of aluminum, exact fit to the cage's internal diameter, either round or oval plunger blocks were milled and had center hand threaded holes placed for attachment of a threaded rod, to which a weight could be attached. (Figure 2.12)

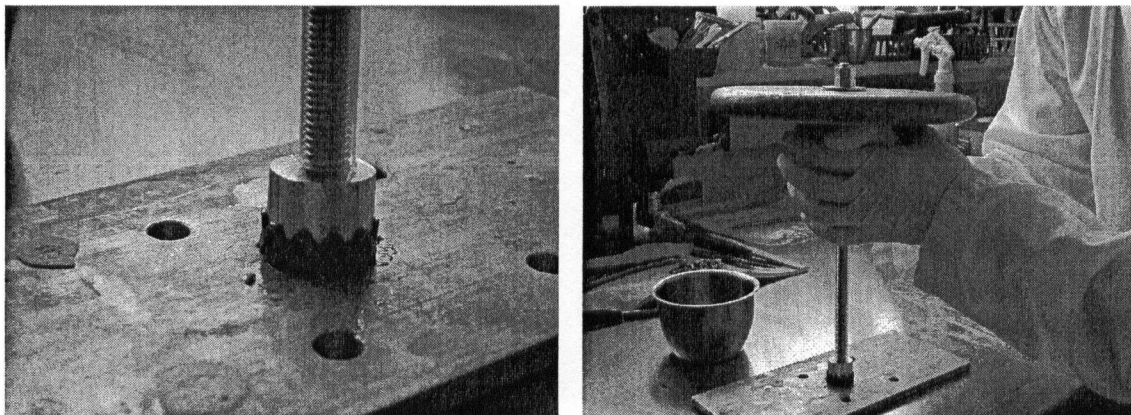


Figure 2.12 Customized metal tip plunger to pack graft within each size cage (left) and standardized force (variable weights for cages) with gravity only (right).

Using the known diameters and surface areas of the cages, both round and oval, (14mm round= 153.9mm^2 , 16mm round= 201.1mm^2 , 17x22mm oval= 293mm^2 , 22x28mm oval= 483.8mm^2) (Using the formula $A = \frac{\pi}{4} \cdot d_1 \cdot d_2$ for oval shapes), and knowing that $\text{Pressure} = F/A$, then $F_1/A_1 = F_2/A_2$. The amount of weight required

then for each size cage was as follows, and was made up with a combination of circular disc weights and lead pellets to make the exact weight specified-

- 14mm diameter round= 2.58 kg
- 16mm diameter round= 3.55 kg
- 17x22 mm oval= 4.78 kg
- 22x28mm oval= 7.88 kg

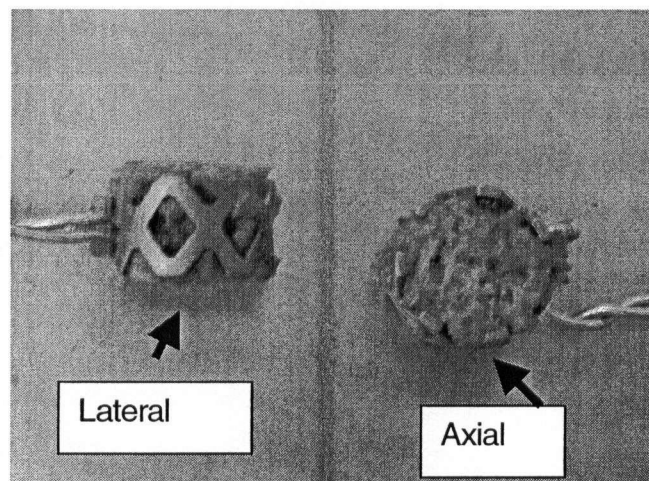


Figure 2.13 Lateral and axial view of 14 mm diameter cage packed with graft

2.10 Measurement of Cage- Bone and Bone- Bone Motion

Motion of the vertebral bodies and cages during the tests were measured using an optoelectric camera system (Optotrak 3020, Northern Digital, Waterloo, Canada). Marker carriers with 4 light emitting diodes (LEDs) (Figure 2.14) were

rigidly attached to the vertebral bodies of each FSU tested. The marker carriers were attached to the vertebral bodies via aluminum couples that were milled in a reciprocal fashion to enable easier and less disruptive addition and removal (Figure 2.15) Braided wires were used to connect these aluminum couples to the marker carriers. A total of 3 marker carriers were used for single cage tests (upper and lower vertebra and cage), and a total of 4 marker carriers for double cage tests (superior and lower vertebra and both cages).

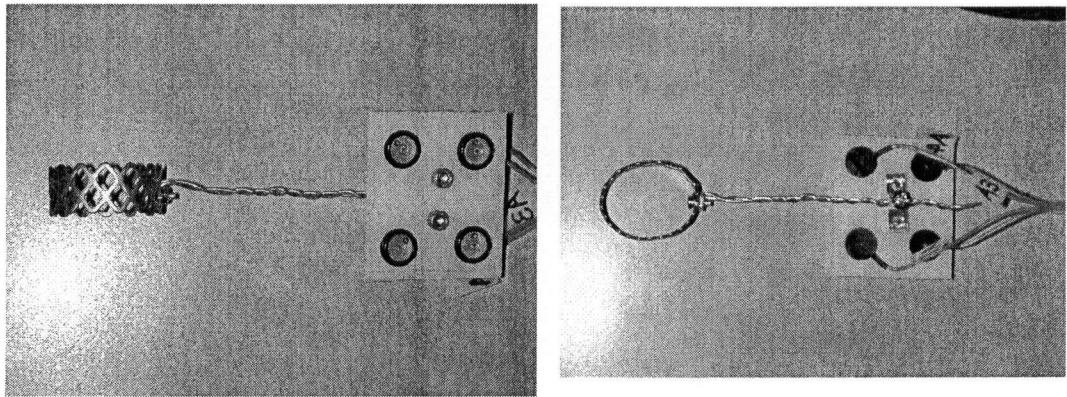


Figure 2.14 Cages with braided wire attaching 4 LED 's for assessment of cage motion.

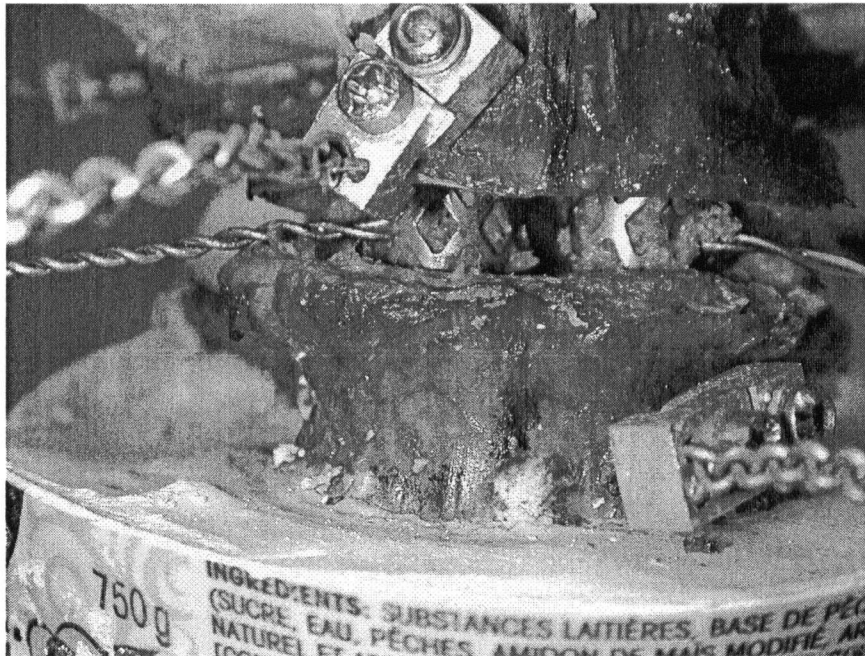


Figure 2.15 Close-up of braided wires coupled to vertebrae and cages.

The optoelectric camera system was set at least 2 meters away from the LED's and the global coordinate system for the camera had its origin at the center camera and cartesian coordinates x,y,z as shown (Figure 2.16)

The cameras were placed such that they were directly in front of the LED's and aligned parallel to the LED's. The frame whereby the camera was attached was locked into place for the duration of the test.

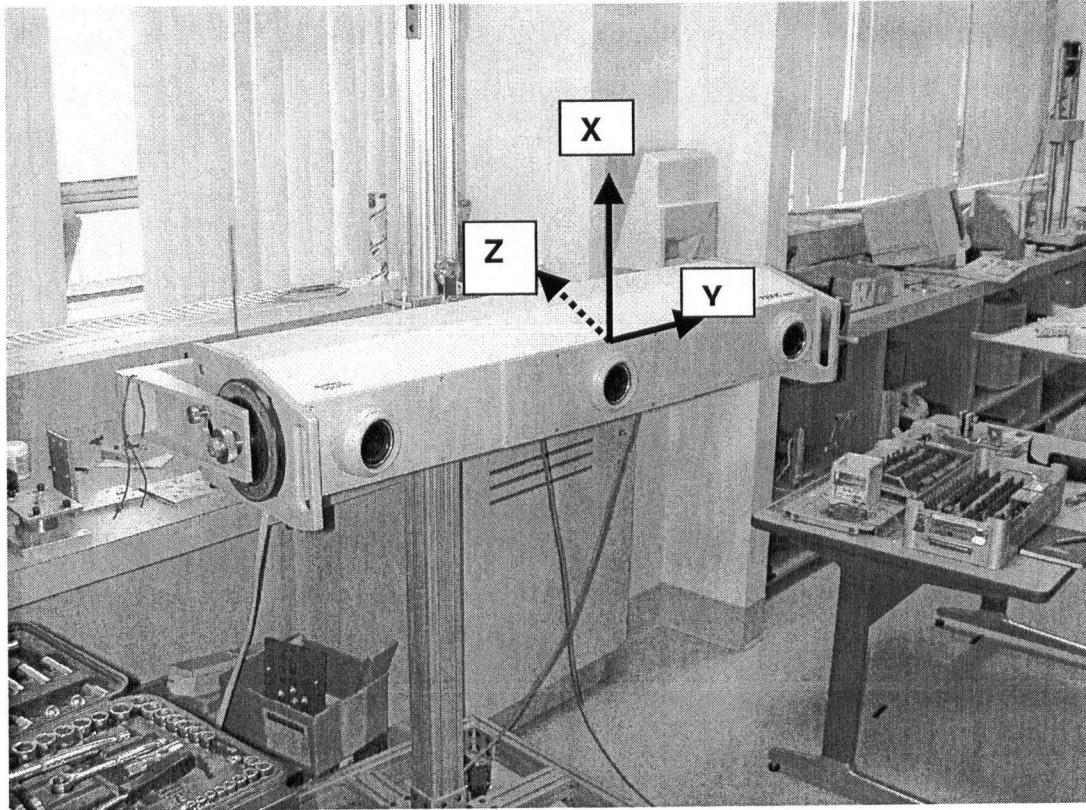


Figure 2.16 Optotrak camera system and global cartesian coordinate system based upon the center camera.

A local co-ordinate system was based upon the 3 LED's mounted rigidly to the testing machine. The specimen was aligned to the plane of these 3 LED's for every test. The three points provided information for the x and y direction of the local coordinate system (Figure 2.17). The origin of this local coordinate system was referenced to the global coordinate system based at the camera (Fig. 2.16).

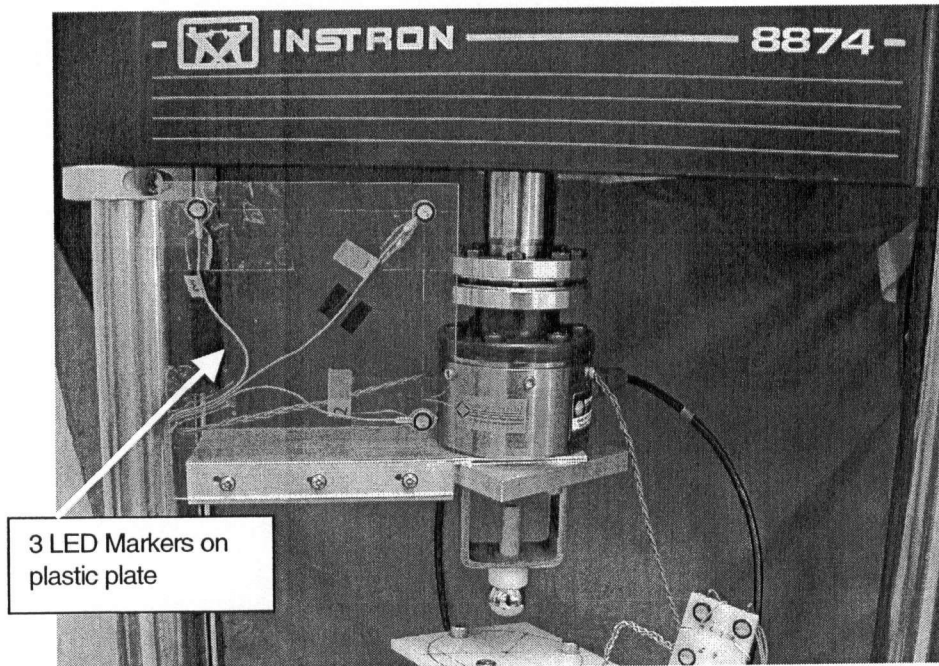


Figure 2.17 Clear plate with 3 LED markers to establish a local coordinate system with cartesian coordinate system as marked.

Before performing each axial compression test on an FSU, whether over 2mm of crosshead distance for the intact disc and without the disc, or over the full 12mm of crosshead displacement for the failure test, with one of the three cage positions in place (to be discussed further in Section 2.11 and 2.12), a 2 second static calibration and digitization of landmarks on the vertebra and cages were performed.

The following points were digitized-

1. Anterior bony point of the superior vertebral body of the FSU being tested (as close to the inferior endplate as possible, in the most anterior position)
2. 3 points around the middle zig-zag band of the titanium mesh cage(s), either equidistant, or as equidistant as possible. These 3 points would be used to calculate the theoretical center point of the cage

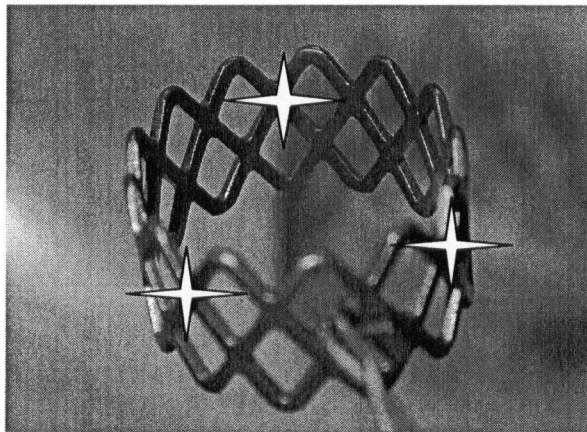


Figure 2.18 Example of points digitized on each cage for calculation of center point of cage.

A 2mm diameter ball tip probe (Northern Digital Inc., Waterloo, Canada) with 6 LED's attached was used to mark these points digitally on the global coordinate system. Accuracy of this system was determined to be ± 0.1 mm through previous tests in the laboratory.

For measurement of bone-bone motion, the motion at the digitized anterior bony point was calculated. For measurement of cage-bone motion, the cage center point was calculated.

Analysis of bone-bone motion utilizes the data of the motion of the marker carriers attached to each vertebra. For this analysis, the origin of the local coordinate system was placed at the digitized anterior bony point and the x, y, and z coordinates aligned with the 3 LED's on the plate set to the crosshead (Figure 2.17). The difference of the motion of these two sets of markers attached to the superior and inferior vertebra, in the local coordinate system, gave the bone-bone motion of the anterior bony point.

Similarly, for the cage-bone motion, the center of the cage was used as the origin and the difference of the motion of the marker carriers attached to the cage and the inferior vertebral bone gave the motion of the cage into the inferior bone.

Finally, an analysis between the marker carriers attached to the cage and the superior vertebral bone gave their relative motion.

The Optotrak capture frequency was 20Hz for all tests, creating 200 data points for a 10 second capture and 1000 points for a 50 second capture. Northern Digital, (Waterloo, Canada) "rigmaker" software and an in-house labview (National Instrumentation) program called "Kin 2000" was used in all analyses.

2.11 Compressive Stiffness Testing- FSU's with Intact Disc and with Disc Removed

After the lower section specimen potting and superior vertebra aluminum plate potting, the test FSU level had 2 screws inserted into the upper and lower vertebral bone in an anterolateral position, so as to not collide with any part of the potting mounting. The LED markers were then attached with the wire and aluminum couples, as described, and then the entire specimen was taken to the servo-hydraulic materials testing machine (Instron 8874, Instron Corporation, Canton, MA) (Figure 2.19).

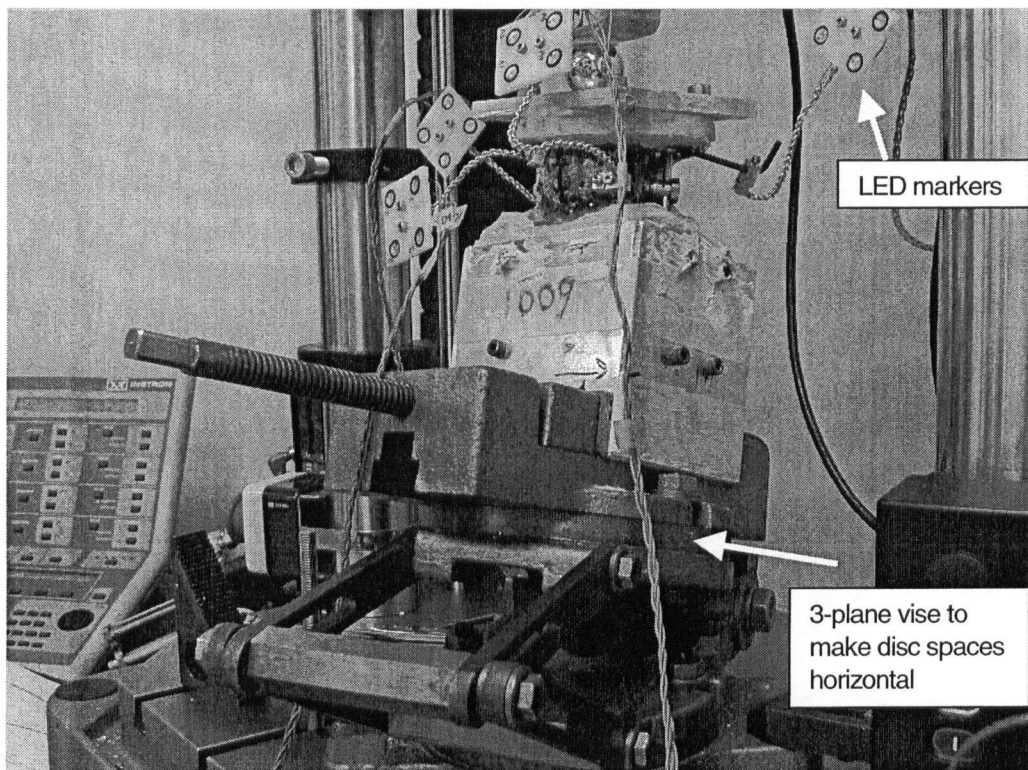


Figure 2.19 FSU with all markers attached mounted in 3 plane leveling vise ready for compression testing in Instron machine.

The Instron controller was connected to a PC via a general- purpose interface bus. Instron supplied software (Fast Trak Console), was used to control each test. All data was acquired by the Instron controller using a 12-bit data acquisition card, sampled at 20 Hz. Force measurements were made using a biaxial load cell (Model 211-113, SensorData Technologies Inc., Sterling Heights, MI; serial number 97533). Original calibration showed that accuracy of the load cell was less than 0.1% of rated output (certified by Instron, November 27, 1998). A shunt calibration was performed each day before testing, and the load cell output was balanced before each test.

Displacement measurements were made using the Instron-supplied LVDT (± 50 mm; serial number 0291). The LVDT calibration was verified with a digital Vernier caliper at the start of the experiment, and positions agreed within 0.3mm over a range of 62mm.

After appropriate calibrations, the specimen in the aluminum block base was set into a 3-plane vise that was able to permit the leveling of the disc space being tested, so that it was parallel to the floor. Visual assessment from both anteroposterior and lateral views confirmed the disc space being level. After locking the vise in the required tilted position to allow for the physiological lumbar lordosis (Figure 2.19), the center point of the superior test vertebra was identified, and position marked on the top of the aluminum top mount, so that the actuator would make contact at the center of the superior test vertebra.

Using the prior marked anterior and lateral points of each vertebra (based upon the initial assessment of the center anterior and lateral points from the superior endplate of L3 during specimen preparation) with ink and metal sharp pins, a “Π” shaped heavy bent wire was placed across the top of the aluminum plate and each hanging arm of the reference wire was aligned with the anterior and then lateral center points of the vertebra, and an ink line was drawn across the top of the aluminum mount, and the intersection marked the center of the superior test vertebra. This procedure was repeated for each test (x3) for each FSU tested (x27). (Figure 2.20)

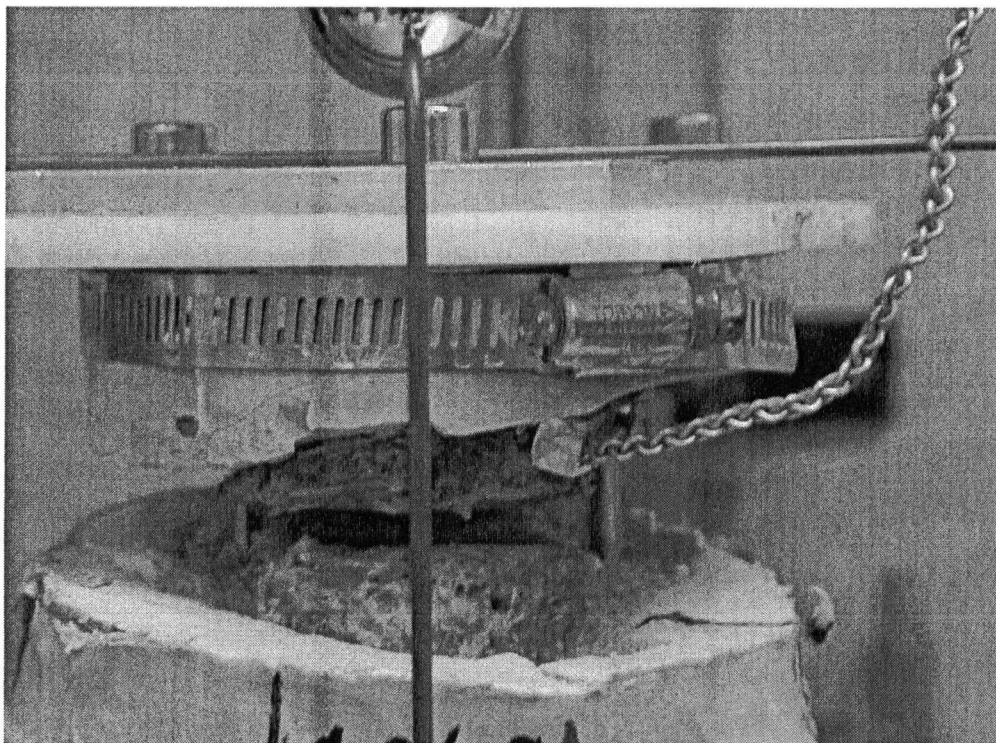


Figure 2.20 Close-up of cross-wire assessment to accurately mark the center of the superior vertebral body for direct axial compression.

The specimen was then positioned under the actuator so that it would make contact at the point of intersection marked with ink on the aluminum plate mount.

All parts of the vise holding the specimen were locked and checked before all tests. The point of load applicator was a 32mm diameter femoral head from a hip replacement prosthesis, made of chrome-cobalt and highly polished, without scratches. The Morse tapered neck was fitted onto a lathed polyethylene stem, attached to an aluminum block mount at the base of the actuator, attached to the moving crosshead. Lubricant (WD40) was applied to the ball-plate interface to decrease friction at the start of each test. The use of a spherical contact was to permit flexion of the plate while a continuous load was applied, without restricting the motion of the FSU with additional loads.

All markers were attached at this point and re-checked. Because no cage tracking was required in the intact disc or without disc stiffness tests, motion of the posterior pedicle screw heads was recorded for a future study assessing the potential motion at the screw-bone interface. Markers were therefore attached to the upper and lower vertebrae, and the pedicle screw heads via hex-shaped keys fitting exactly into the locking inner nut of the pedicle screw on each side (with care to avoid any collision of the wire attached to the markers with the vertebral body or surrounding machine or other wires).

The above vise mounting, centering of the superior vertebra for the actuator, marker attachment, and described optoelectric camera digitization procedure and static data capture was performed identically (allowing for there being one or two cages, in which case the anatomical left cage 3 points were digitized before the

right cage 3 points) before each of the three tests per FSU. Before failure tests, two non-destructive tests were performed for assessment of construct stiffness with 1. an intact disc and 2. with the disc removed and no cages in position. (Figures 2.21 and 2.22). The disc, including all of the anulus fibrosis and nucleus pulposus was removed via anterior and lateral approaches. Complete excision of the anterior and posterior longitudinal ligament and outer annulus was performed. Using scalpel and curettage, the osseous endplates were cleared of all cartilaginous portions, and the osseous endplate was left intact, without any attempt at decortication. There was no excision of any of the bony posterior elements or posterior ligaments or facet joint capsules.

Both tests were considered non-destructive and required a crosshead displacement of 2mm to supply an axial compression force to generate a load-displacement curve so that stiffness values (N/mm) could be calculated. For the first- with disc intact, and second- without disc, tests on the FSU for construct stiffness property assessments; limits set on the Instron were $\pm 5000\text{N}$ with a PID of 15.00dB. After the described Optotrak static data file collection, the Instron had a 1 second delay set, and then a 2 mm crosshead downwards displacement set over 8 seconds (0.25mm/sec), with upward removal of the crosshead at 0.5mm/sec.

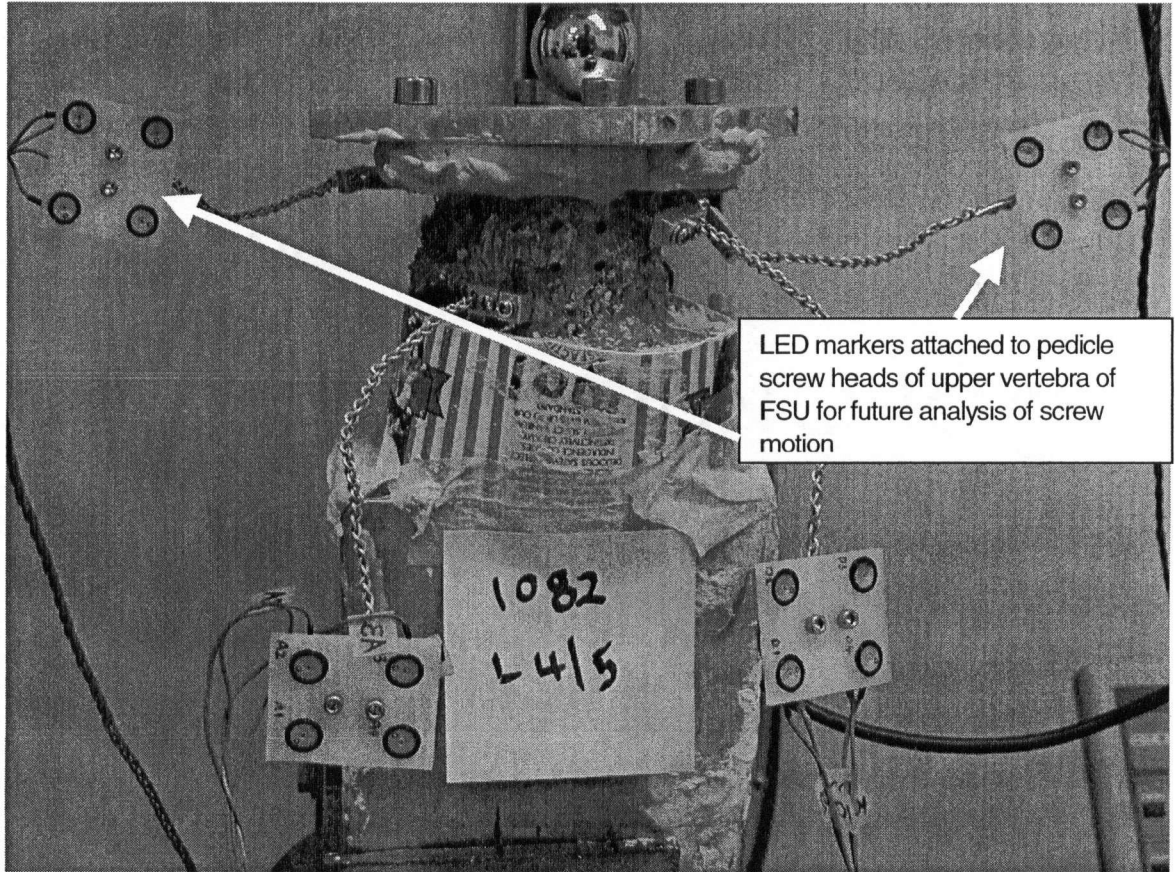


Figure 2.21 Specimen 1082-L4/5, intact disc before 2 mm non-destructive compression for stiffness assessment.

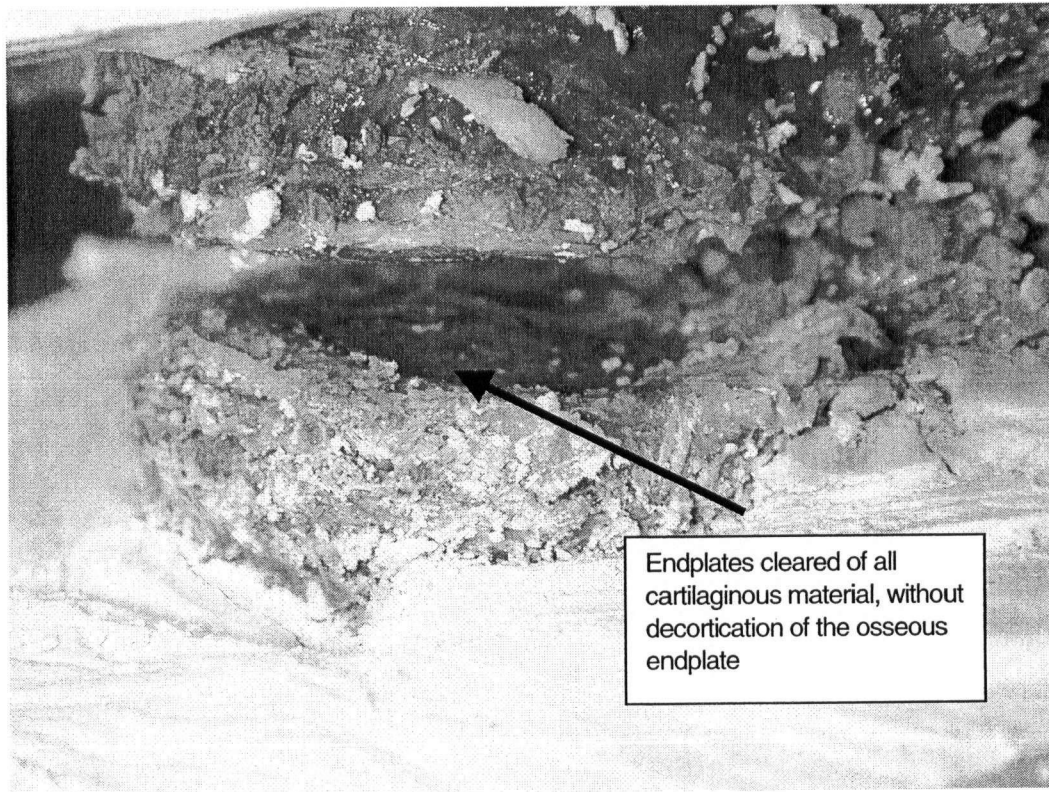


Figure 2.22 Close up of cleared disc space and endplates before 2 mm non-destructive compression test for stiffness assessment.

2.12 Compressive Failure Testing- FSU's with One of Three Cage Patterns Positioned

After the above described compressive stiffness tests (Section 2.11) on each FSU with an intact disc, and then with the disc removed, one of three cage patterns were used to assess the compressive failure strength of the construct and cage/endplate interface, where failure was visually observed, by collapse

and cage subsidence on each experiment. Either a larger oval single cage (17mmx22mm, 10mm height; 22mmx28mm, 12mm height), two smaller posterolaterally positioned cages (14mm diameter round, 9mm height; 16mm diameter round, 10mm height), or two smaller centrally positioned cages (14mm diameter round, 9mm height; 16mm diameter round, 10mm height), were placed through an anterior or lateral approach through the widely cleared disc space at each FSU level tested (Figures 2.23, 2.24, 2.25).

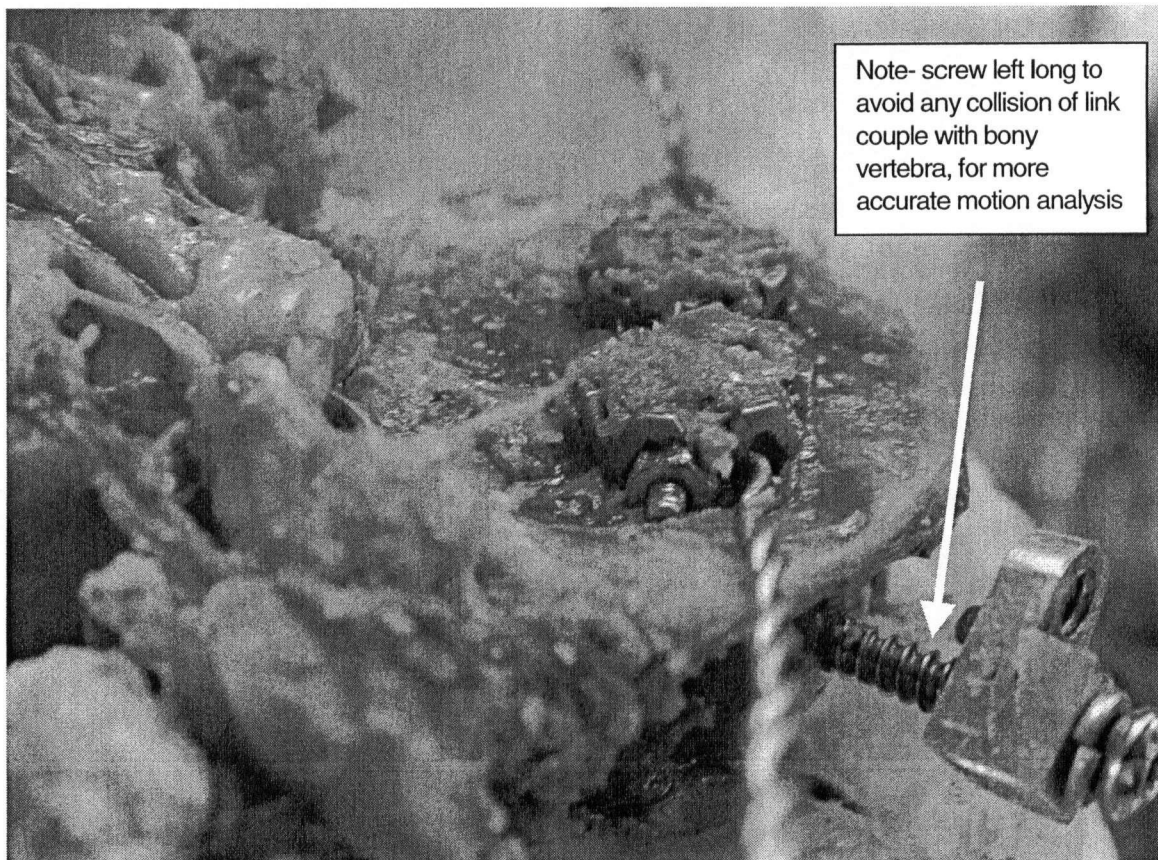


Figure 2.23 Close up view of typical position of 2 central cages (post-test) – note wires attached to cages for marker attachment, and screw in bone for marker attachment via aluminum couple.

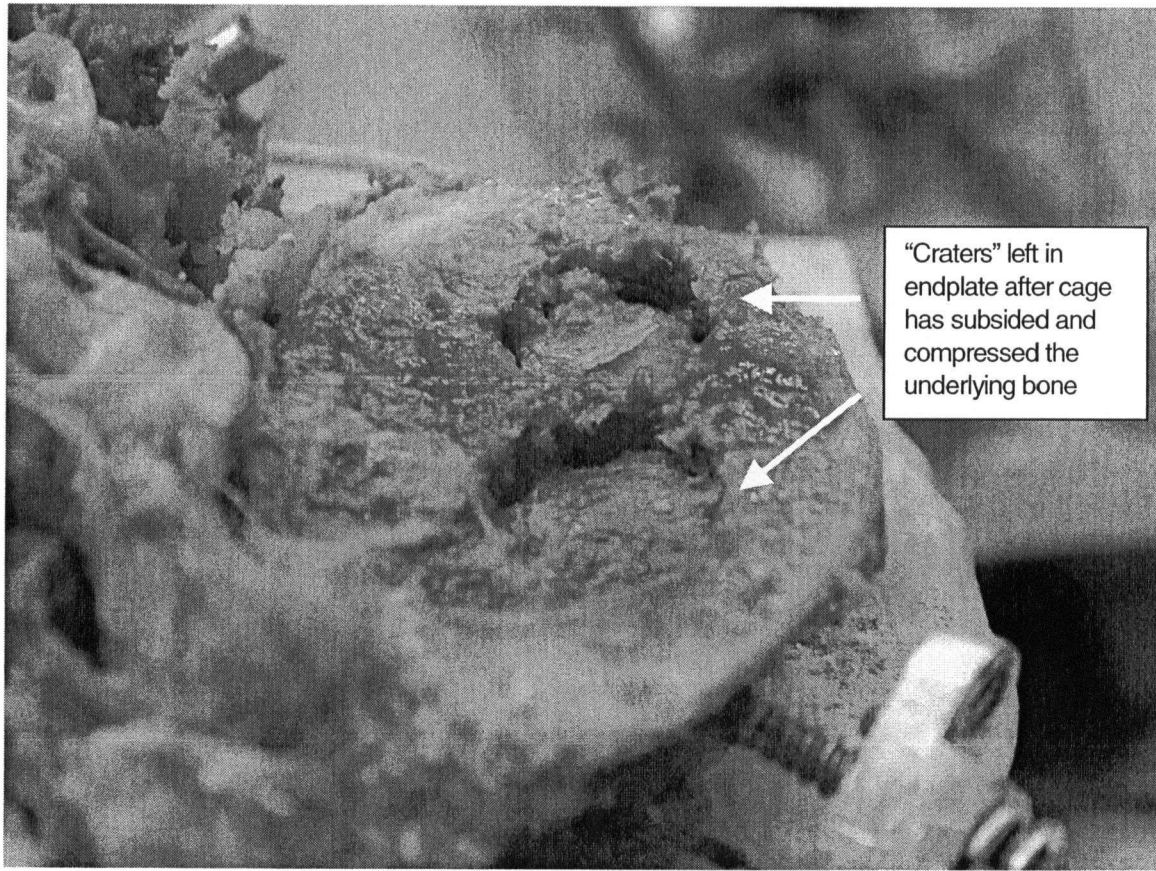


Figure 2.24 Close up view of typical position of 2 central cage position with cages removed (post-test) - note the well-demarcated craters that appear after the endplate has compressed well beyond failure.

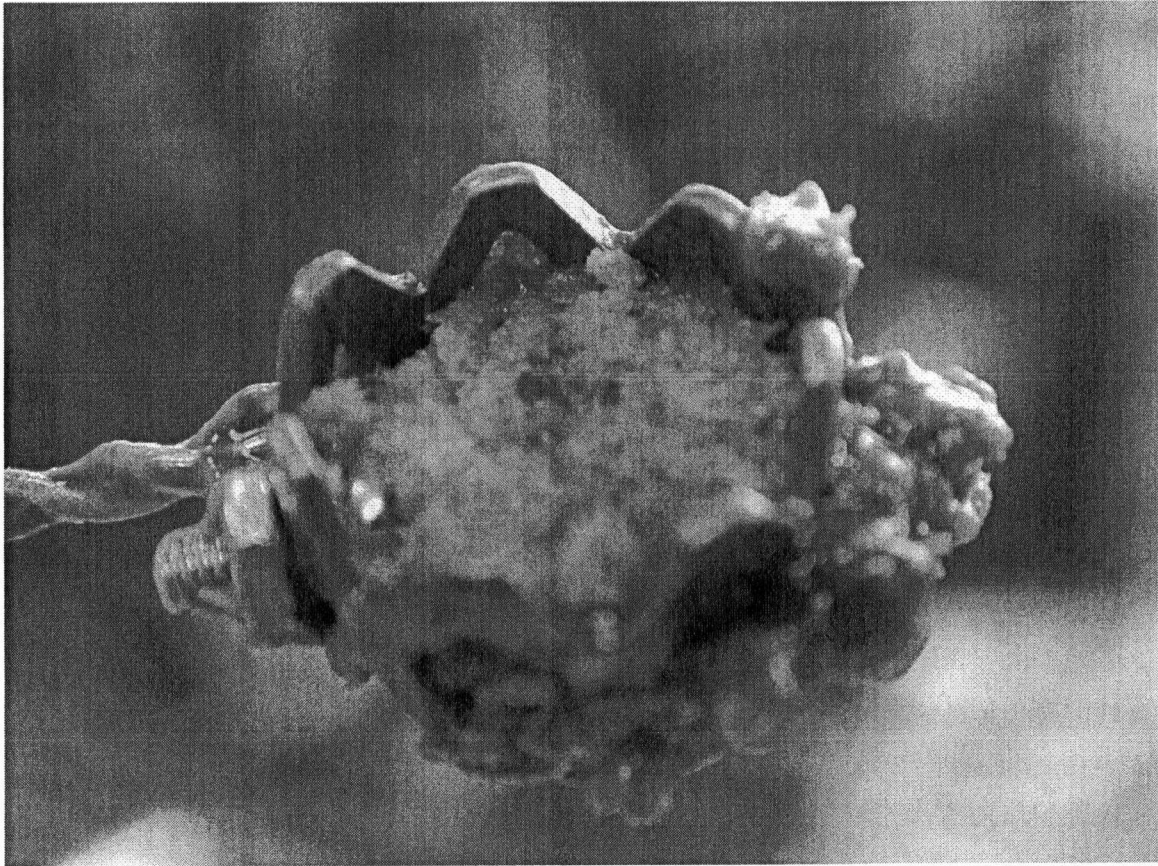


Figure 2.25 Close up view of typical appearance of a titanium mesh cage that has been filled with graft, and preferentially compressed on the endplate side that the cage mostly subsided.

After the cage combination was identified from the randomly distributed list, as described, the cages were packed with the prepared graft and had a standardized amount of force applied through a customized aluminum plunger (Section 2.9). This graft preparation and method of standardized force application had been described. The cage(s) with a twisted double stand of wire attached to the cage by a small bolt and nut, and to the LED marker, were then positioned in the disc space to standardized positions.

The lower vertebral endplate had a line marker across it at the half-way point in an anteroposterior direction. The single large cage was also placed to bisect this line, as was the two smaller centrally placed cages. The single and double central cages were positioned so as to remain in the central portion of the endplate, and avoided the periphery of the endplate, near the outer cortical rimmed margin. The two posterolaterally positioned cages were placed always behind the half-way line, and would not be placed too far back so as to encroach on the neural canal. The cages remained on endplate at all times and did not sit on the pedicles, or posterior cortical rim of the vertebral body. Cages were inserted with some disc distraction via anterior levering on the rim of the vertebral bodies, and gentle distraction of the posterior pedicle screw heads as required. All cages were placed without excessive distraction, or need for excessive disc compression. The wire(s) from the cage(s) with the LED markers attached, were placed so as to leave the wire free to avoid the edge of the vertebral body or any part of the surrounding equipment.

After cage positioning, the specimen mounted in the 3-plane correctable vise, was leveled, as described, to achieve a disc space that was parallel with the floor. The same method for marking the center of the upper vertebral body, for positioning of the actuator in compression, was employed for each FSU test with cage(s) *in situ*.

Optotrak data capture was performed as described with a 2 second static capture, with collection of all fixed points on the specimen, as referenced to the local co-ordinate system (3 LED markers on plate attached to actuator). For each cage, 3 points were digitized around the central zig-zag band of each cage in a symmetrically distributed way, so as to be able to calculate the center point of the cage. This calculated center point was used to reference cage motion, either up or down into the overlying or underlying vertebrae.

Instron limits were set before each cage test to be $\pm 5000\text{N}$ and PID 15.00dB. The crosshead was set to have a 2 second delay before downward displacement of the crosshead at 0.5mm/sec over a total distance of 12 mm for 24 seconds. The actuator at the end of this destructive axial compression test was raised at the same rate, the entire time therefore being a maximum of 50 seconds per test, with Optotrak motion data capture for this time. Before each test, the actuator femoral head 32mm ball, was lowered to the correct position and an amount of lubricant (WD40) was sprayed onto the ball-plate interface.

2.13 Post Compression Testing Vertebral Endplate Analysis

After each compression test to failure with one of the three cages, the spinal column was prepared again for the next level of FSU testing by removal of the superior most post-test vertebra, and had the rods cut with bolt cutters, and capsular and interspinous ligament division- (see Section 2.6.2).

Visual inspection of the endplates was made once the FSU had been opened up, and photographic records of each endplate post-test were made.

2.14 Mode of Endplate Failure Analysis- Macro and Microscopic Qualitative Examination

After all FSU vertebra were tested to failure, and after gross examination and photographing of the damaged endplates, the vertebrae had all metallic implants removed (pedicle screws, anchoring screws, marking pins).

The two endplates of each vertebra were inspected and would often have cage position indentations that did not correspond to the opposite endplate. Using a precision band saw, care was then taken to slice the vertebra through the middle of the indentation area on both endplates. The cuts were made in the coronal plane and therefore permitted the identification of the pedicle screw tracks in plane perpendicular to those tracks.

For each endplate cage indentation area, a 2 mm wafer was cut using a band saw (Exact Model No. 36/122, Exact Apparatebau, Norderstedt, Germany) and then washed with pulsatile lavage to clear any blood and fat from the trabecular bone. The wafer sections were then examined and photographed (Nikon Digital, Coolpix 950) and assessed under stereomicroscopy. All endplates were

assessed for patterns of failure and for patterns of trabecular bone failure. In total, all 54 endplates had a 2 mm wafer section cut to demonstrate the macro and microarchitecture of the endplate failure.

2.15 Data Analysis

Load-displacement values from the non-destructive compression tests, with disc intact, without a disc, and with one of three cages, permitted analysis of stiffness properties and from the destructive tests the construct failure values. Stiffness values (defined as the gradient of the forward loop of the load versus displacement curves) were expressed with respect spinal level tested and cage position tested to see if these variables had an effect. The effect of bone mineral density, based upon a lateral view DEXA scan, was also assessed against stiffness values.

Peak failure and mean failure loads were assessed for the three cage positions, and were expressed with respect to spinal level and cage position to assess if there existed any relationship to these variables. Failure was defined as the point on each load-displacement curve where there was a deviation from the straight portion of the curve, beyond any initial toe region. The author of this thesis and two biomechanical engineers independently assessed these failure points and had values that were identical in almost every test analyzed. The few

discrepancies were discussed amongst the three analysts, and were ultimately unanimously agreed upon. The effect of bone mineral density, based upon a lateral view DEXA scan, was also assessed against failure values.

Motion analysis was performed using the above method (Section 2.10), and anterior vertebral bony motion with respect to the cage was assessed, as was cage motion with respect to the upper and lower vertebrae, for both translation and rotation in x, y, and z planes. Effect of bone mineral density was assessed for direction of cage subsidence.

After measurement of each endplate surface for each FSU tested, a ratio of known available graft surface area for each titanium mesh cage was made with the available bony endplate surface area, and expressed in table form (Table 3.5).

2.16 Statistical Analysis

Construct stiffness with intact disc, no disc, and one of the three cage patterns were compared using repeated measures ANOVA. Failure loads in axial compression for the 3 cage patterns were correlated with bone mineral density values of the adjacent vertebral bodies. One-factor analyses of covariance were conducted for the failure load with BMD as a covariate to assess the effects of cage position and vertebral level with

calculation of Pearson correlation coefficients. Alpha values were set at 0.05 for all tests of significance.

Calculation of sample size and power of the study was largely based upon historical studies (Jost et al, 1998; Lund et al , 1998). Rather than an equivalency study, all test of significance were performed to define a difference between the various effects of cage position.

3.0 Results

3.1 Construct Stiffness Characteristics

Stiffness properties for the constructs tested in this experiment, have been tabulated in Table 3.1. The mean stiffness of the FSU's tested was significantly different ($P < 0.0001$) with respect to having an intact disc, versus having no disc, or any of the three cage patterns (Figure 3.1) and showed no difference with respect to spinal level tested or cage position (Figures 3.2 and 3.3).

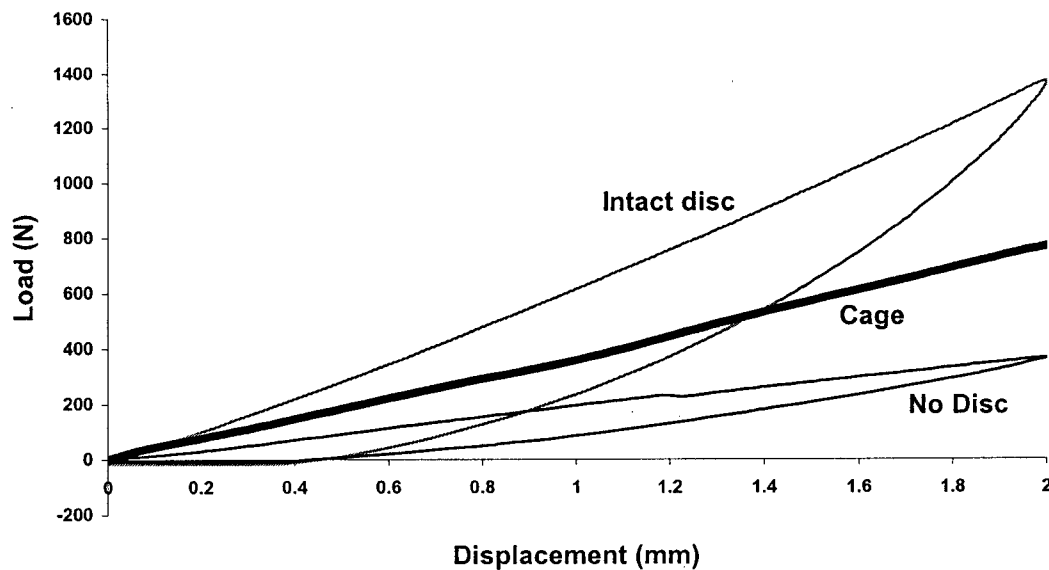


Figure 3.0 Typical appearance of a load-displacement curve (stiffness $-N/mm$, being the gradient of the forward loop) for an FSU with intact disc, no disc, and any of the three cage positions for the first 2mm of crosshead downwards displacement.

For all FSU's, the intact disc had the highest stiffness properties compared with either no disc, or any of the cage patterns. Without the disc, all FSU 's were on average only 20% as stiff as with the intact disc (all degenerate discs). With any of the three cage patterns, the FSU's averaged only 35% of the stiffness compared with the intact disc.

Stiffness values (mean-N/mm; SD-N/mm) for the 2 *posterolateral cage* position FSU's, measured at 2 mm of crosshead displacement, for the intact disc, without disc, and one of the three cage patterns were 855 N/mm, 503; 185 N/mm, 85; 354 N/mm, 122.

Stiffness values (mean-N/mm; SD-N/mm) for the 1 *central cage* position FSU's, measured at 2 mm of crosshead displacement, for the intact disc, without disc, and one of the three cage patterns were 1132 N/mm, 791; 220 N/mm, 158; 330 N/mm, 91.

Stiffness values (mean-N/mm; SD-N/mm) for the 2 *central cage* position FSU's, measured at 2 mm of crosshead displacement, for the intact disc, without disc, and one of the three cage patterns were 754 N/mm, 364; 133 N/mm, 33; 333 N/mm, 132.

Stiffness values related to FSU mean bone mineral density (based upon lateral view DEXA scans) are outlined (Table 3.2).

Table 3.1 Load-Displacement Values for each FSU- Stiffness (N/mm) and Failure (N).

	Specimen	Position	Stiffness- w/disc (N/mm)	Stiffness- w/o disc (N/mm)	Stiffness- w/cage (N/mm)	Failure Load (N)
1	1061L34	2P	749	214	362	2084
2	1061L45	1C	965	166	321	2377
3	1061L51	2C	633	138	347	1494
4	1067L34	1C	736	180	357	2211
5	1067L45	2C	624	157	161	1810
6	1067L51	2P	764	152	255	1848
7	1009L34	2C	872	132	370	1587
8	1009L45	1C	349	128	367	585
9	1009L51	2P	1501	355	585	2332
10	1027L34	2P	115	227	412	3402
11	1027L45	1C	2961	481	382	3617
12	1027L51	2C	1389	123	386	1912
13	1082L34	1C	1500	138	318	1837
14	1082L45	2P	783	182	412	3136
15	1082L51	2C	1028	208	565	1856
16	1031L34	2P	1641	241	424	3631
17	1031L45	2C	968	128	337	3052
18	1031L51	1C	1234	499	449	3933
19	1090L34	1C	659	76	197	789
20	1090L45	2C	720	106	110	2819
21	1090L51	2P	1202	107	221	1869
22	1030L34	2C	147	107	379	1888
23	1030L45	2P	523	108	326	1868
24	1030L51	1C	1334	211	410	2140
25	1036L34	2C	407	102	349	1056
26	1036L45	2P	414	78	191	1853
27	1036L51	1C	450	105	177	843
		MEAN	651	111	262	1681
		SD	388	40	105	665

Table 3.2 Bone Mineral Density for Upper and Lower Vertebra of each FSU. Percentage of Endplate Surface Area Covered by Cage(s) for each FSU.

Specimen	Position	BMD Upper-g/cm ²	BMD Lower-g/cm ²	BMD Average-g/cm ²	Area (%)	
1	1061L34	2P	0.465	0.558	0.512	21.8
2	1061L45	1C	0.558	0.593	0.576	19.6
3	1061L51	2C	0.593	0.716	0.655	18.5
4	1067L34	1C	0.675	0.369	0.522	24.6
5	1067L45	2C	0.369	0.422	0.396	23
6	1067L51	2P	0.422	0.56	0.491	22.7
7	1009L34	2C	0.438	0.506	0.472	21.8
8	1009L45	1C	0.506	0.566	0.536	18.9
9	1009L51	2P	0.566	0.62	0.593	18.4
10	1027L34	2P	0.639	0.68	0.66	17
11	1027L45	1C	0.68	0.902	0.791	19.9
12	1027L51	2C	0.902	1.147	1.025	18
13	1082L34	1C	0.189	0.18	0.185	22.3
14	1082L45	2P	0.18	0.333	0.257	19.9
15	1082L51	2C	0.333	0.547	0.44	19.2
16	1031L34	2P	0.729	0.754	0.742	18.1
17	1031L45	2C	0.754	1.043	0.899	16.1
18	1031L51	1C	1.043	0.928	0.986	13.5
19	1090L34	1C	0.42	0.382	0.401	17.8
20	1090L45	2C	0.382	0.518	0.45	15.4
21	1090L51	2P	0.518	0.595	0.557	16.1
22	1030L34	2C	0.52	0.543	0.532	16.1
23	1030L45	2P	0.543	0.644	0.594	16
24	1030L51	1C	0.644	0.788	0.716	18.1
25	1036L34	2C	0.187	0.184	0.186	19.9
26	1036L45	2P	0.184	0.232	0.208	20.5
27	1036L51	1C	0.232	0.345	0.289	20.9
		MEAN	0.403	0.470	0.437	18.9
		SD	0.169	0.189	0.182	2.1

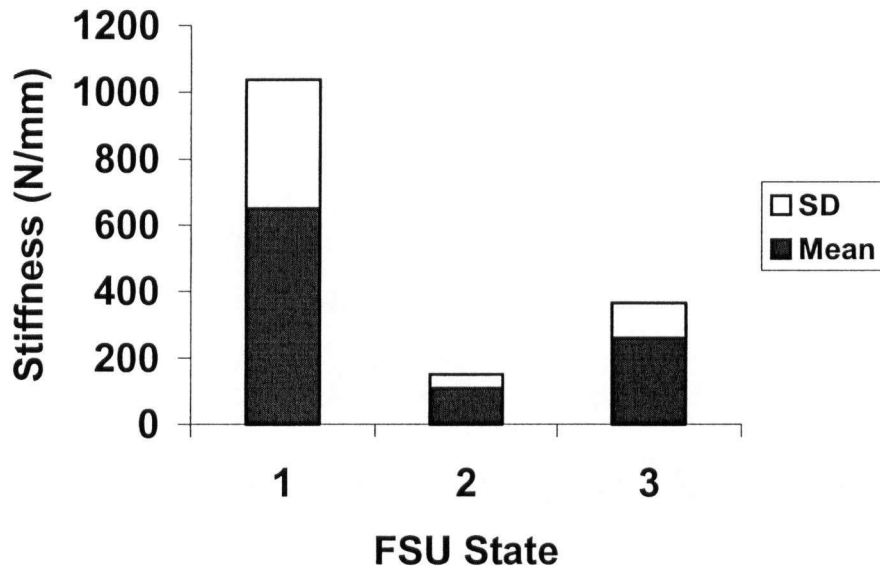


Figure 3.1 Mean stiffness (N/mm) and SD's for all FSU's tested with either Disc Intact (1), No Disc (2), or Cage(s) (3).

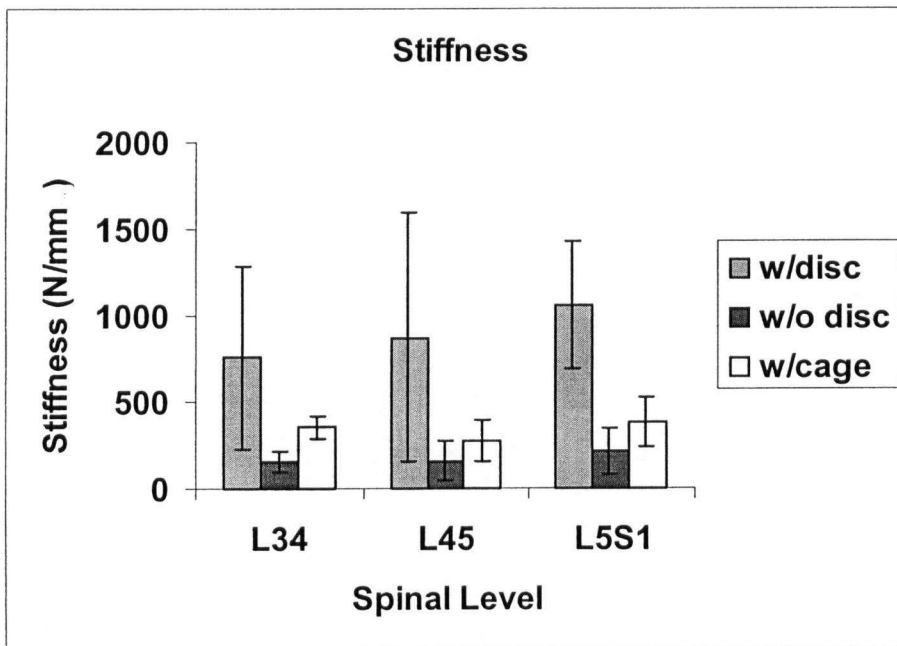


Figure 3.2 Stiffness properties of FSU's with intact disc, without disc, and with cage(s) positioned, with respect to spinal level. $P < 0.0001$ for with disc versus without disc or with cage(s).

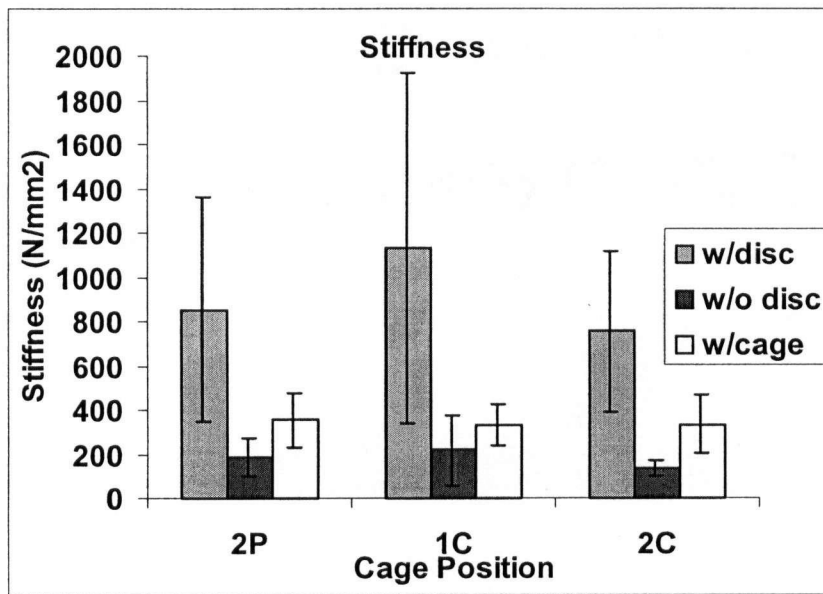


Figure 3.3 Stiffness properties of FSU's with intact disc, without disc, and with cage(s) positioned, with respect to cage position.

3.2 Construct Failure Characteristics

Failure properties for the 27 FSU's tested in this experiment are listed in Tables 3.1. Mean failure values correlated against bone mineral density (Figure 3.4) was shown to be significant ($r= 0.519$; $P=0.007$). Adjusted for cage position- 2 posterolateral, 1 central, or 2 central, the mean failure values again did not appear significantly different ($P= 0.20$) (Figure 3.5), yet there existed a trend towards higher mean failure values for the 2 posterolateral cage position. The failure values, adjusted for spinal level- L3/4, L4/5, L5/1, appeared closely related, without a significant difference ($P= 0.22$) (Figure 3.6).

The mean failure load (N) for the 2 posterolateral cage position FSU was about 20% higher than either 1 central or 2 central cages.

All FSU's tested have a load-displacement graph presented for values with the FSU with an intact disc, without the disc, and a curve for the destructive failure phase of the test with one of the three cage patterns (Appendix A). A representative graph (Figure 3.7) demonstrates the curves with a vertical line representing the failure point of the test with one of the three cage patterns.

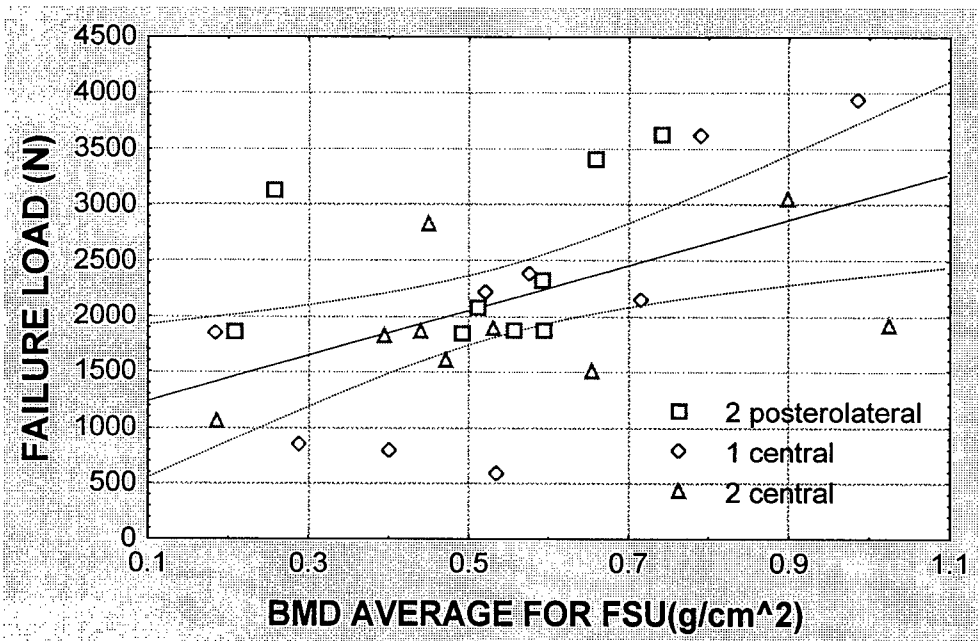


Figure 3.4 Failure load (N) for each FSU with a cage position tested (note- key for subgroups), versus average bone mineral density for that FSU ($r=0.519$; $P=0.007$).

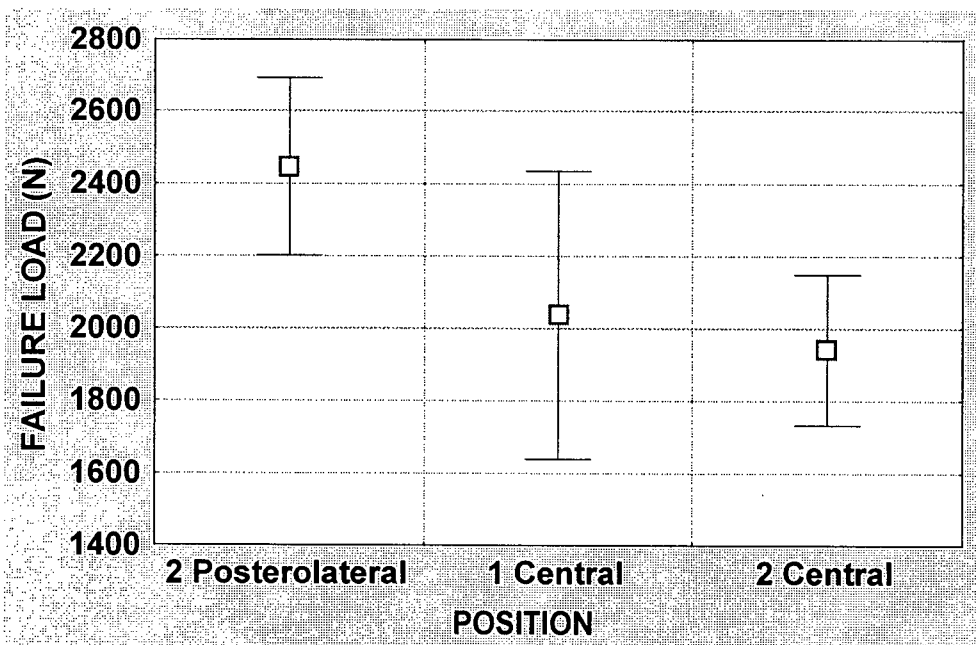


Figure 3.5 Mean peak failure loads (N) and standard error of the mean versus cage position ($P=0.20$).

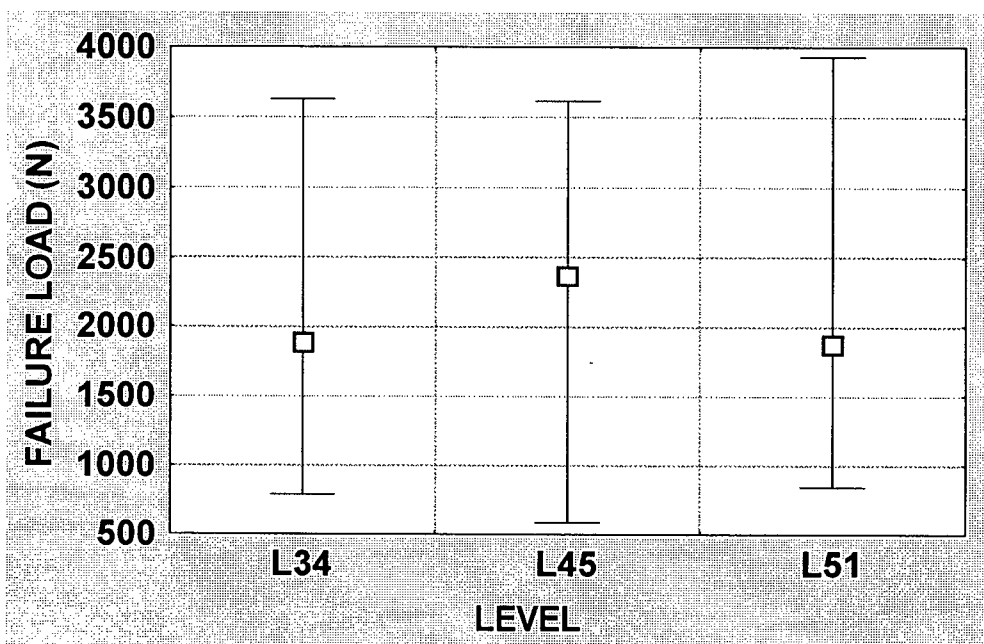


Figure 3.6 Mean peak failure loads (N) and ranges versus spinal levels (P=0.22).

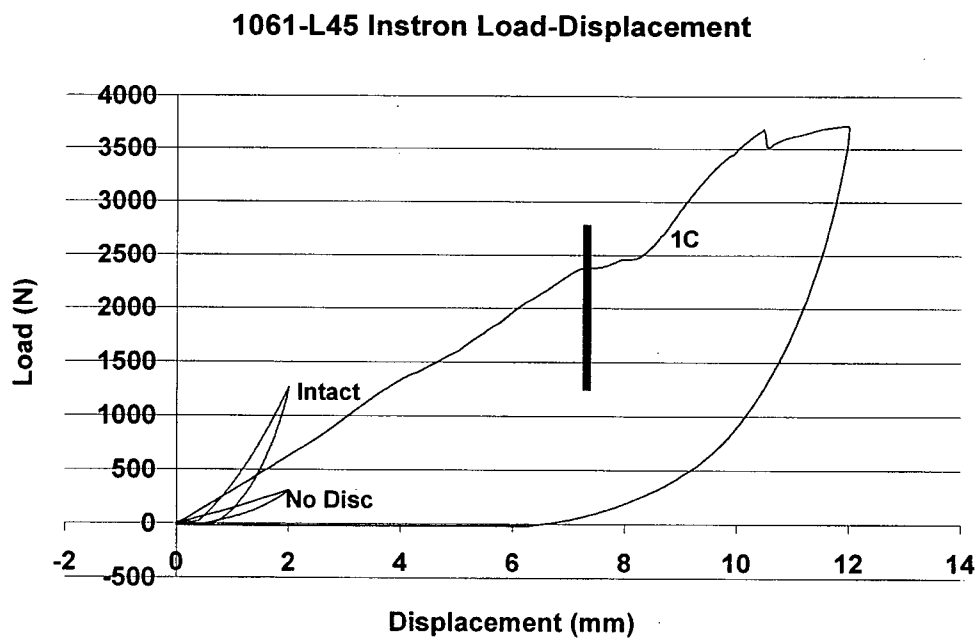


Figure 3.7 Specimen 1061 L4/5 - Load-displacement curves for disc intact, without disc, and 1 central cage (Failure marked with line).

3.3 Motion Analysis of Cage Subsidence

The results of this cage motion has been summarized in Table 3.3 for all cage positions tested. As has been outlined, the cages all underwent mostly downwards or upwards translation in the y plane (following the line of axial compression), with varying amounts of rotation on the x plane (forward flexion). As to whether it was mostly into the upper or lower adjacent endplate of the FSU, it appeared that there was *no* particular pattern of subsidence, either up or down, and this is best seen described in Table 3.4, as it pertains to the adjacent bone mineral densities. Lowest bone mineral density of a particular FSU tested in this study had no predictive role as to whether the cage subsides into one or the other vertebra of the FSU. Table 3.3 displays the values of direction of the double cages, and although not graphically presented in this thesis, it was found that again, *no* particular pattern for direction of cage subsidence was found into either of the endplates in the lumbosacral spine FSU's.

Figure 3.8 demonstrates the coordinate system used when describing either rotation or translation of the cage(s). Figure 3.9 is representative a graph that defines translation in the y plane (following the line of axial compression), with varying amounts of rotation on the x plane (forward flexion) of a single cage. These curves are presented for both movement into the upper and lower vertebra of the FSU. Graphs for all single cage failure tests can be found in Appendix B. Note that all curves include a load-displacement curve with failure points marked as vertical lines on the time axis.

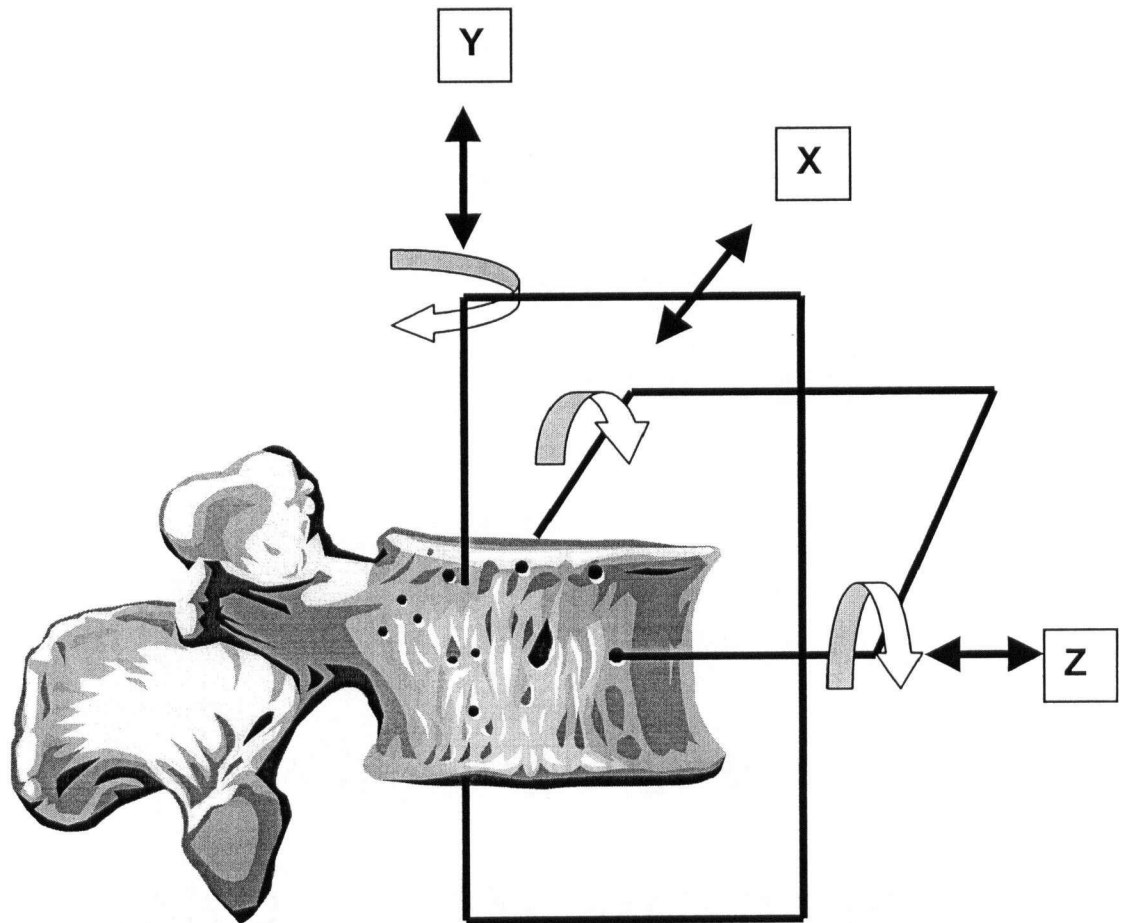


Figure 3.8 Cartesian coordinate system used in describing motion of cage and vertebrae for translation and rotation

1. 1061- L4/5 Single Cage

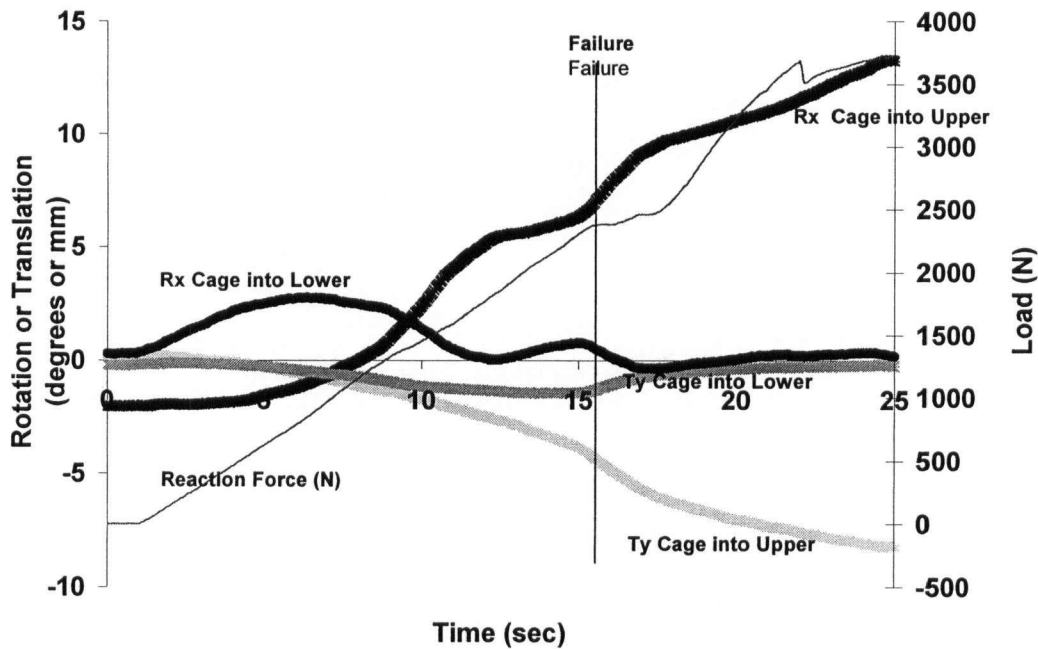


Figure 3.9 Translation (T) and Rotation (R) in both axial- up or down (y plane) and sagittal- forward flexion (x plane) of the single cage in specimen 1061, L4/5, versus time. Reaction Force (N) is plotted versus time, with a failure point as defined by the vertical line.

Qualitative Description for Specimen 1061, L4/5, 1 Central Cage- Pre-failure, the single cage is seen to mostly forward flex (Rx-Lower) into the lower vertebra (superior endplate of L5). Until 5 seconds, very little up or down subsidence occurs, with eventual preferential upwards (Ty-Upper) subsidence of the cage center point into the upper vertebra (inferior endplate of L4) to a depth of around 8 mm. The cage forward flexes (Rx- Upper) into the upper vertebra (inferior endplate of L4) to around 7 degrees at failure. At failure, there was less than 2 mm of subsidence downwards (Ty- Lower) into the lower vertebra (superior endplate of L5). Only small amounts of lateral side bending motion (Rz) and almost no spinning in the axial plane (Ry) was seen (Table 3.3).

Table 3.4 Effect of bone mineral density on cage subsidence. Lowest bone mineral density of each FSU tested with single cage versus direction of cage subsidence.

Specimen Level	Cage Position	BMD- Upper (g/cm ²)	BMD- Lower (g/cm ²)	BMD- Difference (g/cm ²)	Vertebra with Lowest BMD	Majority of Subsidence
1061 L45	1 central	0.558	0.593	0.035	Upper	Upper vertebra (L4)
1067 L34	1 central	0.675	0.369	0.306	Lower	Lower vertebra (L4)
1009 L45	1 central	0.506	0.566	0.06	Upper	Lower vertebra
1027 L45	1 central	0.68	0.902	0.222	Upper	Lower vertebra
1082 L34	1 central	0.189	0.18	0.009	Lower	Lower vertebra (L4)
1031 L51	1 central	1.043	0.928	0.115	Lower	Upper vertebra
1090 L34	1 central	0.42	0.382	0.038	Lower	Upper vertebra
1030 L51	1 central	0.644	0.788	0.144	Upper	Lower vertebra
1036 L51	1 central	0.232	0.345	0.113	Upper	Upper vertebra (L5)

Key: Bold characters represent either vertebra with the lower bone mineral density of the FSU, or a direction of cage subsidence into the lower bone mineral density.

3.4 Mode of Endplate Failure- Macro and Microscopic Qualitative Examination

The typical appearance of a failed vertebral endplate demonstrated an area of osseous endplate collapse into an underlying area of trabecular bone (Figure 3.10). The double cage position specimens revealed a similar appearance, and it appeared that endplate failure occurs in a discrete and well demarcated way, with the thin osseous endplate surface collapsing, leaving the surrounding endplate at the normal anatomical height. Seen on this macroscopic cross sectional image (Figure 3.10), the underlying trabecular bone appeared to be damaged with loss of the normal architecture.

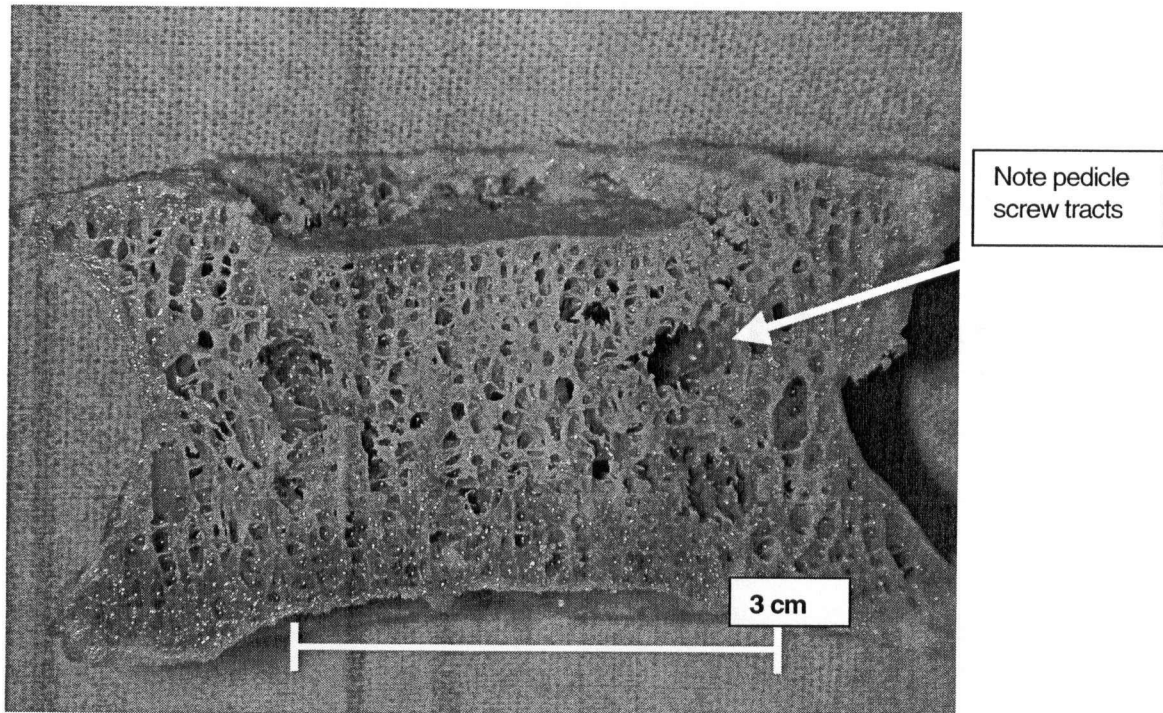


Figure 3.10 Macroscopic cross-section in coronal plane of Specimen –1067 L4 failed superior endplate post-test, single cage.

After examining all 54 endplates and the wafers produced from each, there appeared to be a distinct pattern of endplate failure and failure of the trabecular bone underlying the area of the compressed cage. For both large single cages and for the pairs of smaller cages, it appeared that the thin osseous component of the endplate is very cleanly sheared around its periphery, and then the central round portion of the "cookie-cut" endplate is then driven down into the underlying trabecular bone, with condensation of the immediate sub-endplate trabecular bone. The trabecular architecture distances are reduced and is shown in Figure 3.11 as an example.

It has also been noted that the underlying trabecular bone, beneath the area of endplate compressed by the graft filled cage, demonstrates a typical appearance of mass failure with the appearance of an elliptical area of trabecular bone that has subsided in total. Figure 3.12 demonstrates this finding, and is of an inferior endplate, away from the more superiorly placed pedicle screws.

The potential effect of a pedicle screw, more superiorly, on a cage placed on the upper endplate of a vertebra has been examined. Figure 3.13 highlights the same appearance of immediate sub-endplate bone condensation, and the appearance of a mass shear effect of the underlying bone.

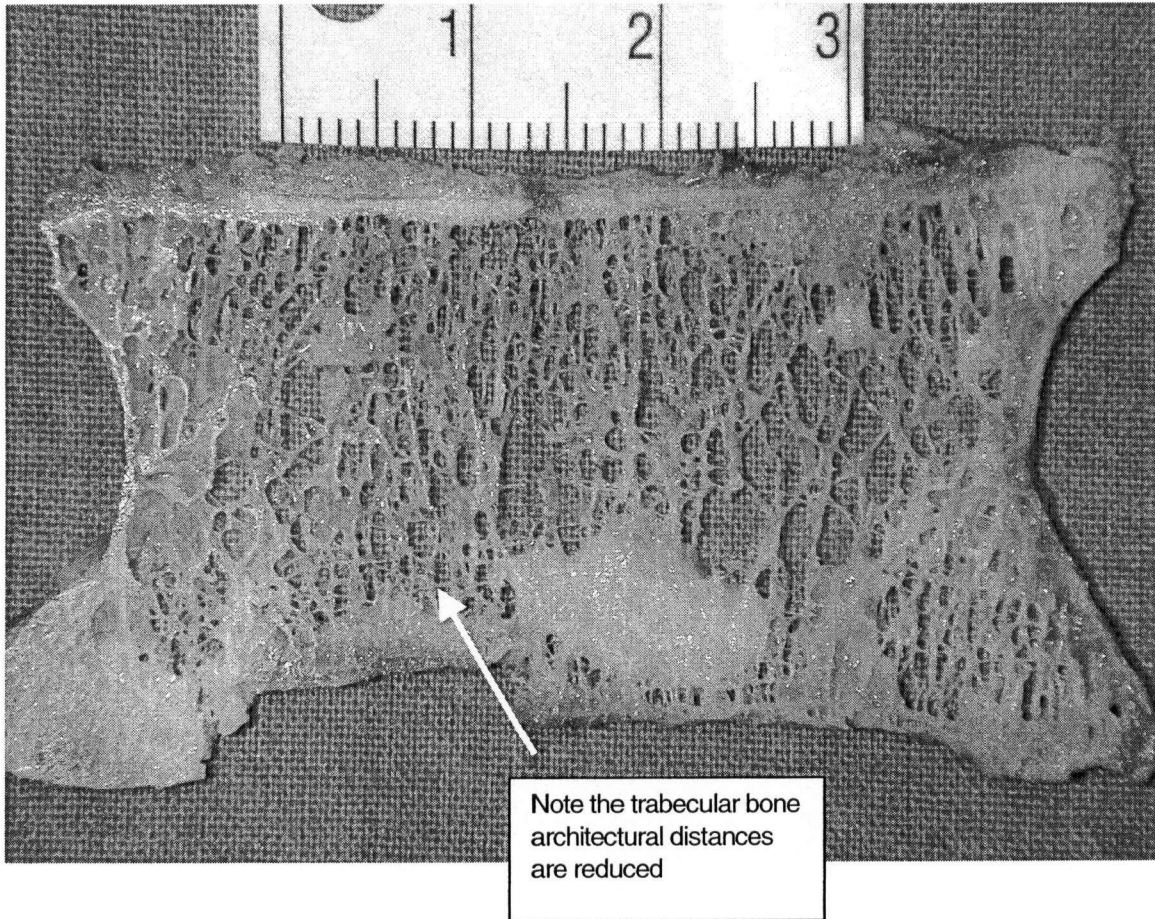


Figure 3.11 2 mm wafer of vertebral body of Specimen 1036- Inferior endplate of L3 highlighted (2 central cages tested). Note the cartilage capped superior endplate of L3 (not tested in experiment).

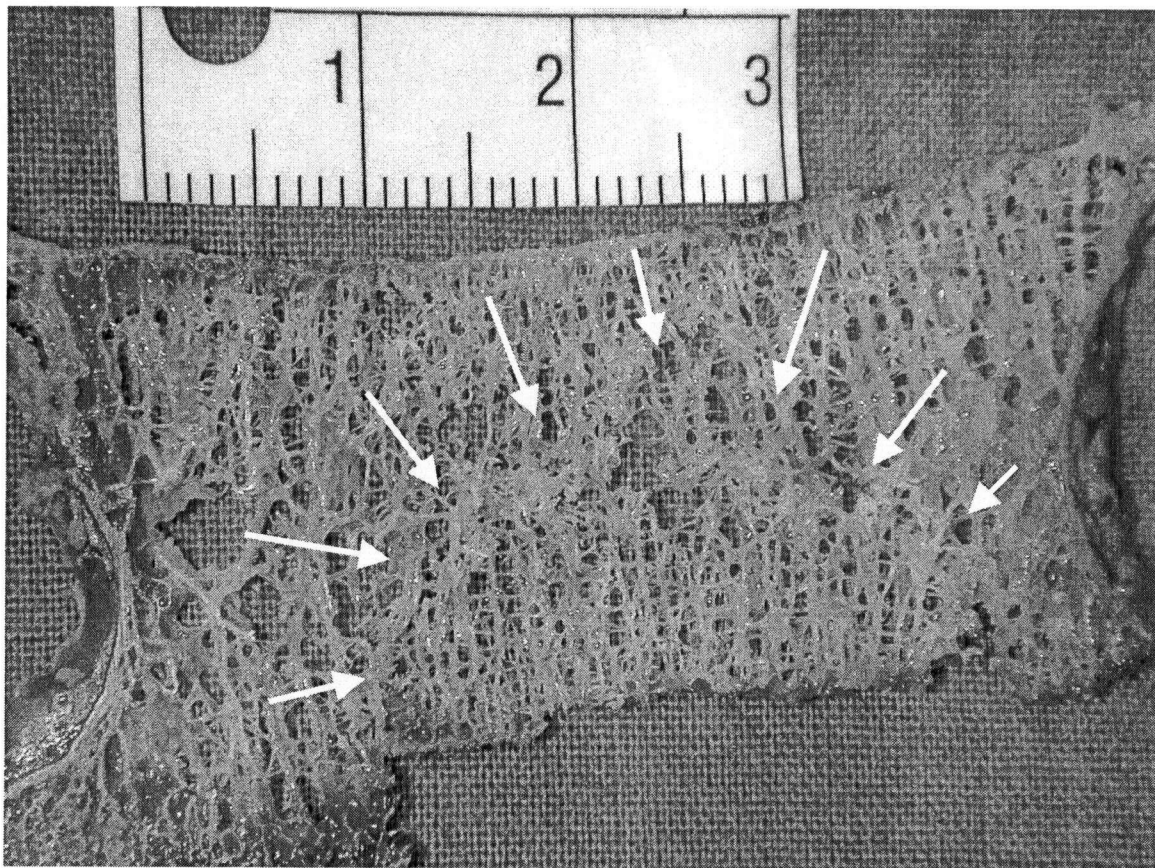


Figure 3.12 2 mm wafer of vertebral body in coronal plane of Specimen 1036- L5 inferior endplate highlighted (1 central cage). Note the margin of trabecular microfractures (arrows) and straight edges to the portion of osseous endplate that has subsided. Note the condensation of trabecular architecture in the immediate sub-endplate region, below the area of cage compression.

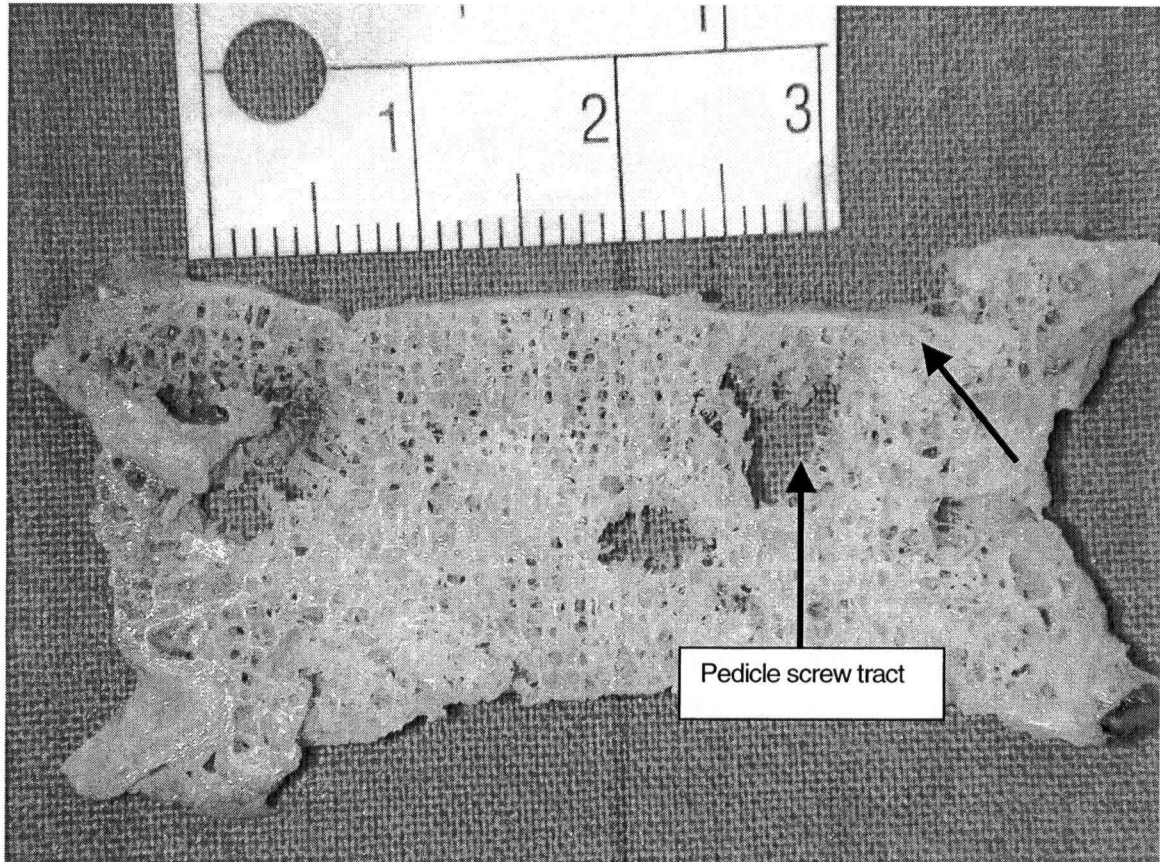


Figure 3.13 2mm wafer of vertebral body cut in coronal plane of Specimen 1067- L5 superior endplate highlighted (2 central cages). Note the pedicle screw tracts more superiorly, and the possible resistance offered to the subsiding cages. Note the consistent appearance of sub-endplate trabecular bone condensation (arrow).

3.5 FSU Intervertebral Disc Degenerative Grading Values

Table 3.5 summarizes the grade of disc degeneration of all the FSU's tested (27). The majority of discs were graded as very degenerate (Grade 4), with yellow-brown pigment and osteophyte formation around the disc margin.

Table 3.5 Intervertebral disc degenerative grades from 1-4 for each level tested for all specimens.

Specimen tested	Disc Grade		
	L3/4	L3/5	L5/S1
1061	4	4	4
1067	4	3	4
1009	4	4	4
1027	4	3	4
1082	4	4	4
1031	3	4	3
1090	4	3	4
1030	4	4	4
1036	3	4	3

Key: Vernon-Roberts and Pirie, (1973) Grading System: 1-mucoid nucleus and dense anulus; 2- non-uniform mucoid / fissured anulus; 3- fibrotic nucleus; 4- yellow-brown pigment / osteophytes.

4.0 Discussion

4.1 Effect of Cage Position Between Lumbosacral Endplates on Construct Stiffness and Failure in Compression

All types of implant surgery, whether it be large joint arthroplasty, or spinal arthrodesis types of surgeries utilizing implants, require a sound knowledge of anatomy and biomechanics to best position the implant. Despite the rapidly developing techniques of spinal disc replacement surgeries, spinal arthrodesis for many indications in both the paediatric and adult populations will remain essential as a surgical option. A better understanding of anterior spinal column biomechanics has led to the greater frequency of surgeries to the anterior column for both reconstruction and arthrodesis. Since the original use of tricortical iliac crest grafts, "keyed in" to the intervertebral body space anteriorly, there has been the development of a multitude of implantable cage devices, used for both anterior stand-alone and posterior approach interbody fusions. There has been a relative paucity of biomechanical data on what is the best position to place such cages.

Many good studies exist on the effect on compressive strength of various cage designs (Jost et al, 1998), yet few on the best biomechanical position of interbody cage placement. Polly et al, (2000), performed a study, that has been discussed, that examined the biomechanical effects of interbody cage (actually, polyethylene blocks) position within the disc space (anterior, middle, or posterior) and variations in posterior

rod diameter (4 or 5 mm) on construct stiffness, posterior rod strain, and interbody cage strain under a compressive flexural loading condition. The authors concluded that construct stiffness was highly sensitive to the position of cages in the sagittal plane and differences in stiffness increased in a linear fashion as cages were shifted from posterior to *anterior*. Using historical controls for pedicle screw systems alone (Cunningham et al, 1993), the authors also concluded that all interbody cage subgroups produced a significant increase in construct stiffness, ranging from six-fold for posteriorly positioned cages to 18-fold for anterior cages. However, the change in rod diameter (4 or 5mm) did not affect construct stiffness. Titanium mesh cages (Surgical Titanium Mesh®, DePuy Acromed, Raynham, MA) were used in their study with Group 1 having two 16mm diameter cages in either anterior, middle, or posterior positions, with 4 mm posterior rods; Group 2 the same, except with 5 mm posterior rods, and Group 3 with a single oval (28 mm x 35 mm) cage and 5 mm posterior rods. The authors concluded that a dual-cage interbody construct positioned *anteriorly* is biomechanically comparable to a single large cage positioned anteriorly. Importantly, the study used a *ultra-high molecular weight polyethylene block vertebrae model*, not human cadaver vertebrae.

It should always be remembered that biomechanical information remains invaluable with regards to predicting the performance of an implant, yet the biomechanically “best position” has to be achievable clinically. This notion detracts from results of all non-cadaver studies, and lends support to the formulation of the model used in this

experiment that closely simulates the commonly performed interbody fusion technique via a posterior approach.

Study results from Grant et al, (2001) post-dating the study described by Polly et al, (2000), raise the question of what effect does the osseous component of the endplate have on the compressive strength of interbody cage constructs, particularly with respect to regional variations in the strength of the lumbosacral endplates, and to the bone mineral density of the vertebral body. As previously discussed, Grant et al, (2001) have demonstrated a regional endplate strength difference in the lumbosacral spine, with posterolateral corners of the endplate being the strongest, the center being the weakest, and the anterior periphery being stronger than the center, yet weaker than the posterolateral corners. A significant difference was also reported between the inferior lumbar vertebral endplates and the sacral endplate, both being stronger than the superior vertebral endplates of the lumbar spine.

More recently, Oxland et al (2002) have presented results that look very carefully at the effect of endplate preparation. This most recent study examined the effects of decorticating half of the "cortical" portion of the bony endplate of seven human lumbar vertebrae (L3-L5). Indentation tests using a 3 mm hemispherical indenter were performed and stiffness and failure load at each site was determined. Conclusions were that removal of the vertebral endplate significantly reduced the local strength and stiffness magnitudes in the lower lumbar vertebral bodies (L3-L5), and that removing

the endplate caused greater strength loss posteriorly and laterally on the vertebral surface.

Many studies, including results such as those from Polly et al, (2000), Grant et al (2001), and the need for better biomechanical validation of currently used surgical techniques of transforaminal and posterior lumbar interbody fusion (TLIF and PLIF) have been the momentum behind the experiment reported in this thesis.

The mean stiffness of the FSU's tested was highly significantly different ($P < 0.0001$) with respect to having an intact disc, versus having no disc, or any of the three cage patterns. The intact disc state FSU's tested, surprisingly, had a very much higher stiffness measured at 2 mm of crosshead displacement compared with any of the three cage position states. This may reflect the effect of a large total surface area contact of mostly degenerative discs (Grade 3 or 4) (Table 3.6) (Vernon-Roberts and Pirie, 1973), allowing a high stiffness property of the posteriorly instrumented FSU.

Mean stiffness values for all of the FSU's tested dramatically dropped with removal of the disc. The stiffness values for any of the three cage positions then increased to approximately 35% of the initial stiffness with the intact disc, regardless of cage position or spinal level. The stiffness values for the FSU with cage(s) may seem initially less than expected, compared with the intact disc state, yet is probably higher than could be expected, if one considers that the mean surface area of the endplates covered by any of the cage patterns is only approximately 20%. The posterior instrumentation is likely

to have a significant contribution to the stiffness of the cage(s) positioned FSU's tested, however with a value that is not quantifiable, since this was not controlled for in the experiment. That is, there were no FSU's tested without posterior instrumentation. The justification for no matched control group of FSU's without instrumentation has been discussed, and is based mostly upon the fact that the two smaller cage positions tested are predominantly clinically used via posterior approaches, with supplemental segmental posterior instrumentation.

Adjusted for cage position- 2 posterolateral, 1 central, or 2 central, the mean failure values again did not appear significantly different ($P= 0.20$), yet trended towards higher mean failure values for the 2 posterolateral cage position. With results that are statistically unable to support this hypothesis, one can see a trend towards the 2 posterolaterally positioned cages being a superior position over 2 central or 1 central. Reasons to explain differences between the results of Grant et al, (2001), may include the nature of the indentation tests that she performed, with a 3 mm indenter versus a relatively large graft packed titanium mesh cage, or perhaps an insufficient sample size for sufficient statistical power. The difference in cage/graft surface area compared to the smaller 3 mm indenter, seems significant, with the distribution of forces across a greater area of the endplates, with possible overlap of anatomical strength regions.

Despite a statistical difference not being shown, the fact remains that an equivalent state exists for stiffness and failure properties of the three cage positions tested. Clinically, this should be useful information to those performing such surgeries, with

knowledge of the acceptability of all three positions, and the achievement of mean failure load values that permit normal mobilization and rehabilitation in the immediate post-operative period and months after the surgery while a biological fusion is achieved. Moreover, the equivalent and satisfactory results of the 2 posterolateral cage position supports the technique employed in transforaminal lumbar interbody fusion (Harms et al,1997), and posterior lumbar interbody fusion utilizing two smaller titanium mesh cages in a posterolateral position.

4.2 Effect of Bone Mineral Density

Bone mineral density has been well established as a significant factor in the compressive strength performance of interbody cages used in the lumbosacral spine (Jost et al, 1998). Bone mineral density has been shown to be statistically significant in the stiffness properties, and mean failure values for all cage positions tested in this experiment.

Mean failure values correlated against bone mineral density (Figure 3.12) was shown to be significant ($r= 0.52$; $P= 0.007$). These results support what has been previously reported in the literature and add support to the notion that pre-operative measurement of BMD may be an effective tool in predicting settling around interbody cages (Jost et al, 1998). More specifically, the use of lateral DEXA scanning in this experiment supports the use of *lateral* BMD scans using DEXA in the accurate determination of the condition

of the bone at the immediate region where the vertebral body is in contact with spinal interbody devices (Goh et al, 2001).

The relationship between bone mineral density and strength in compression of interbody fusion constructs has been well established and discussed with respect to this experiment. Bone mineral density and direction of single cage subsidence has been outlined, and appears *not* show a constant relationship. One would expect that the cage would move into the vertebra of a functional spinal unit that has the lowest bone mineral density. However, results of single cage subsidence in this experiment reveal that only four of the nine single cages moved into the vertebra with the lowest bone mineral density. A review of the *double cage* combinations reveals a similar *unpredictable* direction of cage motion with respect to the vertebra with the lowest bone mineral density.

Possible explanations for this include a sample size that is too small, or the fact that the differences between bone mineral densities of the two vertebra (based upon a lateral DEXA scan) are usually small (Table 3.4).

4.3 Direction of Interbody Cage Subsidence in the Lumbosacral Spine

Radiographic evidence of cage subsidence into adjacent vertebral endplates of an interbody fusion site can be noted on weight-bearing post-operative lateral radiographs of the lumbosacral spine, and may be associated with symptoms, including pain. These findings would usually suggest clinical failure of the attempt to reconstruct the interbody height of the anterior spinal column, and may continue to be symptomatic, also with the possibility of a failed spinal arthrodesis. Despite this well reported unfortunate clinical occurrence, little has been reported on either the possible preferential direction of cage subsidence.

The relevance of such a question- *which direction do cages preferentially subside?*, pertains to the concept of there being an anatomical, regional strength map for the lumbosacral endplates, and a difference in the strength of the inferior lumbar endplate, being stronger, than the superior lumbar endplate (Grant et al, 2001). One could hypothesize that an interbody cage in the lumbosacral spine is more likely to subside into the superior lumbar endplate of the vertebra below in the FSU, as supported by Grant's et al, (2001) work, with some degree of uncertainty at the L5/S1 FSU level due to the fact that the sacral endplate is close in strength to the inferior endplate of L5.

After an extensive literature review, it appears that no other published study has looked so accurately at the direction of cage motion in an interbody fusion biomechanical experiment. This experiment has employed the use of an optoelectric camera system

(Optotrak 3020, Northern Digital Inc., Waterloo, Canada) and light emitting diodes attached carefully to the cages to allow tracking of the cages throughout the compression test. Using a previously unreported technique of digitizing three points of each titanium mesh cage and the calculation of a necessary center point of the cage in space, the experiment performed involved the tracking of the cages through six degrees of freedom, including rotation and translation.

As to whether it was mostly into the upper or lower adjacent endplate of the FSU, it appeared that there was *no* particular pattern of subsidence, either up or down, and this is best seen described in Table 3.4, as it pertains to the adjacent bone mineral densities. It was found that *no* particular pattern for direction of cage subsidence was found into either of the endplates in the lumbosacral spine FSU's, for single or double cage patterns.

Not being able to detect a trend, nor supporting the hypothesis that the cages should preferentially subside into the superior lumbar endplates in a test lumbosacral FSU (that is, the endplate below the cage *in situ*), may be explained by the sample size used in this experiment, or it may be that there is no preferential subsidence, as a measure of a strength difference between superior and inferior endplates, of titanium mesh cages. This possible non-preferential subsidence state may be explained by the fact that the area of the cage and bone graft is large enough to negate any smaller anatomical regional differences in strength of the endplates, or it may be something intrinsic to the design of the cylindrical mesh cage packed with bone graft.

4.4 Theoretical Mode of Endplate Failure with Bone Graft Packed Titanium Mesh Cages

Mode of endplate failure from an anatomical and biomechanical perspective appears to not have been described after searching all published literature. The findings of this anatomical study of sectioning the failed endplates and vertebral bodies into 2 mm wafers, through the area of endplate subsidence, has revealed several consistent findings.

The cylindrical titanium mesh cage packed with bone graft, appears to offer considerable resistance to the endplate surface, and does permit some preferential "cookie-cutting" of the periphery of the cage. However, the interesting mode of failure of the endplates for both larger single and smaller double cage patterns, appears to be that of a neat cleavage by the rim of the mesh cage of the bony endplate, and then subsidence of the thin osseous portion of the endplate beneath the cage into the underlying trabecular bone. The deeper portions of the underlying trabecular bone appears to subside in a mass effect with what appears to be shear type forces, leaving an elliptical fracture line at the base of the compressed trabecular bone mass. This pattern appears to the same whether into upper or lower endplate.

Importantly, it appears that the superior endplate compression tests, that compressed a cage into regions that overlie the more superiorly placed pedicle screws in the vertebral body, may have resulted in the trabecular bone shear driven subsidence to have been

restricted by the nearby screw. This potential effect has been at least standardized throughout the experiment, and may have greater clinical applications, this potential supporting effect of the pedicle screw being used to the surgeons advantage-particularly in osteoporotic bone. Interestingly, when assessing the direction of cage subsidence, there was not a majority of cages subsiding into the inferior endplate (upper vertebra) of the FSU's being tested. This may have been predicted, if one assumes that the pedicle screws nearer to the upper endplate of a vertebral body, do provide some resistance to trabecular bone collapse under a cage packed with graft.

4.5 Support for the Proposed Lumbosacral Endplate Strength Map

Grant et al (2001) has reported there being a regional variation in strength in compression of the lumbosacral vertebral endplates. This study has been well discussed (Section 1.3.3) and formed a large proportion of the basis to the experimental design in this study.

After performing the indentation tests, Grant et al (2001), concluded that both the failure load and stiffness varied significantly across the endplate surfaces ($p < 0.0001$), with the posterolateral corners of the endplate being stronger and more stiff than the central regions. The sacral and inferior lumbar endplates were both found to be stronger than the superior lumbar endplates (sacrum $p = 0.054$); (inferior $p = 0.008$) but they themselves were not significantly different. The authors also concluded that that the center of the bone, where implants are

often placed, is the weakest part of the lumbar endplates and is not the strongest region of the sacral endplate.

The results of this experiment have shown that there exists a trend that two posterolaterally positioned cages in the posteriorly instrumented interbody fusion model tested, appears to have a higher mean failure load in axial compression. This finding, which was not statistically significant, permits a biomechanical validation of that position for two smaller cages in such surgeries as transforaminal lumbar interbody fusion (TLIF).

Highlighting the fact that Grant et al, (2001) used a 3 mm diameter indenter that was compressed only 3 mm into the lumbosacral endplates, it is important to contrast the use of a much larger surface area cage/graft- "indenter", used in this experiment. The fact remains that larger areas of regional overlap may have existed in this study, and more subtle compression strength differences, as suggested by Grant et al, (2001), may have been masked.

It appears that at the very least, a satisfactory biomechanical validation of a current surgical technique, such as the use of two small cages in TLIF surgery, has been achieved through the results of this project. Moreover, the concept of a regional lumbosacral endplate strength map that has variation, has been at least supported in a highly clinically flavored biomechanical model that exploits the possibilities of placing cages in an anatomically significantly different position.

4.6 Strengths and Weaknesses of the Experimental Model

Perhaps the greatest *strength* of the study was that the model so closely simulated what is achieved with posteriorly approached lumbar interbody fusion surgeries such as transforaminal lumbar interbody fusion (TLIF) and posterior lumbar interbody fusion (PLIF). The model also simulated a surgery that may employ a separate anterior approach and interbody fusion cage placement, with then the addition of posterior segmental instrumentation, through a posterior approach. Although not exactly a posteriorly approached interbody fusion model, with the preservation of the facet joints posteriorly, the model permitted very accurate endplate preparation and accurate cage placement via an anteriorly approached disc space. *With the addition* of rigid posterior segmental instrumentation, it was thought that the biomechanical contribution and effect of the facet joint would become negligible. The benefits of accurate endplate preparation, and cage positioning – being a main question in the study, was deemed to outweigh the need to partially destroy the posterior pair of facet joints.

Another *strength* of the study was the fact that it addressed a biomechanical question that had never been addressed by using a human cadaver spine model, as opposed to other studies that have looked at cage position in compression using ultra-high molecular weight polyethylene (Polly et al, 2000), with such a closely simulated surgical technique and implant insertion. Using surgical

descriptions based on that of Harms et al, (1997), and Lowe and Tahernia, (2002), with details down to even the most commonly used mesh cage sizes, the use of titanium mesh cages and standard prepared graft, as well as commonly used segmental posterior pedicle screw fixation, the human cadaver experiment has come close to reflecting what is done in the operating room. Local experience at BC Children's Hospital, with such a surgical technique as is used for higher grades of spondylolisthesis at the lumbosacral junction, and experience at Vancouver General Hospital with surgeries employing TLIF and PLIF techniques, has also influenced the formulation of this experiment.

Assessment of interbody cage motion during axial compression is also a *strength* of the model. Such accurate assessment of both translation and rotation of the cage(s) during compression has never been published, according to our review of the literature, and has allowed a better understanding of how endplate failure may occur during axial compression.

A *weakness* of the experiment was perhaps the sample size (27 FSU's). Although by published biomechanical standards, the number of FSU's used is at the higher end of most experimental sample size designs, it could always be suggested that more samples tested may have rendered a statistically significant difference for both the effect of a possibly superior posterolateral cage position. Power calculation before the study was performed and, as with most laboratory

based bench top biomechanical studies with uncertain outcomes, historical sample sizes were heavily relied upon.

Another potential *weakness* of the study was not having a cage position that included either one single or two cages anterior in the intervertebral space. Due to sample size limitations mostly, and the fact that this position is not often clinically utilized, the decision was made not to include this cage position. Acknowledging the results of the study presented by Polly et al (2001), that concluded that all interbody cage subgroups that they studied, produced a significant increase in construct stiffness, ranging from six-fold for posteriorly positioned cages to 18-fold for anterior cages. The obvious effect of placing a more anteriorly placed graft/cage to “hold-up” the anterior column at the end of a pedicle screw combination that has a center of gravity for that FSU closer to the screw-rod junction, is clearly understood. However, the relative difficulty in preparing this region of anterior endplate, especially from a posterior approach, and the benefit of placing bone graft more anteriorly, so it can be seen on a post-operative lateral radiograph (“sentinel graft”), remain clinical reasons as to not placing cages in a more anterior position.

4.7 Clinical Correlations to Posterior Lumbar Interbody Fusion (PLIF) and Transforaminal Lumbar Interbody Fusion (TLIF)

A potential benefit of two smaller sized, round, titanium mesh cages is the fact that they can be inserted posteriorly through monoportal, transforaminal, approaches to achieve anterior interbody fusion (Harms et al, 1997); Lowe and Tahernia, 2002). The advantage of this transforaminal posterior interbody fusion (TLIF) technique is the ability to insert two smaller round cages into the interbody space, through a unilateral posterior bony element exposure, preserving contralateral lamina for bone graft surface area. The second cage is rolled “blindly” into the far, unexposed side of the interbody space. Specifically, this requires only one whole, or part of one, facet joint to be excised at the disc space level that is being arthrodesed. Assuming neural foramen decompression is not required on the other non-excised side, the TLIF technique, with the monoportal approach decreases the risk of a neural injury to the unexposed spinal nerve, and minimizes the risk of excessive cauda or conus retraction by having intact midline structures (interspinous ligament).

The results of this study have biomechanically supported the use of three cage positions, with emphasis on the satisfactory strength in compression offered by two posterolaterally positioned cages, placed via a posterior approach, with supplemental segmental posterior pedicle screw fixation.

4.8 Future Directions and Further Study

It would seem a logical progression to direct further study, which utilizes human cadaver spine functional spinal units, towards a model that assesses similar cage positioning questions via an anterior approach with and without anterior instrumentation- such is anterior lumbar stand-alone surgeries. The other potential focus of such a study could be having eccentrically loaded compressive forces, with various cage positions, so as to simulate a spinal deformity in either sagittal, or especially coronal plane deformities, such as found in a scoliosis. Use of titanium mesh cages, especially in the upper lumbar spine, has become common place for many surgeons who deal with correction of scoliosis. The cages permit possible correction of the coronal plane deformity, and assist in restoration of the normal lumbar lordosis, in the sagittal plane. Considering the complexity of forces that must go through such regions of spinal deformity, it would be useful to know what is the best position to place a cage(s), and whether even a single cage, say in the posterolateral corner of a cleared disc space, could support the compressive force going through that region of spine, and resist subsidence. All such study results could be correlated against lateral view DEXA scan bone mineral density values, which has been well established as a useful tool in possible prediction of compressive strengths of interbody fusion constructs.

5.0 Conclusions

The *compressive stiffness* of the construct at all spinal levels were significantly higher with the intact disc (897N/mm; SD 539) compared to without the disc (175N/mm; SD 83), and with any of the three cage patterns (334N/mm; SD 109), and these differences were highly significant ($p= 0.0001$). This result supports the concept that an intact disc, despite it being highly degenerate, can provide a high level of physiological strength and stiffness to the *in vivo* FSU. With any of the three cage patterns tested, only one-third of the stiffness of the intact disc state was achieved, albeit with only around 20 % of the surface area of the endplates covered by cage/graft.

Mean *failure loads* in compression for the three cage positions ranged between 2000N and 2500N and were not significantly different, though tended to be higher for the 2 posterolateral cage position ($p=0.20$). This supported the findings of a study (Grant et al, 2001) that has found a regional difference in compressive strength of the lumbar vertebral endplates, with the posterolateral regions being the strongest. There was no significant difference for mean failure loads versus spinal level tested.

Motion analysis of the cage- either single or double combinations, revealed no trend for either superior or inferior subsidence into the endplates. The mode of endplate failure was assessed anatomically, and appears to involve the local collapse of the bony endplate under the graft filled cage, and a sharp sectioning of the bony endplate with

the edges of the cylindrical mesh cage. Underlying trabecular bone appeared to subside with a mass effect with a shear type fracture pattern of the trabecular architecture.

Bone mineral density values did relate significantly to the peak failure loads for all cage patterns. Bone mineral density did not appear to be predictive in what direction a cage would subside, using the model described in this experiment.

Failure loads in compression in excess of 2000N, which are values encountered immediately post spinal surgery, were achieved with all three of the cage positions described in the posteriorly instrumented cadaver spine model tested. The cage/graft to endplate surface ratio was approximately 20% for all FSU's. These values lend support to the biomechanical validity of PLIF and especially TLIF type surgeries, with the often preferred placement of two smaller posterolaterally positioned titanium mesh cages (Harms et al, 1997). Results of the mode of endplate failure may promote further study and provide a better understanding of how implants that support the anterior bony spinal column may fail. Avoidance of subsidence, whether it be in attempts to reconstruct and arthrodesis the anterior spinal column, or whether it be for more recently popularized attempts at seating an implant for disc replacement surgery, will remain a fundamental objective for the spinal surgeon.

6.0 References

1. Abumi, K., M. M. Panjabi, et al. (1990). "Biomechanical evaluation of lumbar spinal stability after graded facetectomies." Spine 15(11): 1142-7.
2. Amstutz, H. C. and H. A. Sissons (1969). "The structure of the vertebral spongiosa." J Bone Joint Surg Br 51(3): 540-50.
3. Anglin, C., P. Tolhurst, et al. (1999). "Glenoid cancellous bone strength and modulus." J Biomech 32(10): 1091-7.
4. Bagby, G. W. (1988). "Arthrodesis by the distraction-compression method using a stainless steel implant." Orthopedics 11(6): 931-4.
5. Behrens, J. C., P. S. Walker, et al. (1974). "Variations in strength and structure of cancellous bone at the knee." J Biomech 7(3): 201-7.
6. Blechner, M.H., Kanim, L.E.A., Patel, M., Grewal, R, Delamarter, R.B., Dawson, E.G., "Clinical evaluation of the distractive properties of interbody cages for anterior spinal fusion." Meeting of the Orthopaedic Research Society, 1999, p 1001.
7. Blume, H.G., Rojas, C.H. (1981) " Unilateral lumbar interbody fusion (posterior approach) utilizing dowel graft." J Neurol Orthop Surg 2: 171-175.
8. Bogduk, N. (1997). "Clinical anatomy of the lumbar spine and sacrum". 3rd edition, Churchill Livingstone, London.
9. Boos, N., D. Marchesi, et al. (1993). "Treatment of severe spondylolisthesis by reduction and pedicular fixation. A 4-6-year follow-up study." Spine 18(12): 1655-61.
10. Boxall, D., Bradford, D.S., Winter, R.B., Moe, J.H., (1981) "Management of severe spondylolisthesis in children and adolescents." J Bone Joint Surgery 63A: 619-626.
11. Brantigan, J. W., A. D. Steffee, et al. (1991). "A carbon fiber implant to aid interbody lumbar fusion. Mechanical testing." Spine 16(6 Suppl): S277-82.
12. Brodke, D. S., J. C. Dick, et al. (1997). "Posterior lumbar interbody fusion. A biomechanical comparison, including a new threaded cage." Spine 22(1): 26-31.

13. Buttermann, G. R., T. A. Garvey, et al. (1998). "Lumbar fusion results related to diagnosis." Spine 23(1): 116-27.
14. Calvo, L.J. (1957). "Observations on the growth of the female adolescent spine and its relation to scoliosis." Clin Orthop 10: 40-46.
15. Chen, D., L. A. Fay, et al. (1995). "Increasing neuroforaminal volume by anterior interbody distraction in degenerative lumbar spine." Spine 20(1): 74-9.
16. Closkey, R. F., J. R. Parsons, et al. (1993). "Mechanics of interbody spinal fusion. Analysis of critical bone graft area." Spine 18(8): 1011-5.
17. Cloward, R.B. (1953). "The treatment of ruptured intervertebral discs by vertebral body fusion." J Neurosurg 10: 154-168.
18. Cunningham, B. W., Oda, I., Haggerty, C.J., McAfee, P.C.,(1999) "Biomechanical effects of posterior rod diameter and anterior column reconstruction on multisegmental spinal stability." Trans Orthop Res Soc 24: 1011.
19. Cunningham, B. W. and D. W. Polly, Jr. (2002). "The use of interbody cage devices for spinal deformity: a biomechanical perspective." Clin Orthop(394): 73-83.
20. Cunningham, B. W., J. C. Seftor, et al. (1993). "Static and cyclical biomechanical analysis of pedicle screw spinal constructs." Spine 18(12): 1677-88.
21. Dick, W. T. and B. Schnebel (1988). "Severe spondylolisthesis. Reduction and internal fixation." Clin Orthop(232): 70-9.
22. Eck, K. R., K. H. Bridwell, et al. (2002). "Mesh cages for spinal deformity in adults." Clin Orthop(394): 92-7.
23. Edwards, C. C. and D. S. Bradford (1994). "Instrumented reduction of spondylolisthesis." Spine 19(13): 1535-7.
24. Eyring, E. J. (1969). "The biochemistry and physiology of the intervertebral disk." Clin Orthop 67: 16-28.
25. Flynn, M. J. and D. D. Cody (1993). "The assessment of vertebral bone macroarchitecture with X-ray computed tomography." Calcif Tissue Int 53(Suppl 1): S170-5.

26. Freebody, D., R. Bendall, et al. (1971). "Anterior transperitoneal lumbar fusion." J Bone Joint Surg Br 53(4): 617-27.
27. Freeman, B. L., 3rd and N. L. Donati (1989). "Spinal arthrodesis for severe spondylolisthesis in children and adolescents. A long-term follow-up study." J Bone Joint Surg Am 71(4): 594-8.
28. Frennered, A. K., B. I. Danielson, et al. (1991). "Midterm follow-up of young patients fused in situ for spondylolisthesis." Spine 16(4): 409-16.
29. Gaines, R. W. and W. K. Nichols (1985). "Treatment of spondyloptosis by two stage L5 vertebrectomy and reduction of L4 onto S1." Spine 10(7): 680-6.
30. Gill, K. (1989). "Introduction to interbody fusion." In: Lin, P.M., and Gill, K., Eds. Lumbar interbody fusion, Rockville, Aspen, Maryland, pp 3-7.
31. Glazer, P. A., O. Colliou, et al. (1997). "Biomechanical analysis of multilevel fixation methods in the lumbar spine." Spine 22(2): 171-82.
32. Goh, J. C., J. S. Tan, et al. (2001). "Linear correlation between axial and lateral bone mineral density of lumbar vertebrae." J Clin Densitom 4(1): 31-6.
33. Gooding, C.A, Neuhauser, E.B.D. (1965) "Growth and development of the vertebral body in the presence and absence of normal stress." Am J Roentgenol 93 :388-394.
34. Grant, J. P., T. R. Oxland, et al. (2001). "Mapping the structural properties of the lumbosacral vertebral endplates." Spine 26(8): 889-96.
35. Harms, J., Jeszensky, D., Stohize, D., et al, (1997) "True spondylolisthesis reduction and more segmental fusion" In: Bridwell, K.H., and De Wald, R.L., eds, The Textbook of Spinal Surgery, 2nd Ed, Philadelphia, Lippincott-Raven, 1337-1347.
36. Hanson, D.S., Antonacci, M.D., Heggeness, M.H. "A histologic study of human vertebral endplates." Presented at the 9th annual meeting of the North American Spine Society, October, 1994.
37. Harris, I. E. and S. L. Weinstein (1987). "Long-term follow-up of patients with grade-III and IV spondylolisthesis. Treatment with and without posterior fusion." J Bone Joint Surg Am 69(7): 960-9.
38. Hoffer, Z., Oxland, T.R., Nydegger, T., Nolte, L.P. "Cyclic loading decreases the stabilization provided by lumbar interbody cages." Presented at the International Society for the study of the Lumbar Spine, 1998, p 70.

39. Hollowell, J. P., D. G. Vollmer, et al. (1996). "Biomechanical analysis of thoracolumbar interbody constructs. How important is the endplate?" Spine 21(9): 1032-6.
40. Hoshijima, K., R. W. Nightingale, et al. (1997). "Strength and stability of posterior lumbar interbody fusion. Comparison of titanium fiber mesh implant and tricortical bone graft." Spine 22(11): 1181-8.
41. Ito, M., K. Hayashi, et al. (1993). "Relationship of osteophytes to bone mineral density and spinal fracture in men." Radiology 189(2): 497-502.
42. Johnson, J.R., Kirwin, E.O.,(1983) "The long term results of fusion in situ for severe spondylolisthesis." J Bone Joint Surgery 65B : 43-46.
43. Jost, B., P. A. Cripton, et al. (1998). "Compressive strength of interbody cages in the lumbar spine: the effect of cage shape, posterior instrumentation and bone density." Eur Spine J 7(2): 132-41.
44. Kandziora, F., R. Pflugmacher, et al. (2001). "Biomechanical comparison of cervical spine interbody fusion cages." Spine 26(17): 1850-7.
45. Keller, T. S., T. H. Hansson, et al. (1989). "Regional variations in the compressive properties of lumbar vertebral trabeculae. Effects of disc degeneration." Spine 14(9): 1012-9.
46. Keller, T. S., E. Moeljanto, et al. (1992). "Distribution and orientation of bone in the human lumbar vertebral centrum." J Spinal Disord 5(1): 60-74.
47. Kuslich, S.D., Oxland, T.R., Jansen, R.C., Ulstrom, C.L. "The BAK interbody fusion system;early clinical results of a treatment for chronic low back pain." Presented at North American Spine Society annual meeting, 1993, p 175.
48. Kuslich, S. D., C. L. Ulstrom, et al. (1998). "The Bagby and Kuslich method of lumbar interbody fusion. History, techniques, and 2-year follow-up results of a United States prospective, multicenter trial." Spine 23(11): 1267-78; discussion 1279.
49. Lee, C. K., P. Vessa, et al. (1995). "Chronic disabling low back pain syndrome caused by internal disc derangements. The results of disc excision and posterior lumbar interbody fusion." Spine 20(3): 356-61.
50. Lenke, L. G. and K. H. Bridwell (2002). "Mesh cages in idiopathic scoliosis in adolescents." Clin Orthop(394): 98-108.

51. Lenke, L. G., K. H. Bridwell, et al. (1992). "Results of in situ fusion for isthmic spondylolisthesis." J Spinal Disord 5(4): 433-42.
52. Lin, P. M. (1985). "Posterior lumbar interbody fusion technique: complications and pitfalls." Clin Orthop(193): 90-102.
53. Lowe, T. G., A. D. Tahernia, et al. (2002). "Unilateral transforaminal posterior lumbar interbody fusion (TLIF): indications, technique, and 2-year results." J Spinal Disord Tech 15(1): 31-8.
54. Lund, T., T. R. Oxland, et al. (1998). "Interbody cage stabilisation in the lumbar spine: biomechanical evaluation of cage design, posterior instrumentation and bone density." J Bone Joint Surg Br 80(2): 351-9.
55. Magerl, F. (1982) "External skeletal fixation of the lower thoracic and the lumbar spine." In: Uthoff, H.K. (Ed.) Current concepts of external fixation of fractures, Berlin, Springer.
56. Maurice, H. D. and T. R. Morley (1989). "Cauda equina lesions following fusion in situ and decompressive laminectomy for severe spondylolisthesis. Four case reports." Spine 14(2): 214-6.
57. McAfee, P. C., G. A. Lee, et al. (2002). "Anterior BAK instrumentation and fusion: complete versus partial discectomy." Clin Orthop(394): 55-63.
58. Meyerding, H.W. (1932) "Spondylolisthesis" Surg Gynecol Obstet 54: 371.
59. Molinari, R. W., K. H. Bridwell, et al. (2002). "Anterior column support in surgery for high-grade, isthmic spondylolisthesis." Clin Orthop(394): 109-20.
60. Nachemson, A. (1960). "Lumbar intradiscal pressure. Experimental studies on postmortem material." Acta Orthop Scand (Suppl) 43: 1-104.
61. Nakabayashi, Y., H. W. Wevers, et al. (1994). "Bone strength and histomorphometry of the distal femur." J Arthroplasty 9(3): 307-15.
62. Nibu, K., M. M. Panjabi, et al. (1997). "Multidirectional stabilizing potential of BAK interbody spinal fusion system for anterior surgery." J Spinal Disord 10(4): 357-62.
63. Nibu, K., M. M. Panjabi, et al. (1998). "Intervertebral disc distraction with a laparoscopic anterior spinal fusion system." Eur Spine J 7(2): 142-7.

64. Oxland, T.R., Grant J.P., et al. (2002) "Effects of endplate removal on the structural properties of the lower lumbar vertebral bodies" Currently accepted for publication in Spine.
65. Oxland, T. R. and T. Lund (2000). "Biomechanics of stand-alone cages and cages in combination with posterior fixation: a literature review." Eur Spine J 9 Suppl 1: S95-101.
66. Oxland, T. R., T. Lund, et al. (1996). "The relative importance of vertebral bone density and disc degeneration in spinal flexibility and interbody implant performance. An in vitro study." Spine 21(22): 2558-69.
67. Panjabi, M., K. Abumi, et al. (1989). "Spinal stability and intersegmental muscle forces. A biomechanical model." Spine 14(2): 194-200.
68. Panjabi, M. M., T. R. Oxland, et al. (1994). "Mechanical behavior of the human lumbar and lumbosacral spine as shown by three-dimensional load-displacement curves." J Bone Joint Surg Am 76(3): 413-24.
69. Perey, O. (1957). "Fracture of the vertebral endplate in the lumbar spine: an experimental biomechanical investigation." Acta Orthop Scand Suppl. 25:1-101.
70. Polly, D.W., Klemme, W.R., Cunningham, B.W., et al, (1998) "Biomechanical analysis of anterior scoliosis constructs using intervertebral cages." Trans Scoliosis Res Soc 81.
71. Polly, D. W., Jr., W. R. Klemme, et al. (2000). "The biomechanical significance of anterior column support in a simulated single-level spinal fusion." J Spinal Disord 13(1): 58-62.
72. Poussa, M., D. Schlenzka, et al. (1993). "Surgical treatment of severe isthmic spondylolisthesis in adolescents. Reduction or fusion in situ." Spine 18(7): 894-901.
73. Rathonyi, G. C., T. R. Oxland, et al. (1998). "The role of supplemental translaminar screws in anterior lumbar interbody fixation: a biomechanical study." Eur Spine J 7(5): 400-7.
74. Ray, C.D. (1993). "Threaded titanium cages for lumbar interbody fusions." Presented at the North American Spine Society annual meeting, 1993, p77.
75. Ray, C. D. (1997²). "Threaded fusion cages for lumbar interbody fusions. An economic comparison with 360 degrees fusions." Spine 22(6): 681-5.

76. Ray, C. D. (1997¹). "Threaded titanium cages for lumbar interbody fusions." Spine 22(6): 667-79; discussion 679-80.
77. Reid, I. R., M. C. Evans, et al. (1991). "The influence of osteophytes and aortic calcification on spinal mineral density in postmenopausal women." J Clin Endocrinol Metab 72(6): 1372-4.
78. Riew, K. D. and J. M. Rhee (2002). "The use of titanium mesh cages in the cervical spine." Clin Orthop(394): 47-54.
79. Rizzoli, R., D. Slosman, et al. (1995). "The role of dual energy X-ray absorptiometry of lumbar spine and proximal femur in the diagnosis and follow-up of osteoporosis." Am J Med 98(2A): 33S-36S.
80. Roberts, S., I. W. McCall, et al. (1997). "Does the thickness of the vertebral subchondral bone reflect the composition of the intervertebral disc?" Eur Spine J 6(6): 385-9.
81. Roberts, S., J. Menage, et al. (1989). "Biochemical and structural properties of the cartilage end-plate and its relation to the intervertebral disc." Spine 14(2): 166-74.
82. Sandhu, H. S., S. Turner, et al. (1996). "Distractive properties of a threaded interbody fusion device. An in vivo model." Spine 21(10): 1201-10.
83. Saunders, J.B. deC.M., Inman, V.T. (1940) "Pathology of the intervertebral disk." Arch Surg 40 ;380-416.
84. Schmorl, G. and Jungerhanns, H. (1959) "The human spine in health and disease". New York and London, Grune and Stratton.
85. Schoenecker, P. L., H. O. Cole, et al. (1990). "Cauda equina syndrome after in situ arthrodesis for severe spondylolisthesis at the lumbosacral junction." J Bone Joint Surg Am 72(3): 369-77.
86. Seitsalo, S., K. Osterman, et al. (1990). "Severe spondylolisthesis in children and adolescents. A long-term review of fusion in situ." J Bone Joint Surg Br 72(2): 259-65.
87. Stauffer, R. N. and M. B. Coventry (1972). "Posterolateral lumbar-spine fusion. Analysis of Mayo Clinic series." J Bone Joint Surg Am 54(6): 1195-204.
88. Steffen, T., A. Tsantrizos, et al. (2000). "Effect of implant design and endplate preparation on the compressive strength of interbody fusion constructs." Spine 25(9): 1077-84.

89. Tan, J.S., Wong, H.K., Goh, J.C.H., Wong, D. (2000) "Influence of bone mineral density on the penetration load of lumbar spine vertebra with titanium mesh cage." International Society for the Study of the Lumbar Spine, Adelaide, Australia, p98.
90. Taylor, J. R. (1975). "Growth of human intervertebral discs and vertebral bodies." J Anat 120(1): 49-68.
91. Tencer, A. F., D. Hampton, et al. (1995). "Biomechanical properties of threaded inserts for lumbar interbody spinal fusion." Spine 20(22): 2408-14.
92. Tiusanen, H., D. Schlenzka, et al. (1996). "Results of a trial of anterior or circumferential lumbar fusion in the treatment of severe isthmic spondylolisthesis in young patients." J Pediatr Orthop B 5(3): 190-4.
93. Vernon-Roberts, B. and C. J. Pirie (1973). "Healing trabecular microfractures in the bodies of lumbar vertebrae." Ann Rheum Dis 32(5): 406-12.
94. Walmsley, R. (1953). "Growth and development of the intervertebral disc." Edinburgh Med J. 60: 341-364.
95. Weaver, J. K. (1966). "The microscopic hardness of bone." J Bone Joint Surg Am 48(2): 273-88.
96. Wenger, K.H., Pross, A., Wilke, H.J., et al, "Bone mineral density of the vertebral endplate: an in vitro comparison of normals, degenerations, and osteoporotics." Presented at the International Society for the Study of the Lumbar Spine, 1999, p 56.
97. Wetzel, F.T., and LaRocca, H. (1990) "The failed posterior lumbar interbody fusion." Spine 16 (7):839-845.
98. White, A.A., and Panjabi, M.M., (1990) "Clinical biomechanics of the spine." 2nd Ed., Philadelphia: JB Lippincott.
99. Wong, D., Tan, J.S., Wong, H.K., Goh, J.C.H., "Subsidence of Moss-Miami cage implant in PLIF with and without posterior fixation. Presented at the International Society for the Study of the Lumbar Spine, Adelaide, Australia, 2000, p279.

7.0 Appendices

Appendix A - Load-Displacement Graphs for Functional Spinal Units Tested

1061-L34 Instron Load-Displacement

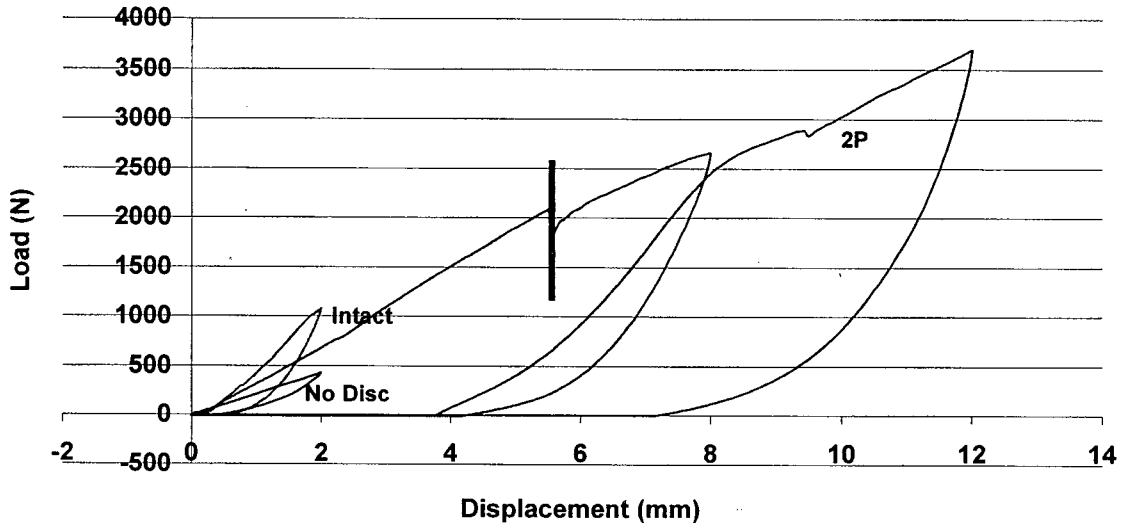


Figure A.1 Specimen 1061 L3/4- Load-displacement curves for disc intact, without disc, and 2 posterolateral cages (Failure marked with line)

1061-L45 Instron Load-Displacement

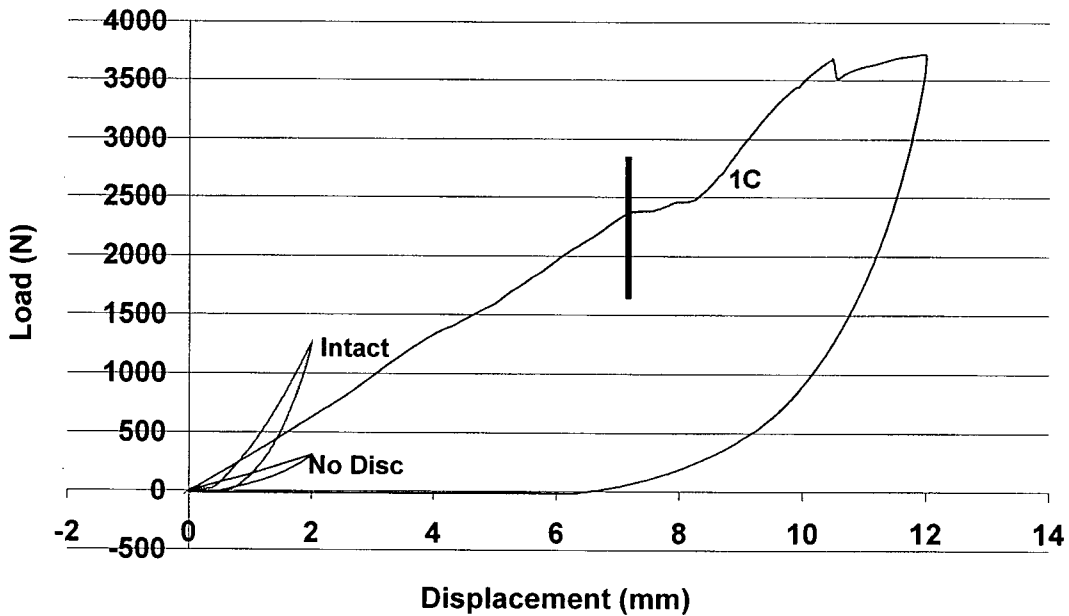


Figure A.2 Specimen 1061 L4/5 - Load-displacement curves for disc intact, without disc, and 1 central cage (Failure marked with line)

1061-L5-S1 Instron Load-Displacement

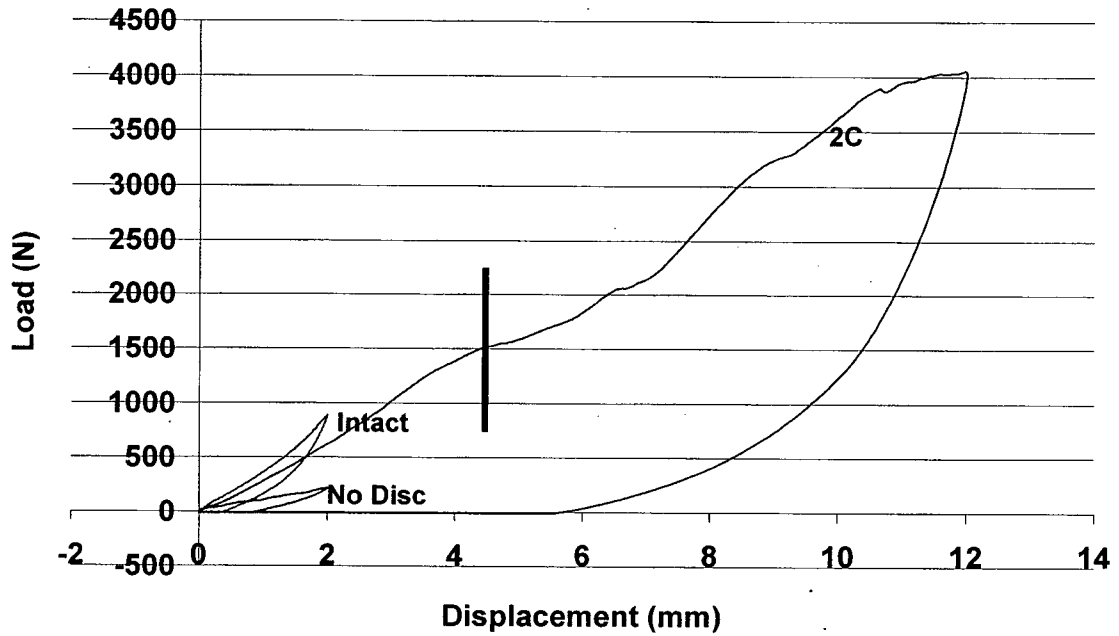


Figure A.3 Specimen 1061 L5/S1- Load-displacement curves for disc intact, without disc, and 2 central cages

1067-L34 Instron Load-Displacement

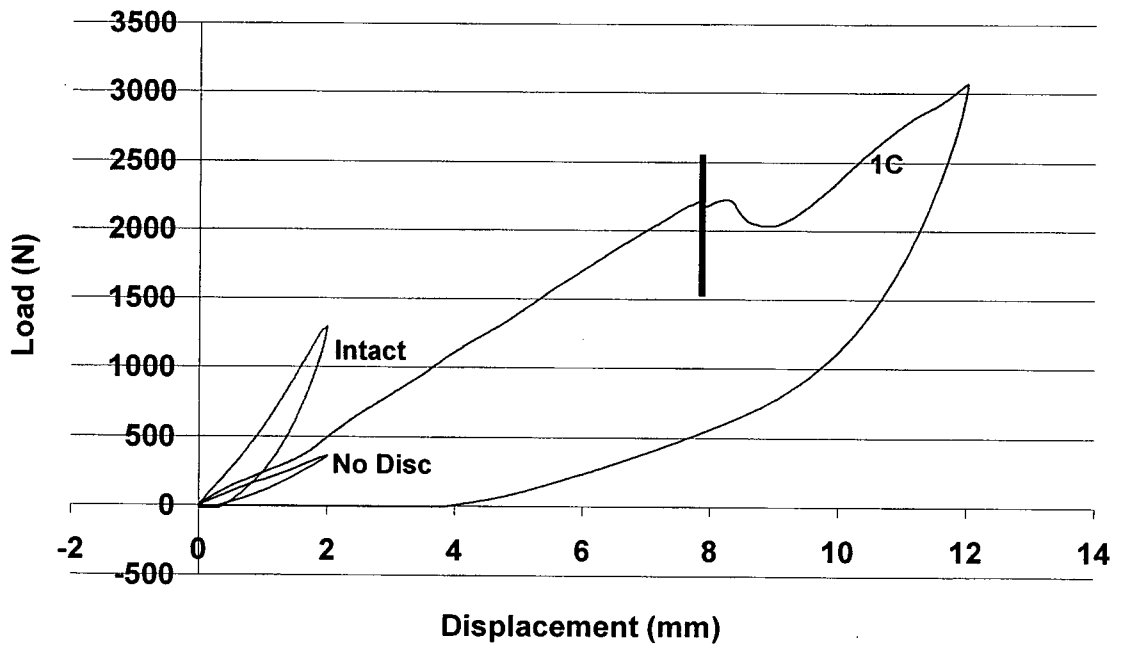


Figure A.4 Specimen 1067 L3/4- Load-displacement curves for disc intact, without disc, and 1 central cage

1067-L45 Instron Load-Displacement

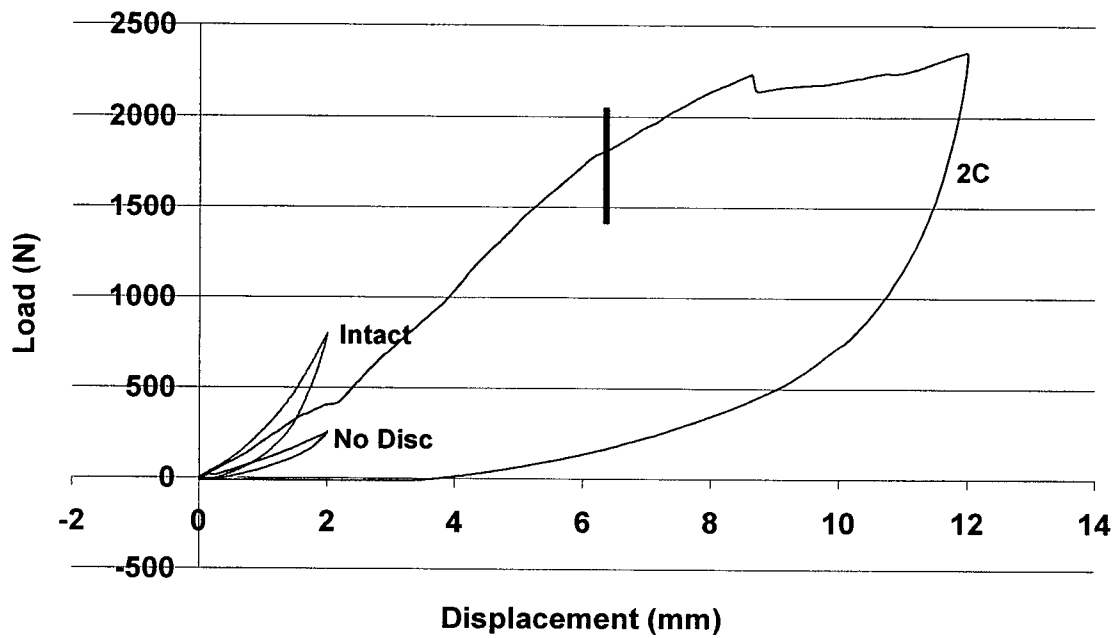


Figure A.5 Specimen 1067 L4/5- Load-displacement curves for disc intact, without disc, and 2 central cages

1067-L5-S1 Instron Load-Displacement

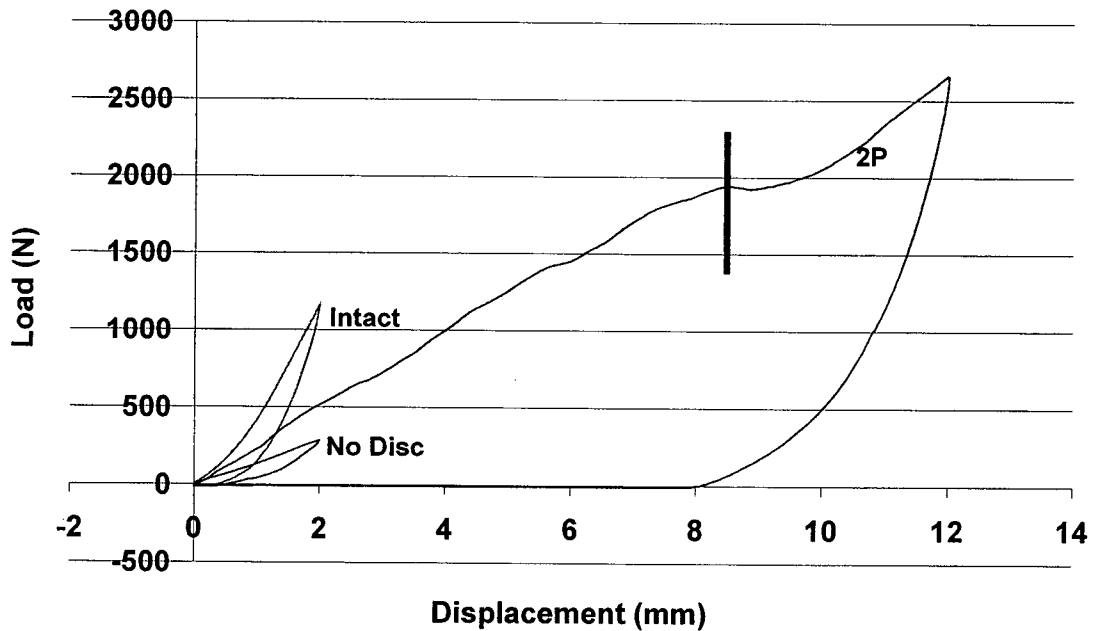


Figure A.6 Specimen 1067 L5/S1- Load-displacement curves for disc intact, without disc, and 2 posterolateral cages

1009-L34 Instron Load-Displacement

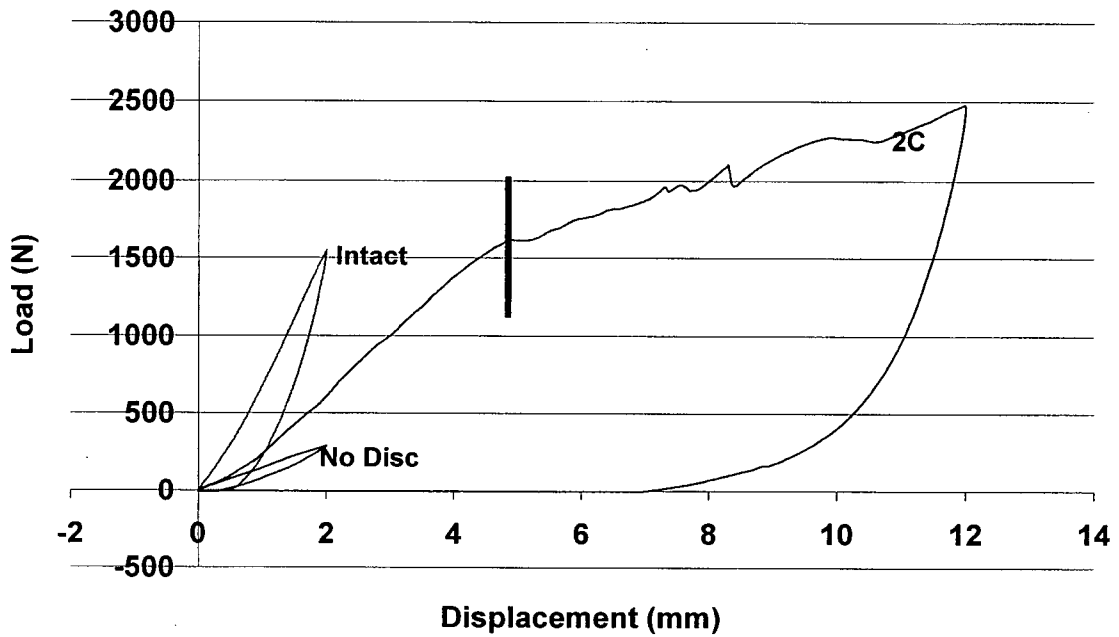


Figure A.7 Specimen 1009 L3/4- Load-displacement curves for disc intact, without disc, and 2 central cages

1009-L45 Instron Load-Displacement

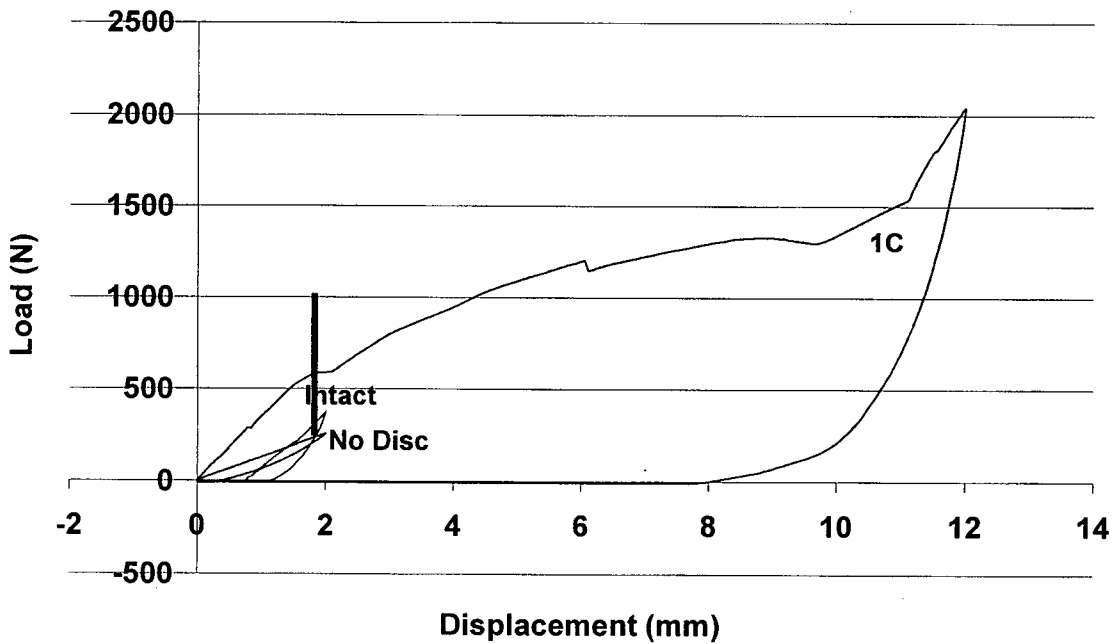


Figure A.8 Specimen 1009 L4/5- Load-displacement curves for disc intact, without disc, and 1 central cage

1009-L5-S1 Instron Load-Displacement

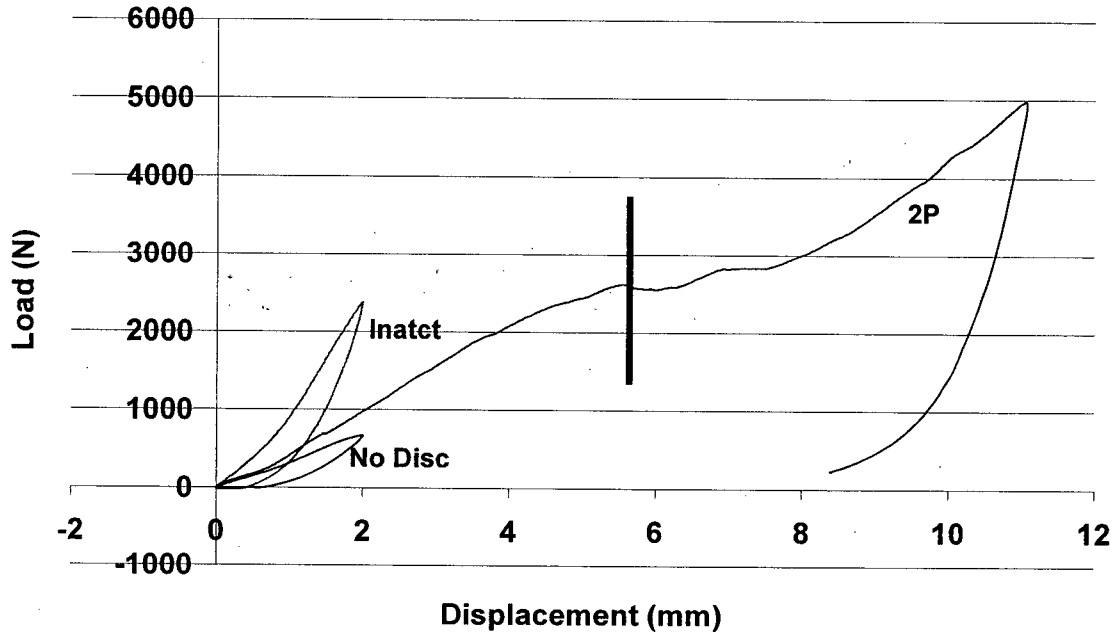


Figure A.9 Specimen 1009 L5/S1- Load-displacement curves for disc intact, without disc, and 2 posterolateral cages

1027-L34 Instron Load-Displacement

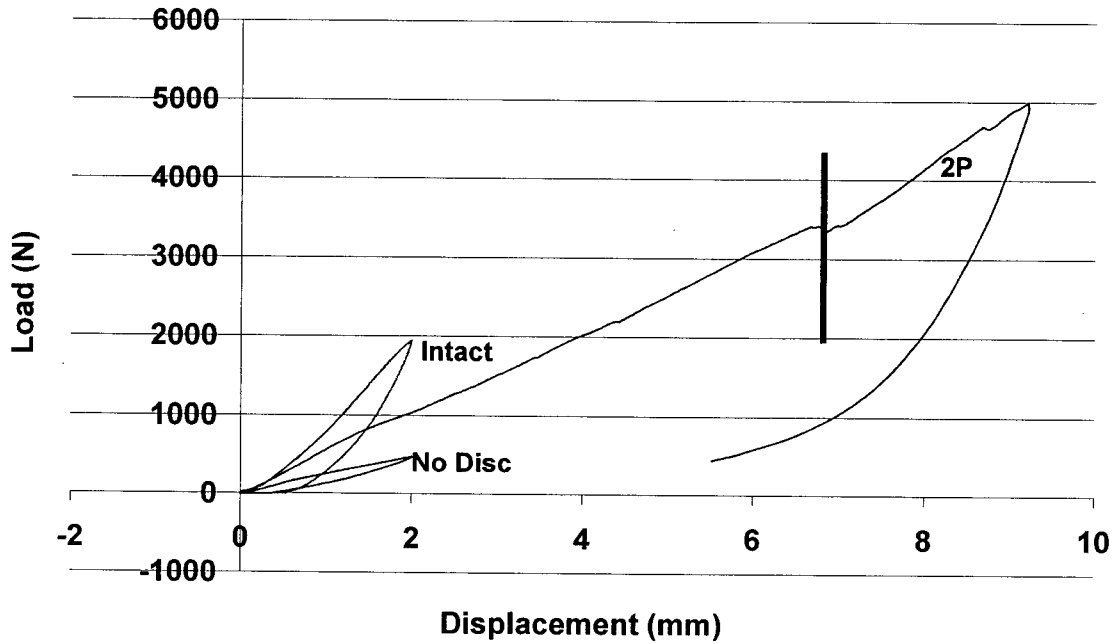


Figure A.10 Specimen 1027 L3/4- Load-displacement curves for disc intact, without disc, and 2 posterolateral cages

1027-L45 Instron Load-Displacement

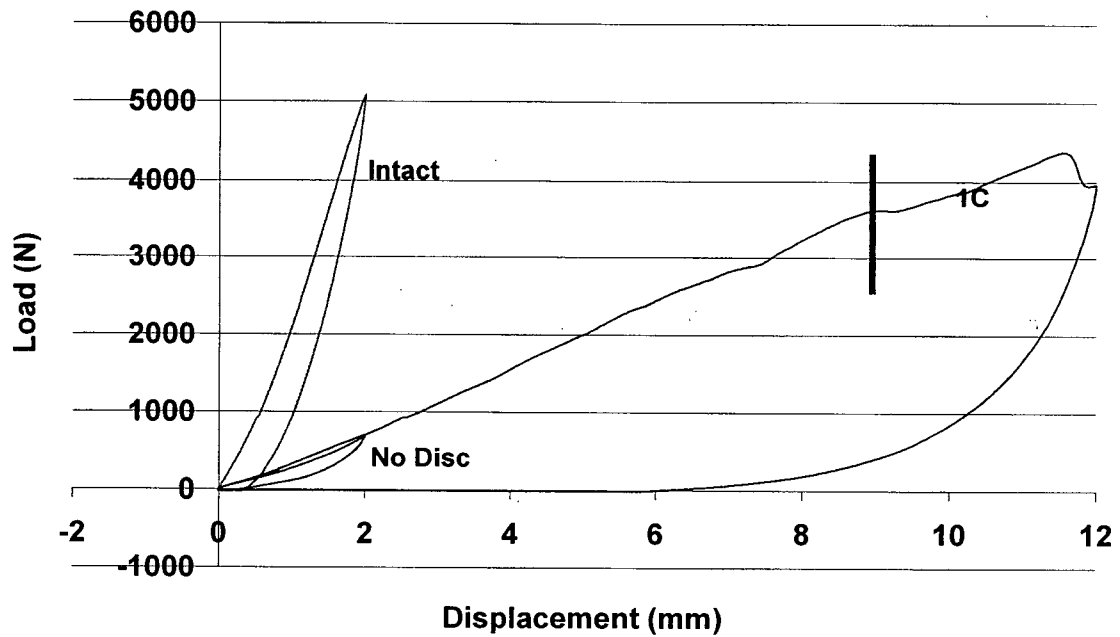


Figure A.11 Specimen 1027 L4/5 Load-displacement curves for disc intact, without disc, and 1 central cage

1027-L5-S1 Instron Load-Displacement

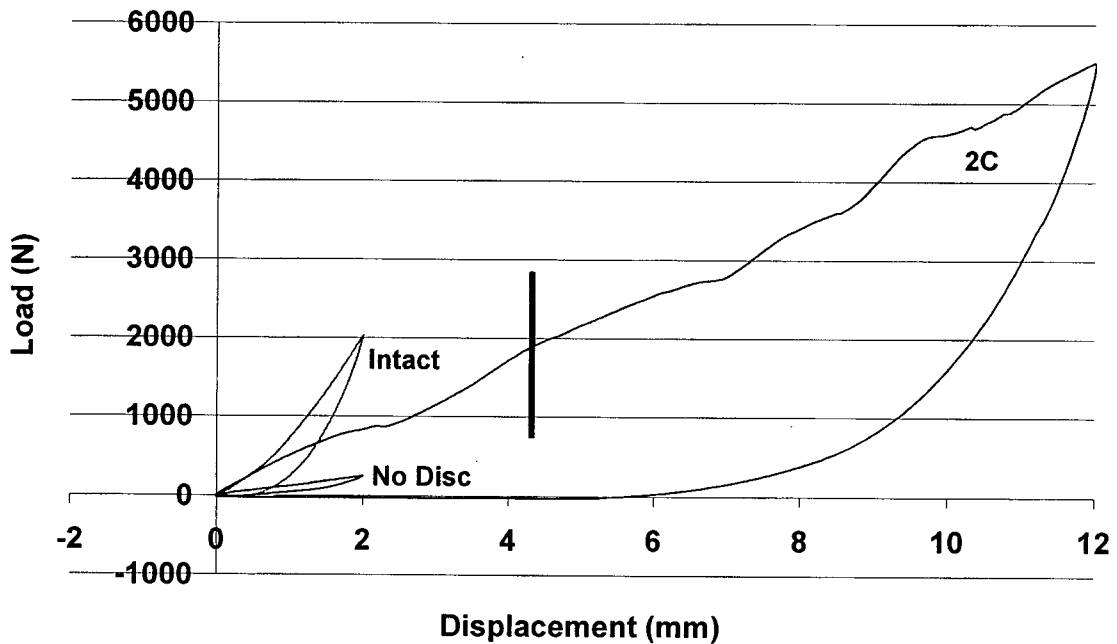


Figure A.12 Specimen 1027 L5/S1 Load-displacement curves for disc intact, without disc, and 2 central cages

1082-L34 Instron Load-Displacement

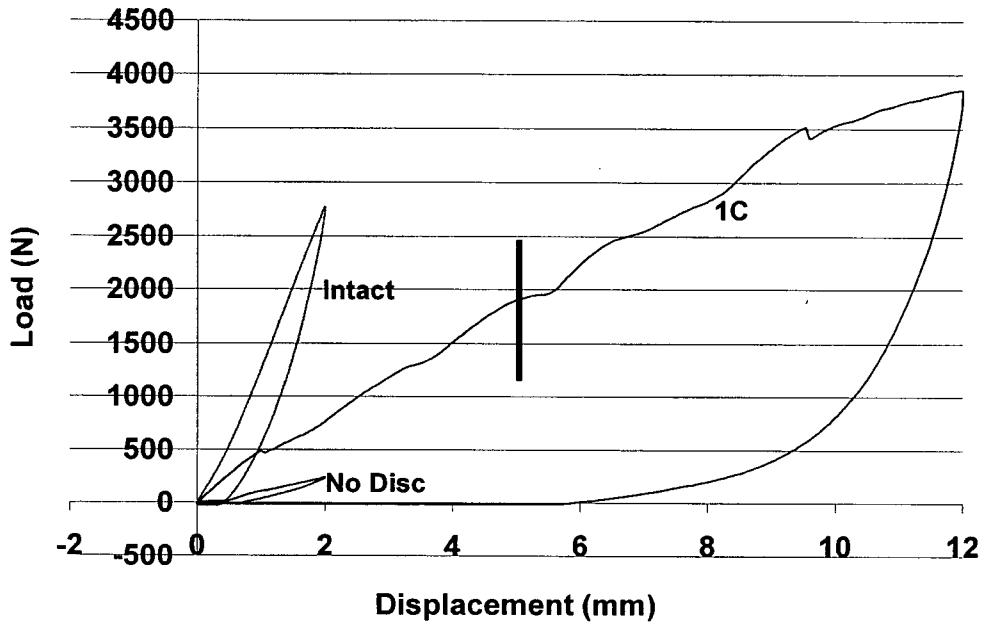


Figure A.13 Specimen 1082 L3/4- Load-displacement curves for disc intact, without disc, and 1 central cage

1082-L45 Instron Load-Displacement

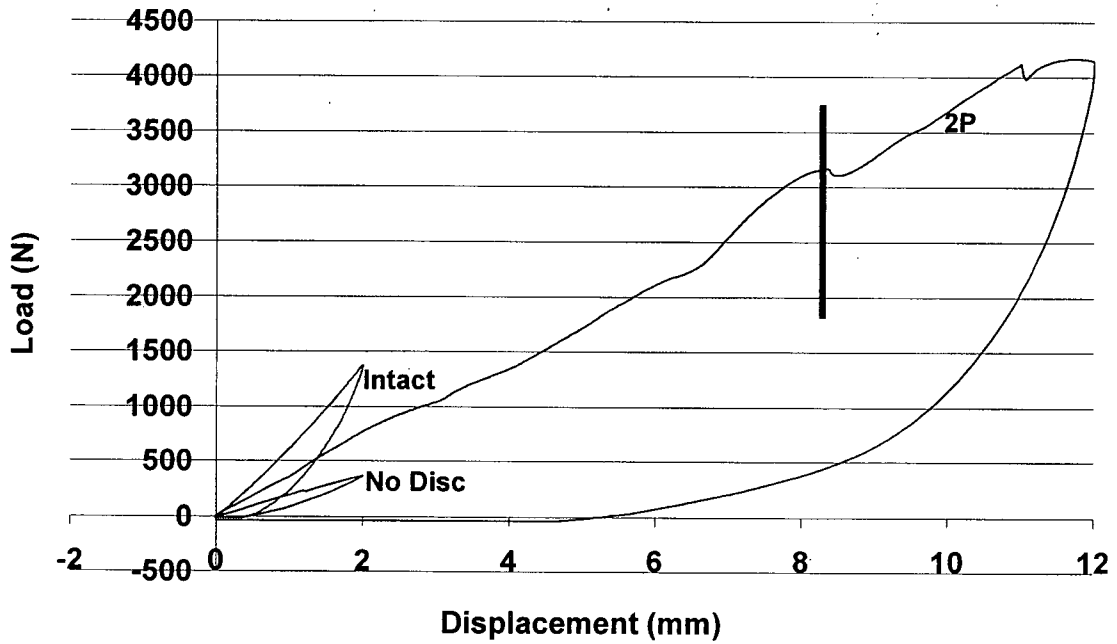


Figure A.14 Specimen 1082 L4/5- Load-displacement curves for disc intact, without disc, and 2 posterolateral cages

1082-L5-S1 Instron Load-Displacement

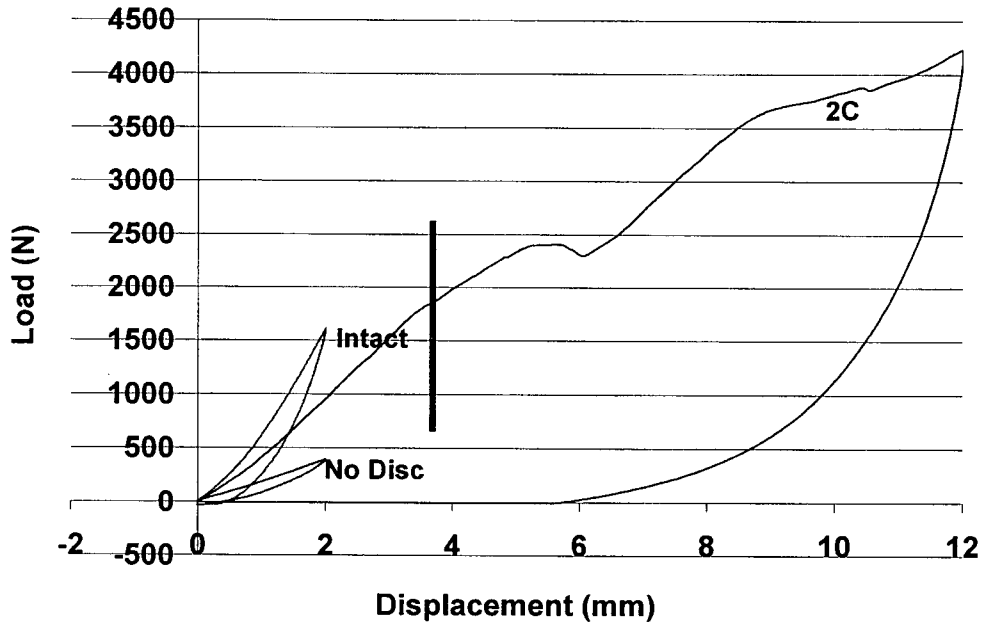


Figure A.15 Specimen 1082 L5/S1- Load-displacement curves for disc intact, without disc, and 2 central cages

1031-L34 Instron Load-Displacement

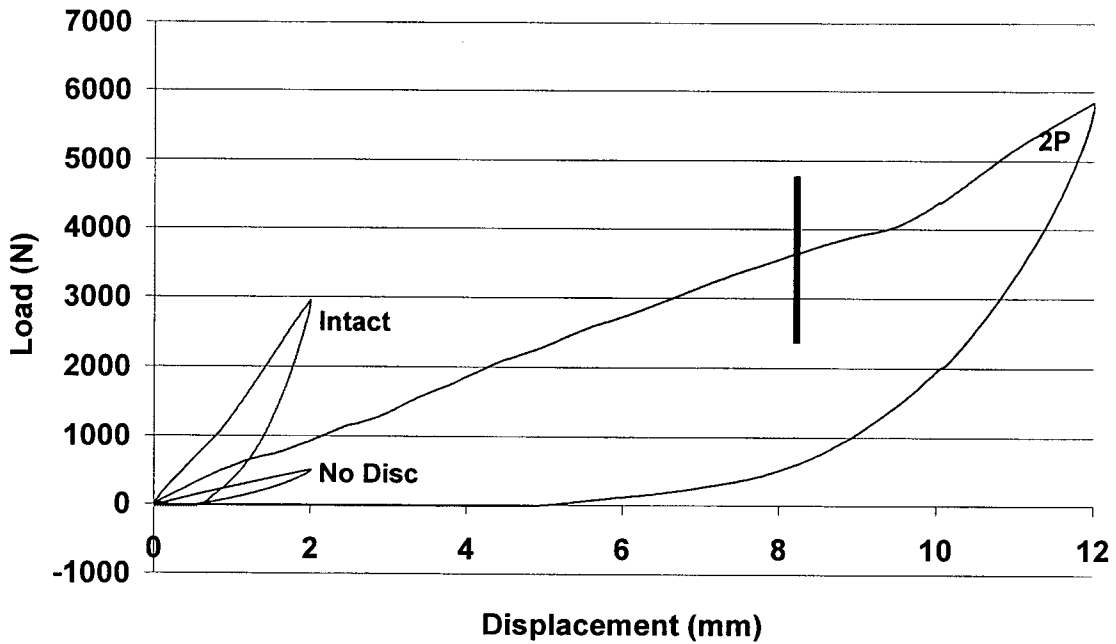


Figure A.16 Specimen 1031 L3/4- Load-displacement curves for disc intact, without disc, and 2 posterolateral cages

1031-L45 Instron Load-Displacement

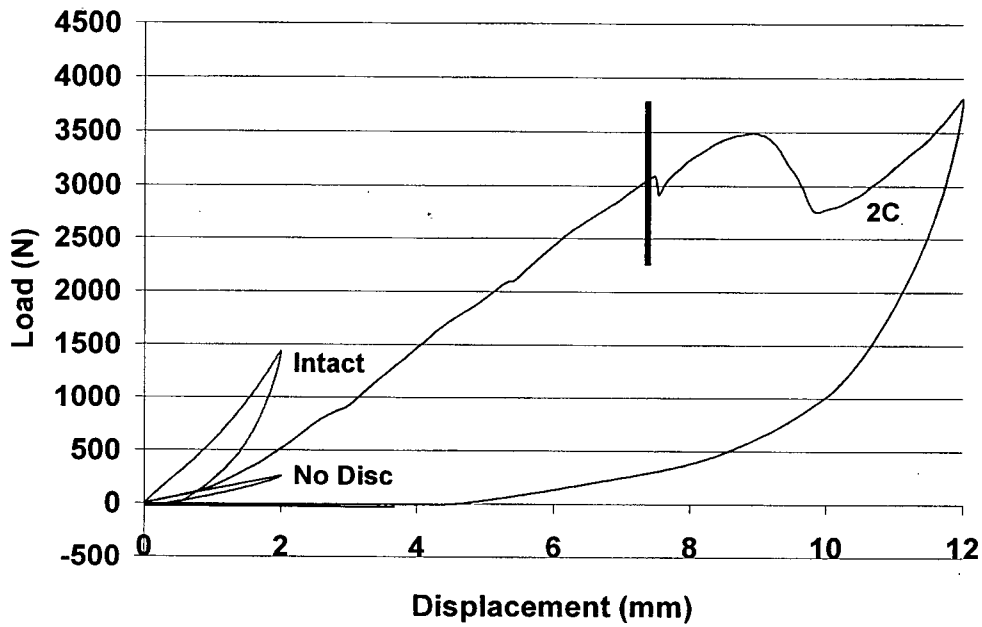


Figure A.17 Specimen 1031 L4/5- Load-displacement curves for disc intact, without disc, and 2 central cages

1031-L5-S1 Instron Load-Displacement

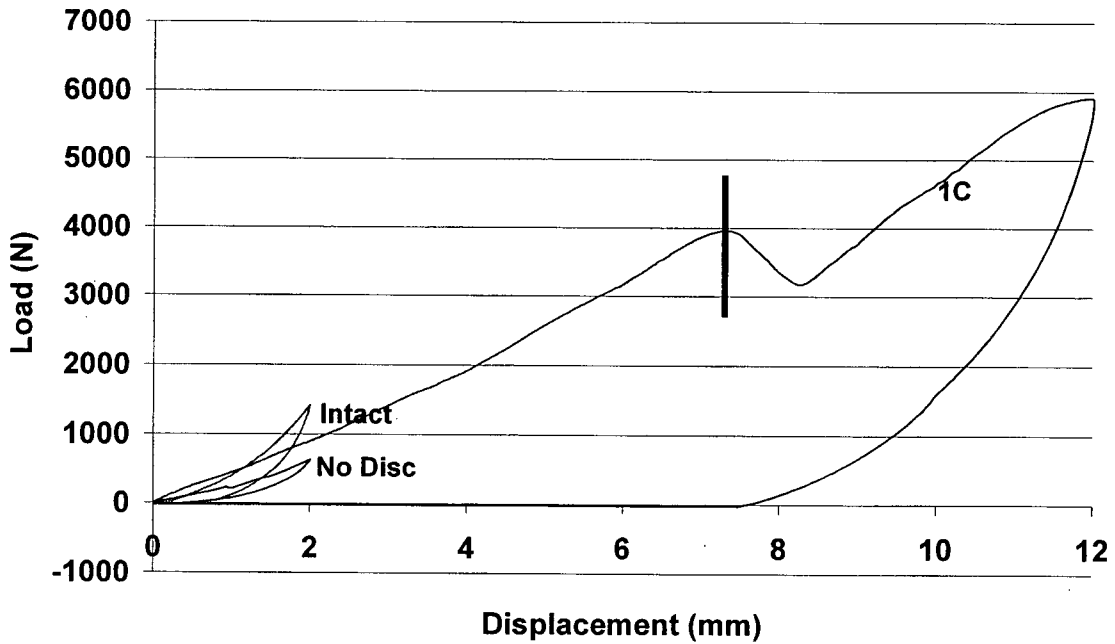


Figure A.18 Specimen 1031 L5/S1- Load-displacement curves for disc intact, without disc, and 1 central cage

1090-L34 Instron Load-Displacement

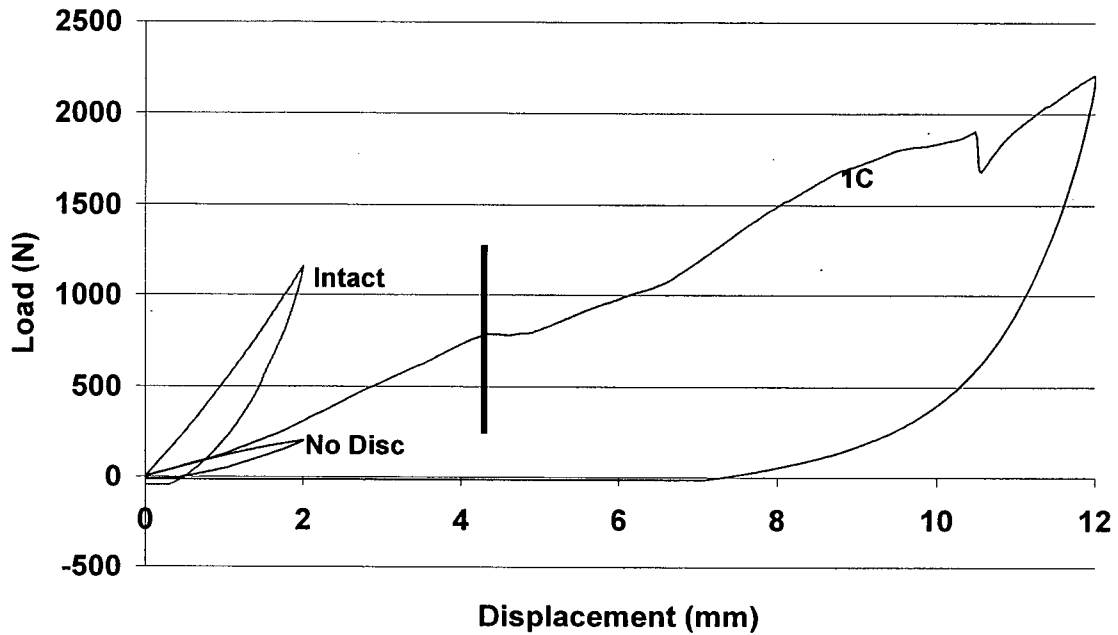


Figure A.19 Specimen 1090 L3/4- Load-displacement curves for disc intact, without disc, and 1 central cage

1090-L45 Instron Load-Displacement

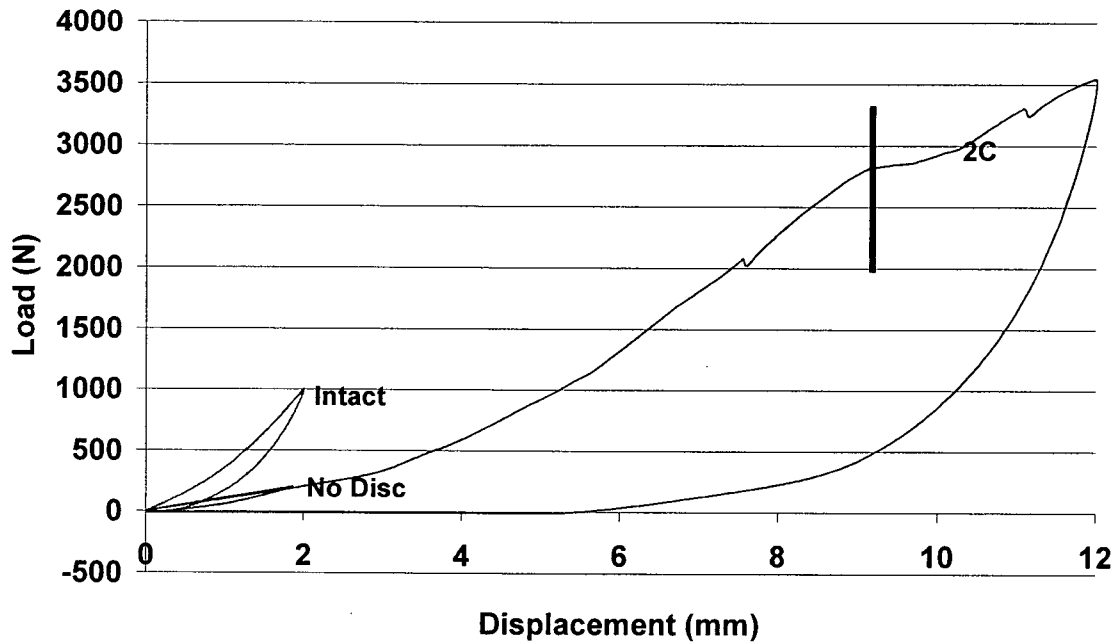


Figure A.20 Specimen 1090 L4/5 Load-displacement curves for disc intact, without disc, and 2 central cages

1090-L5-S1 Instron Load-Displacement

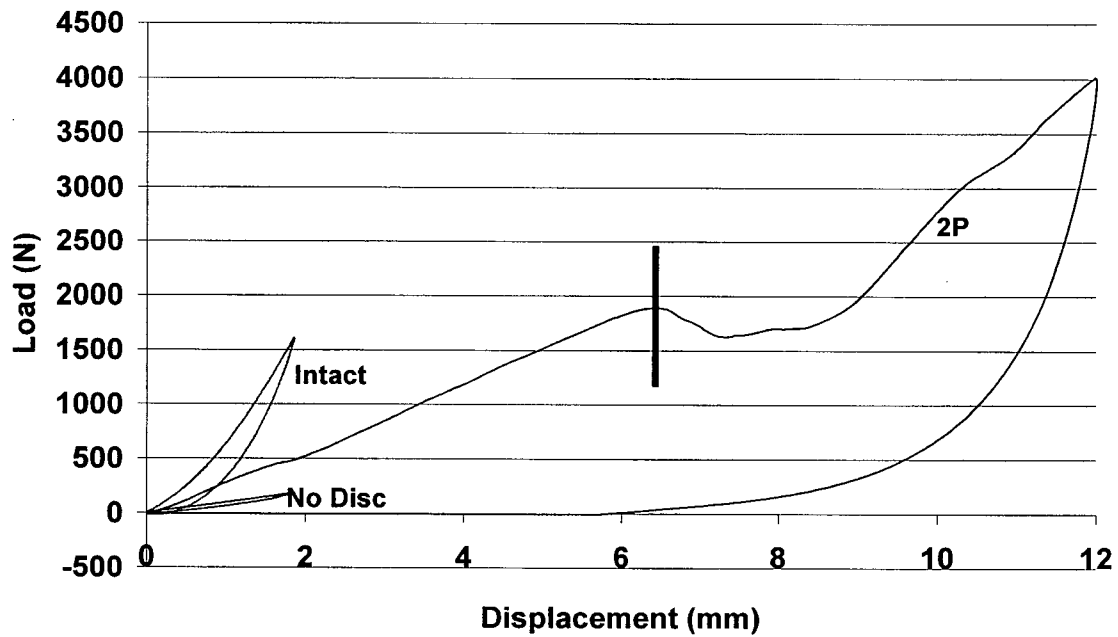


Figure A.21 Specimen 1090 L5/S1- Load-displacement curves for disc intact, without disc, and 2 posterolateral cages

1030-L34 Instron Load-Displacement

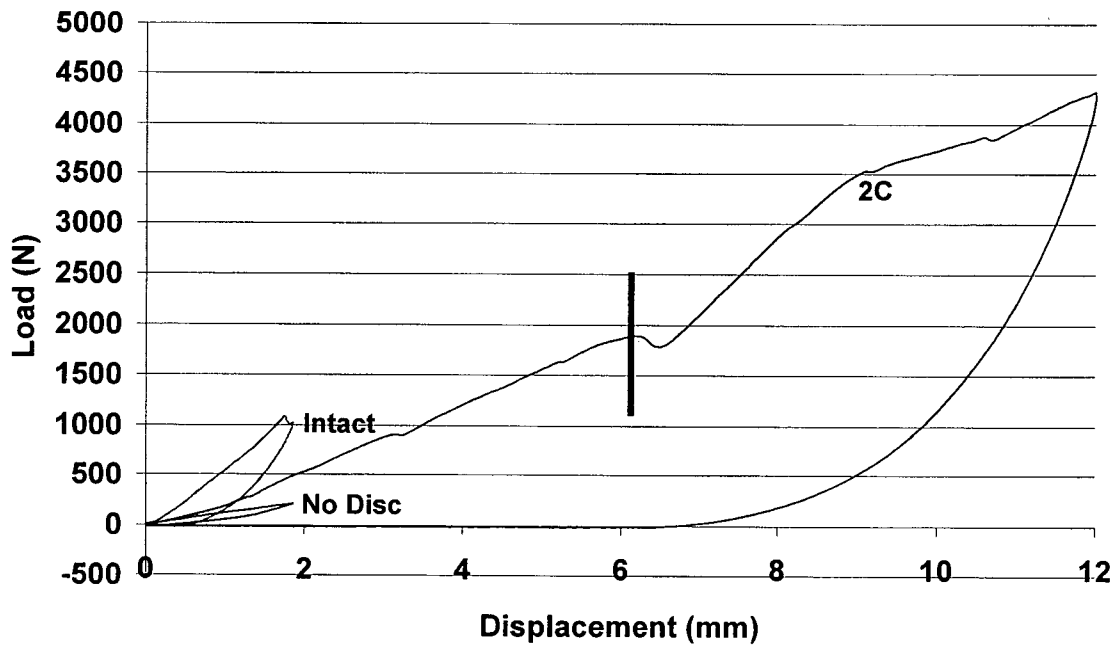


Figure A.22 Specimen 1030 L3/4- Load-displacement curves for disc intact, without disc, and 2 central cages

1030-L45 Instron Load-Displacement

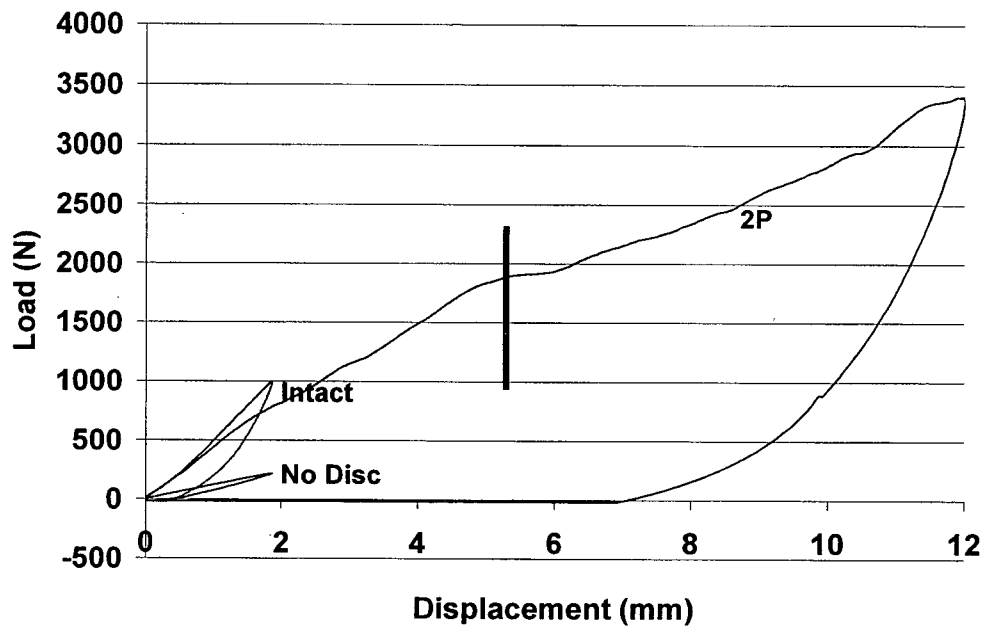


Figure A.23 Specimen 1030 L4/5 Load-displacement curves for disc intact, without disc, and 2 posterolateral cages

1030-L5-S1 Instron Load-Displacement

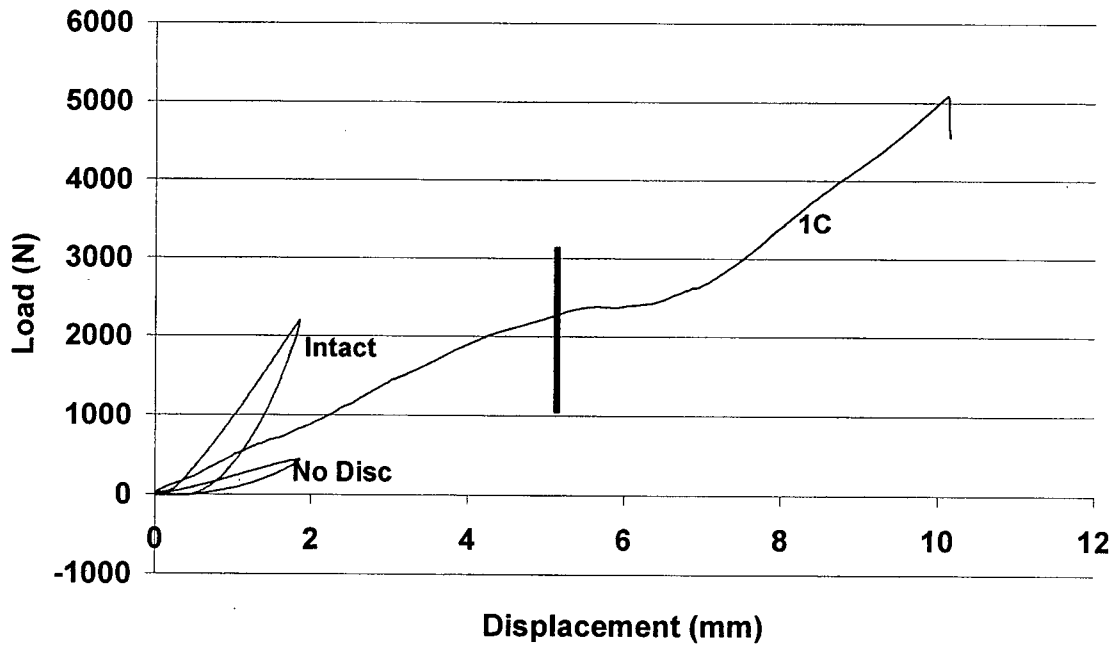


Figure A.24 Specimen 1030 L5/S1- Load-displacement curves for disc intact, without disc, and 1 central cage

1036-L34 Instron Load-Displacement

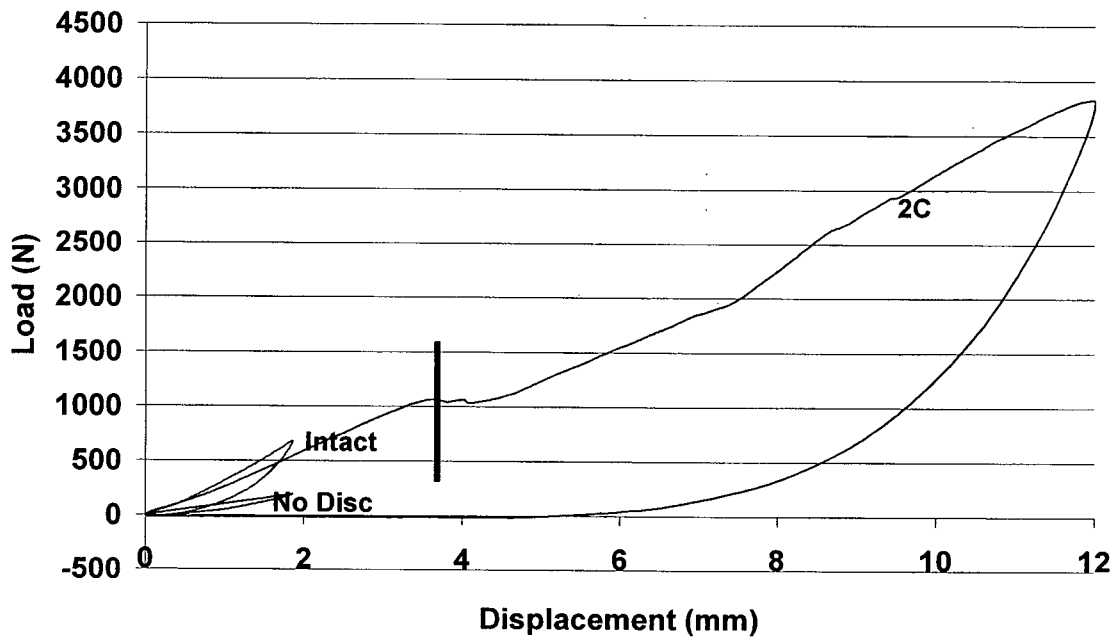


Figure A.25 Specimen 1036 L3/4- Load-displacement curves for disc intact, without disc, and 2 central cages

1036-L45 Instron Load-Displacement

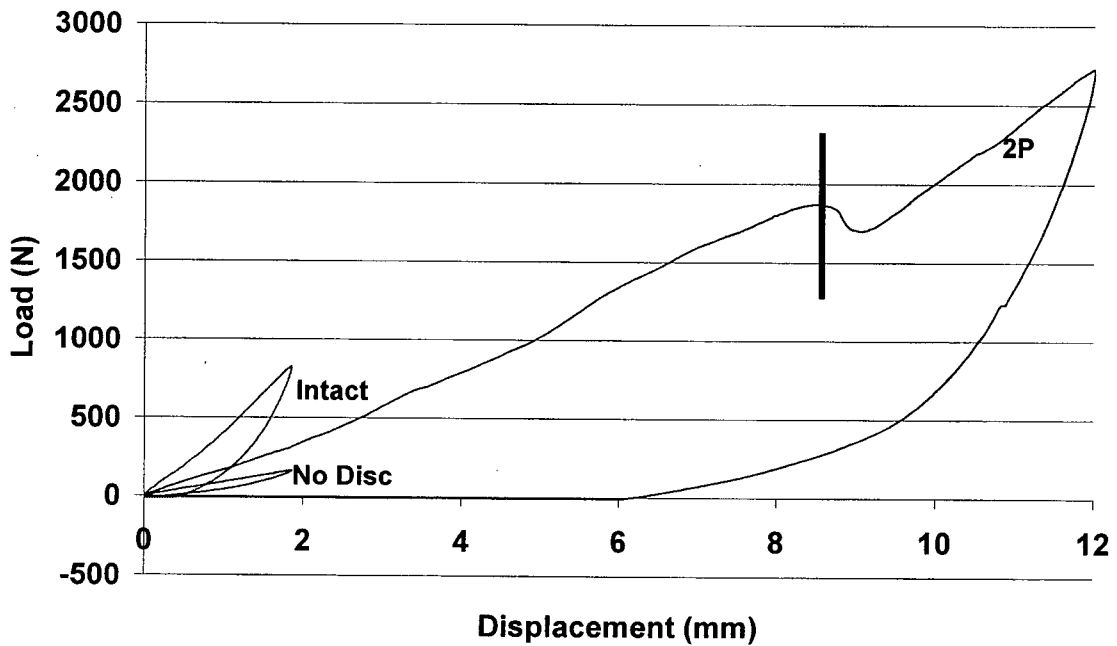


Figure A.26 Specimen 1036 L4/5- Load-displacement curves for disc intact, without disc, and 2 posterolateral cages

1036-L5-S1 Instron Load-Displacement

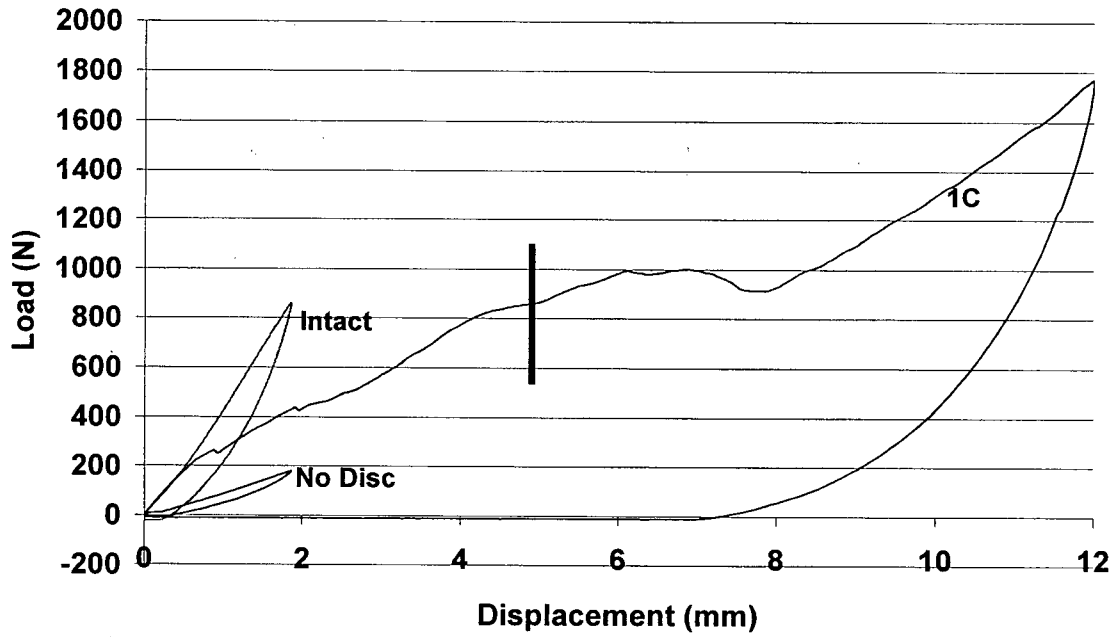


Figure A.27 Specimen 1036 L5/S1- Load-displacement curves for disc intact, without disc, and 1 central cage (Failure marked on cage curve with line)

Appendix B - Translation and Rotation Graphs for Single Cages and Qualitative Description of Motion for Single Cage Position Tests

1. 1061- L4/5 Single Cage

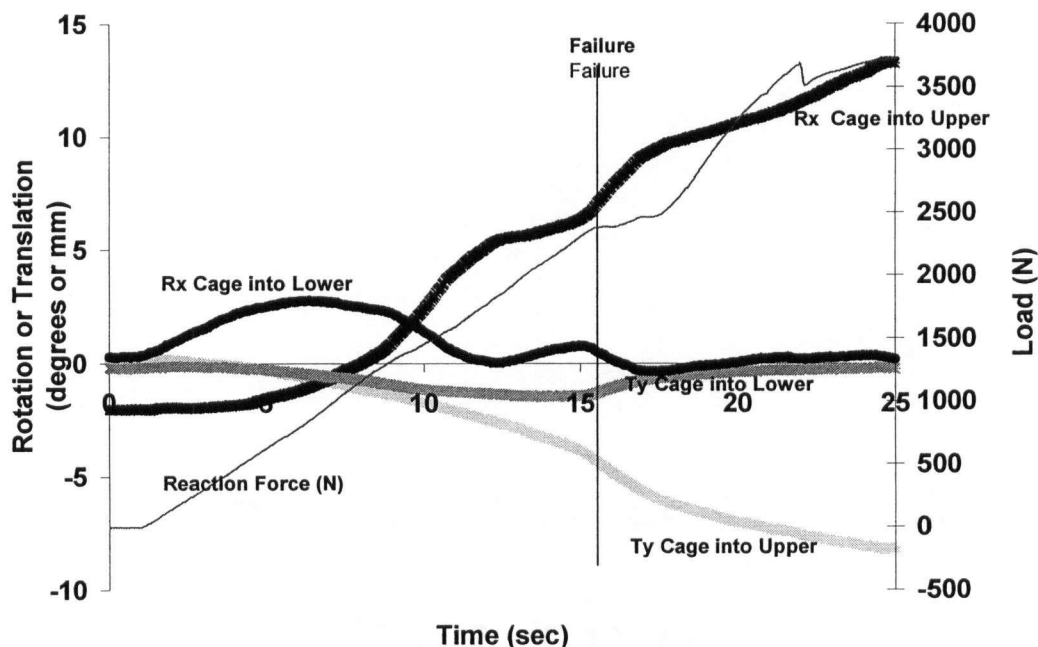


Figure B.1 Translation (T) and Rotation (R) in both axial- up or down (y plane) and sagittal- forward flexion (x plane) of the single cage in specimen 1061, L4/5, versus time. Reaction Force (N) is plotted versus time, with a failure point as defined by the vertical line.

Qualitative Description- Pre failure, the single cage is seen to mostly forward flex (Rx- Lower) into the lower vertebra (superior endplate of L5). Until 5 seconds, very little up or down subsidence occurs, with eventual preferential upwards (Ty-Upper) subsidence of the cage center point into the upper vertebra (inferior endplate of L4) to a depth of around 8 mm. The cage forward flexes (Rx- Upper) into the upper vertebra (inferior endplate of L4) to around 7 degrees at failure. At failure, there was less than 2 mm of subsidence downwards (Ty- Lower) into the lower vertebra (superior endplate of L5).

Only small amounts of lateral side bending motion (R_z) and almost no spinning in the axial plane (R_y) was seen (Table 3.3).

2. 1067- L3/4 Single Cage

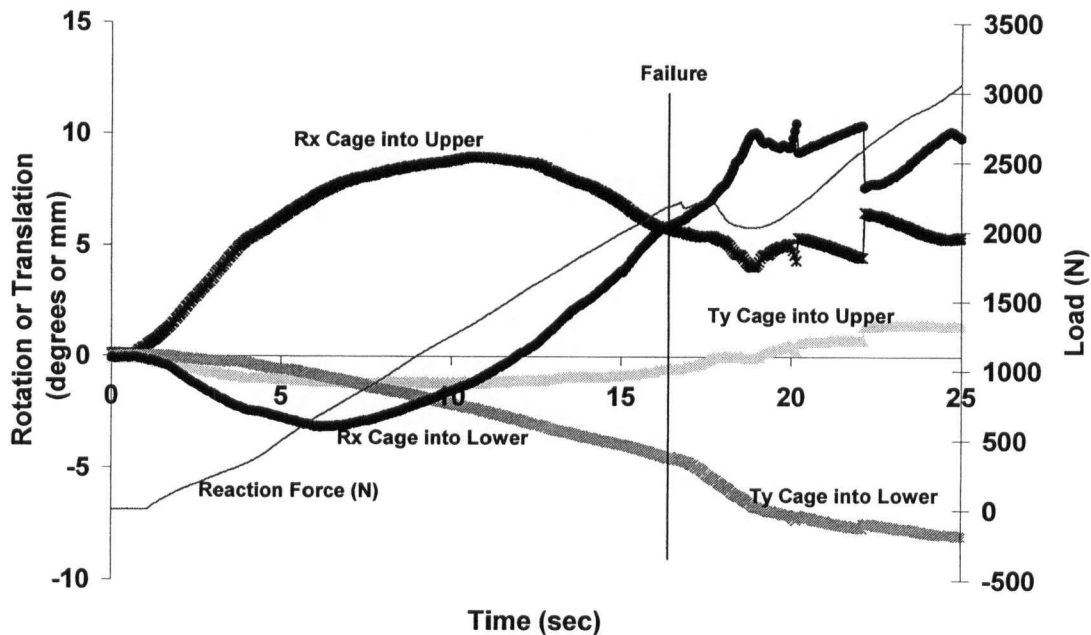


Figure B.2 Translation (T) and Rotation (R) in both axial- up or down (y plane) and sagittal- forward flexion (x plane) of the single cage in specimen 1067, L3/4, versus time. Reaction force (N) is plotted versus time, with a failure point as defined by the vertical line.

Qualitative Description- Pre-failure, the single cage was seen to mostly forward flex (Rx-Upper) into the upper vertebra (inferior endplate of L3). Only after 10 seconds, does the downward movement (Ty- Lower) become more significant, with nearly 5 mm of downward displacement into the lower vertebra (superior endplate of L4). Very little translation upwards (Ty- Upper) of the cage center point occurred. At failure, a significant amount of forward flexion (Rx- Lower) had occurred with the cage forward flexing into the lower vertebra (superior endplate of L4). Only small amounts of lateral

side bending motion (R_z) and almost no spinning in the axial plane (R_y) was seen (Table 3.3).

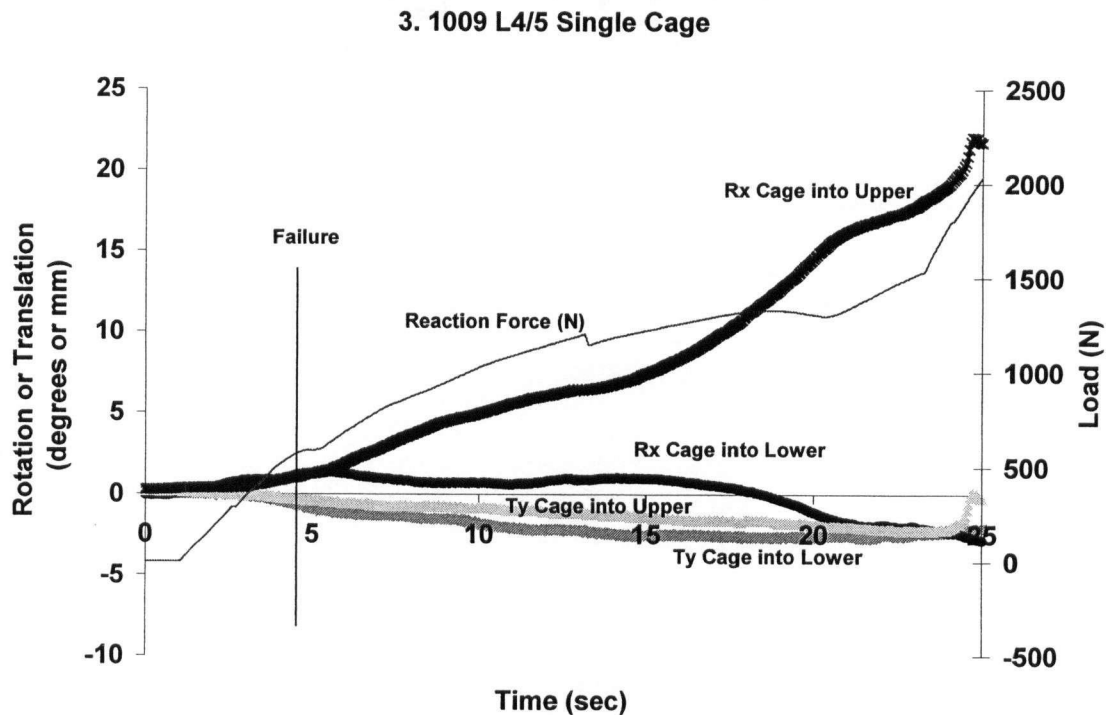


Figure B.3 Translation (T) and Rotation (R) in both axial- up or down (y plane) and sagittal- forward flexion (x plane) of the single cage in specimen 1009, L4/5, versus time. Reaction force (N) is plotted versus time, with a failure point as defined by the vertical line.

Qualitative Description- Failure is seen to occur just before 5 seconds, and remains the earliest failure of all cage(s) tested. Pre-failure, the single cage is seen to mostly rotate into both the upper and lower vertebra by only a few degrees (R_x –upper and Lower). Post-failure, the cage mostly moves into the upper vertebra (inferior endplate of L4) with a forward flexion motion (R_x - Upper), and moves by about 20 degrees by the end of the 12 second test. Only small amounts of lateral side bending motion (R_z) and almost no spinning in the axial plane (R_y) was seen (Table 3.3).

4. 1027 L4/5 Single Cage

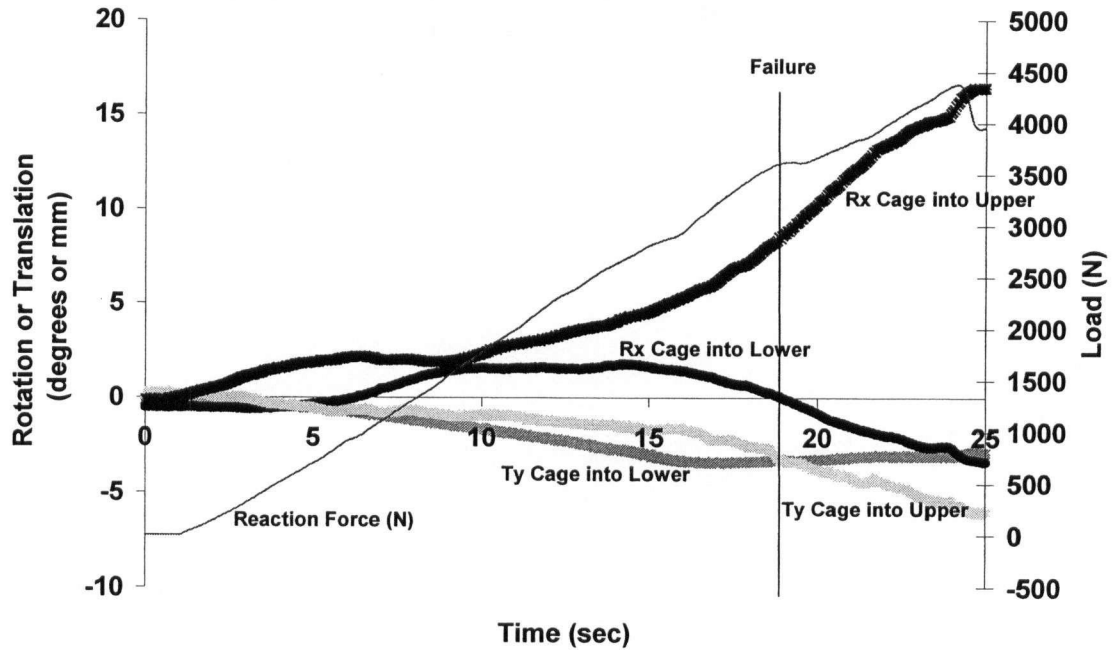


Figure B.4 Translation (T) and Rotation (R) in both axial- up or down (y plane) and sagittal- forward flexion (x plane) of the single cage in specimen 1027, L4/5, versus time. Reaction force (N) is plotted versus time, with a failure point as defined by the vertical line.

Qualitative Description – Pre-failure, the single cage is seen to rotate up into the inferior endplate of L4 (Rx-Upper). At failure, there is almost equal amounts of subsidence of the cage center point into both upper and lower vertebra to a depth of about 3 mm (Ty- Lower, Ty- Upper). At failure, the cage has predominantly rotated up into the upper vertebra (inferior endplate of L4), by approximately 8 degrees. Only small amounts of lateral side bending motion (Rz) and almost no spinning in the axial plane (Ry) was seen (Table). Only small amounts of lateral side bending motion (Rz) and almost no spinning in the axial plane (Ry) was seen (Table 3.3).

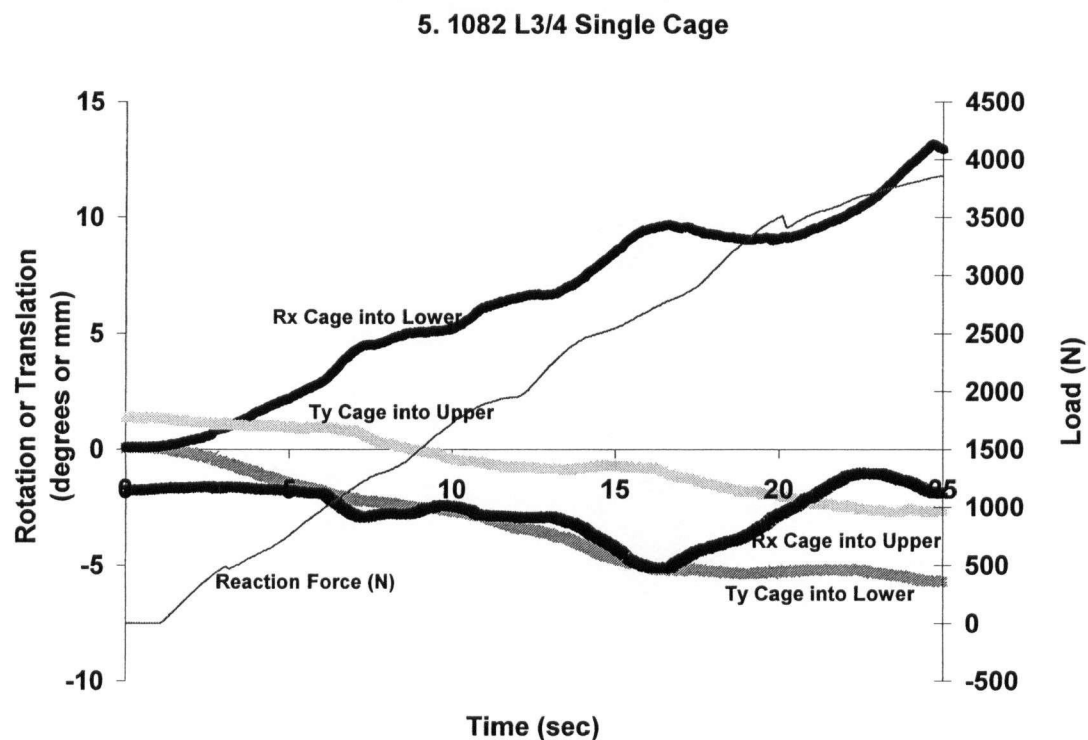


Figure B.5 Translation (T) and Rotation (R) in both axial- up or down (y plane) and sagittal- forward flexion (x plane) of the single cage in specimen 1082, L3/4,

versus time. Reaction force (N) is plotted versus time, with a failure point as defined by the vertical line.

Qualitative Description – Pre-failure, the single cage is seen to mostly rotate down into the lower vertebra (Rx- Lower) by around 7 degrees, with almost no upwards translation (Ty) of the cage into the upper vertebra (inferior endplate of L3). At failure, there is approximately 3 mm of downwards translation (Ty- Lower) into the superior endplate of L4, and almost no translation of the cage center point into the upper vertebra (inferior endplate of L3). Only small amounts of lateral side bending motion (Rz) and almost no spinning in the axial plane (Ry) was seen (Table 3.3).

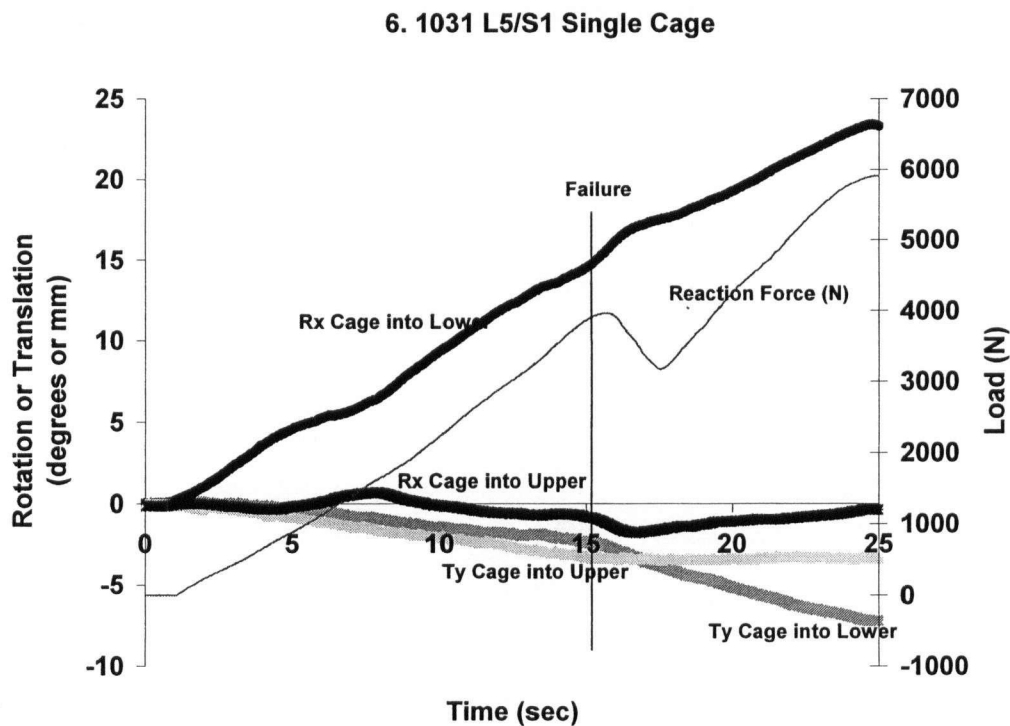


Figure B.6 Translation (T) and Rotation (R) in both axial- u or dwn (y plane) and sagittal- forward flexion (x plane) of the single cage in specimen 1031, L5/S1,

versus time. Reaction force (N) is plotted versus time, with a failure point as defined by the vertical line.

Qualitative Description – Pre-failure, the cage does almost nothing but forward rotate down (Rx- Lower) into the upper endplate of S1 by a total of 15 degrees at failure. This rotation forwards down into the lower vertebra remains the predominant cage motion throughout the test. At failure, only a few millimeters of cage center point translation up or down (Ty-Upper, Ty- Lower) had occurred. Almost no rotation of the cage into the upper vertebra (Rx- Upper) has occurred. Only small amounts of lateral side bending motion (Rz) and almost no spinning in the axial plane (Ry) was seen (Table 3.3).

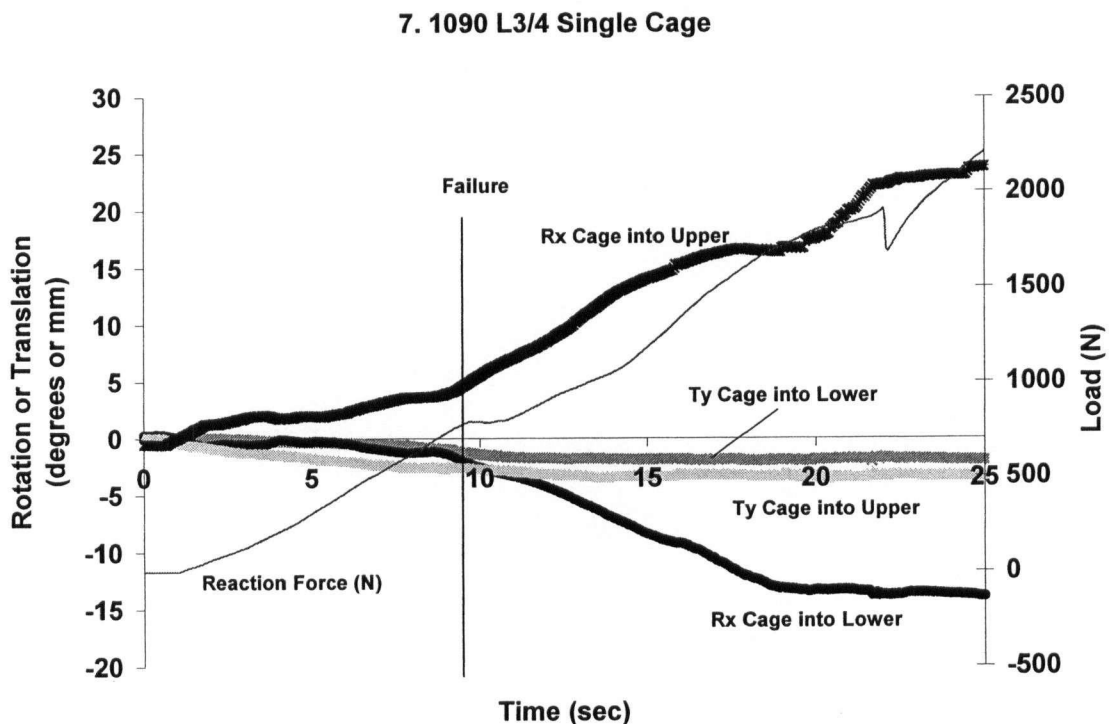


Figure B.7 Translation (T) and Rotation (R) in both axial- up or down (y plane) and sagittal- forward flexion (x plane) of the single cage in specimen 1090, L3/4, versus time. Reaction force (N) is plotted versus time, with a failure point as defined by the vertical line.

Qualitative Description- Pre-failure, the center point single cage translates only a few millimeters into the upper vertebra (Ty-Upper), with almost no translation into the lower vertebra (Ty-Lower). At failure, there is approximately 5 degrees of rotation (Rx- Upper) of the cage into the upper vertebra (inferior endplate of L3). Interestingly, post-failure, the cage continues to rotate into the upper and lower vertebrae, yet does not translate more than a few millimeters into either the upper or lower vertebra (Ty-Upper, Ty-Lower). Only small amounts of lateral side bending motion (Rz) and almost no spinning in the axial plane (Ry) was seen (Table 3.3).

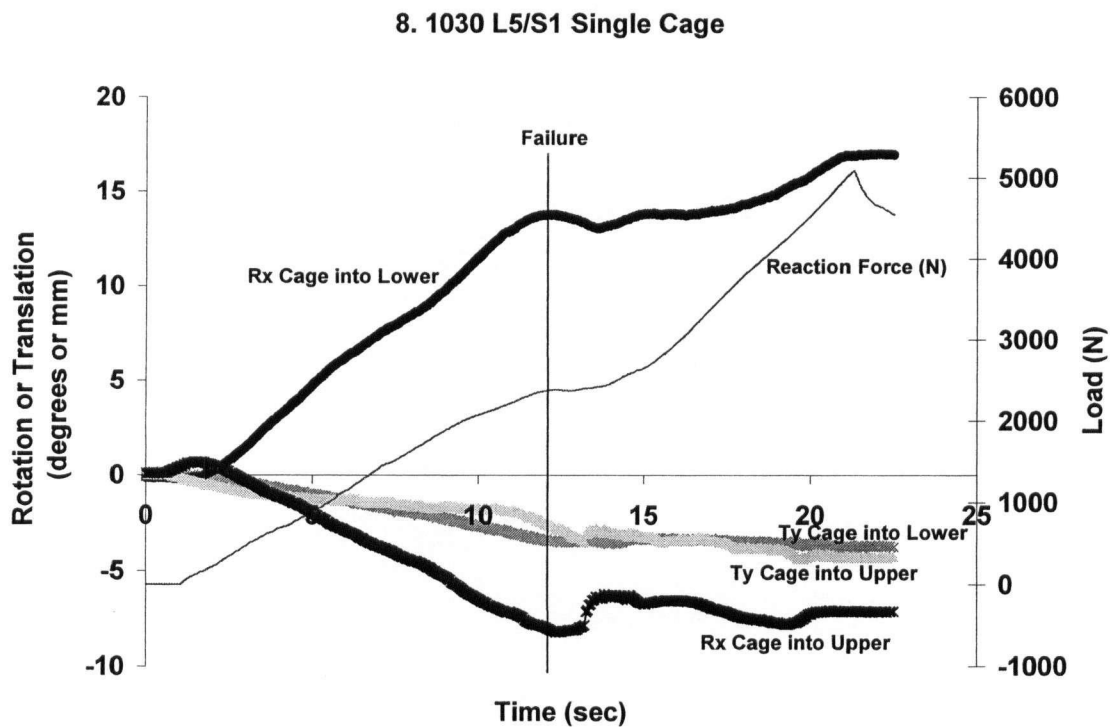


Figure B.8 Translation (T) and Rotation (R) in both axial- up or down (y plane) and saggital- forward flexion (x plane) of the single cage in specimen 1030, L5/1, versus time. Reaction force (N) is plotted versus time, with a failure point as defined by the vertical line.

Qualitative Description – Pre-failure, the cage does little translating or rotating in the first 2 seconds of the test. After 2 seconds, the cage dramatically rotates forwards (Rx- Lower) into the lower vertebra (superior endplate of S1), with rotation of the posterior part of the cage up (Rx- Upper) into the inferior endplate of L5. At failure, the cage forward rotates through approximately 14 degrees. At failure, the center point of the single cage had only translated a few millimeters into the upper and lower vertebra (Ty- Upper, Ty- Lower). Only small amounts of lateral side bending motion (Rz) and almost no spinning in the axial plane (Ry) was seen (Table 3.3).

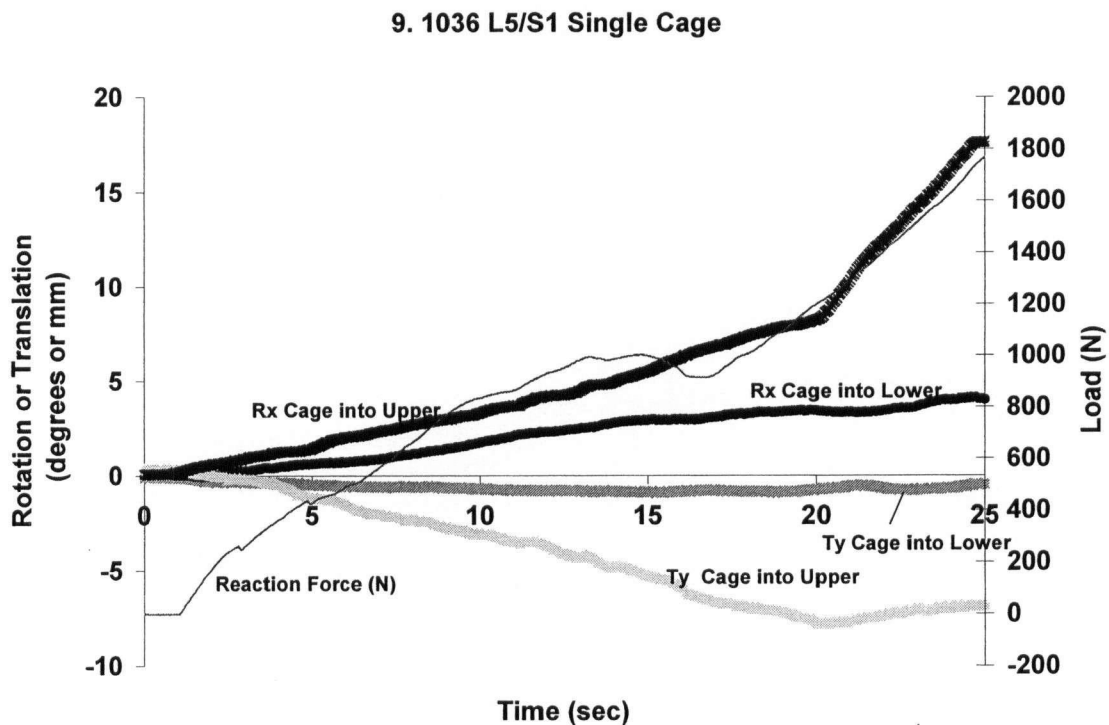


Figure B.9 Translation (T) and Rotation (R) in both axial- up or down (y plane) and sagittal- forward flexion (x plane) of the single cage in specimen 1036, L5/1,

versus time. Reaction force (N) is plotted versus time, with a failure point as defined by the vertical line.

Qualitative Description – Pre-failure, the cage motion does little for the first few seconds of the test. By 5 seconds, the has rotated into the upper vertebra by a few degrees (Rx- Upper). At failure, (approximately 10 seconds) has rotated (Rx- Upper) and translated (Ty- Upper) by approximately 3 degrees and 3mm into the upper vertebra (inferior endplate of L5). Almost no downwards translation (Ty- Lower) into the lower vertebra (superior endplate of S1) occurs throughout the test. Only small amounts of lateral side bending motion (Rz) and almost no spinning in the axial plane (Ry) was seen (Table 3.3).